Winter 12-15-2017

Extrinsic and Intrinsic Control of Integrative Processes in Neural Systems

Anirban Nandi
Washington University in St. Louis

WASHINGTON UNIVERSITY IN ST.LOUIS

School of Engineering & Applied Science
Department of Electrical and Systems Engineering

Dissertation Examination Committee:
ShiNung Ching, Chair
Jr-Shin Li
Baranidharan Raman
Jason T. Ritt
Heinz Schättler

Extrinsic and Intrinsic Control of Integrative Processes in Neural Systems

by

Anirban Nandi

A dissertation presented to
The Graduate School
of Washington University in
partial fulfillment of the
requirements for the degree
of Doctor of Philosophy

December 2017
St. Louis, Missouri

Table of Contents

List of Figures

Acknowledgments

I have to start this section by offering my sincerest gratitude to my advisor, Dr. ShiNung Ching. I don't think I'd be here today without his patience, support and guidance along the way. I definitely had my share of lows during these five years, ranging from paper rejections to running circles around research problems, and he was always accessible in these times to address my concerns or point me in the right direction. As I reflect on my experience as a Ph.D. student, I realize that I could not have asked for a better advisor.

I would like to thank Dr. Heinz Schättler, who amid all his commitments found time to help me in my research. I was fortunate enough to attend all his graduate level courses at Washington University, which form a significant arc of the theoretical knowledge I acquired during my Ph.D. I would also like to acknowledge the rest of my committee members: Dr. Jr-Shin Li, Dr. Jason T. Ritt, and Dr. Baranidharan Raman, with whom I had the pleasure of collaborating with at some point or another during my Ph.D. Their insights, comments, and encouragement have undoubtedly made me a better researcher. I'd like to take this opportunity to thank Dr. Humberto Gonzalez, as well, for all his helpful inputs in my research.

I also had the good fortune to work and spend time with one of the smartest, most creative, group of researchers: my colleagues at the Brain Dynamics Lab. I treasure those long

conversations (sometimes hours long) in the lab which started as innocent questions and digressed into something completely unrelated. I also want to thank my friends both in St. Louis, USA, and in India, who were constant sources of support in my life over the past five years.

The final word goes to my family - my parents, R.K. and Nupur Nandi, and my sister Susmita, to whom I owe everything in life. I also thank my girlfriend Stephanie for being there for me every step of the way.

Anirban Nandi

Washington University in Saint Louis

December 2017

Dedicated to my parents R.K. Nandi & Nupur Nandi.

ABSTRACT OF THE DISSERTATION

Extrinsic and Intrinsic Control of Integrative Processes in Neural Systems

by

Anirban Nandi

Doctor of Philosophy in Electrical Engineering

Washington University in St. Louis, 2017

Professor ShiNung Ching, Chair

At the simplest dynamical level, neurons can be understood as integrators. That is, neurons accumulate excitation from afferent neurons until, eventually, a threshold is reached and they produce a spike. Here, we consider the control of integrative processes in neural circuits in two contexts. First, we consider the problem of extrinsic neurocontrol, or modulating the spiking activity of neural circuits using stimulation, as is desired in a wide range of neural engineering applications. From a control-theoretic standpoint, such a problem presents several interesting nuances, including discontinuity in the dynamics due to the spiking process, and the technological limitations associated with underactuation (i.e., many neurons controlled by the same stimulation input). We consider these factors in a canonical problem of selective spiking, wherein a particular integrative neuron is controlled to a spike, while other neurons remain below threshold. This problem is solved in an optimal control framework, wherein several new geometric phenomena associated with the aforementioned nuances are revealed. Further, in an effort to enable scaling to large populations, we develop relaxations and alternative approaches, including the use of statistical models within the control design framework. Following this treatment of extrinsic control, we turn attention to a scientifically-driven question pertaining to intrinsic control, i.e., how neurons in the brain may themselves be controlling higher-level perceptual processes. We specifically postulate that neural activity

is decoded, or "read-out" in terms of a drift-diffusion process, so that spiking activity drives a latent state towards a detection/perception threshold. Under this premise, we optimize the neural spiking trajectories according to several empirical cost functions and show that the optimal responses are physiologically plausible. In this vein, we also examine the nature of 'optimal evidence' for the general class of threshold-based integrative decision problems.

Chapter 1

Introduction

In the nervous system, a neuronal action potential, i.e., a 'spike', is generally thought to be the primary unit of information processing [1]. Neurons interact in highly nontrivial ways to produce patterns of spiking that, ultimately, culminate in a certain behavioral or functional outcome. In some cases, spiking may coalesce into rhythmic or oscillatory patterns [2, 3], while in others, spiking exhibits a more asynchronous character [4]. Over the past decades, the field of neuroscience (and, in particular, computational neuroscience) has made major strides in positing relationships between these neural activity patterns and the functions that they ostensibly enable (in neuroscience, referred to as neural coding, i.e., how neurons 'code' information or actions). However, the complexity of neuronal networks has meant that, despite these advances, many questions remain regarding the precise functional role of spikes, the mechanisms by which they realize complex patterns of neural activity and the extent to which this activity can be controlled exogenously. In other words, much remains unknown about the control properties of neurons and networks thereof. Understanding the control properties of brain networks at spatial scales commensurate with individual neurons has three related and important implications in neuroscience and neural engineering.

First, achieving spatially and temporally precise control in such networks would provide a substantial tool for probing different hypothesis pertaining to neural coding, such as the level of spike temporal precision that is consequential for information processing in the brain. Second, knowing the control properties of such networks may aid in understanding basic issues around how networks of neurons intrinsically self-coordinate their activity. Third, these insights may enable new strategies for devising extrinsic neural control systems as part of clinical brain stimulation technologies or emerging neural prostheses. The overall goal of this dissertation is to provide fundamental control-theoretic analysis, engineering design methodology and scientific insight towards these long-term objectives.

1.1 Neurocontrol

The manipulation of networks of neurons in the brain through the use of extrinsic controls – neurocontrol – is a key problem in experimental neuroscience [5]. Such capability has the potential to advance our understanding of how the firing activity of brain cells is related to the processing of sensory information [6]. Moreover, improving the use of neurostimulation may aid the refinement of how such technology is used in clinical settings [7, 8].

The use of stimulation in the study of neural coding is itself an established paradigm in neuroscience. The general idea is straightforward: by inducing neural activity and observing the consequent behavior of the organism, one can infer the functional role of the region in question. For example, cortical microstimulation of certain brain regions has been shown to induce behavioral changes in the context of perceptual tasks such as visual decision-making [9, 10]. Recently, several key advances in neurostimulation technology, such as the advent of optogenetics [11], have made neurocontrol possible at unprecedented spatial scales. Thus, experimentalists are able to assess the functional role not simply of different neural

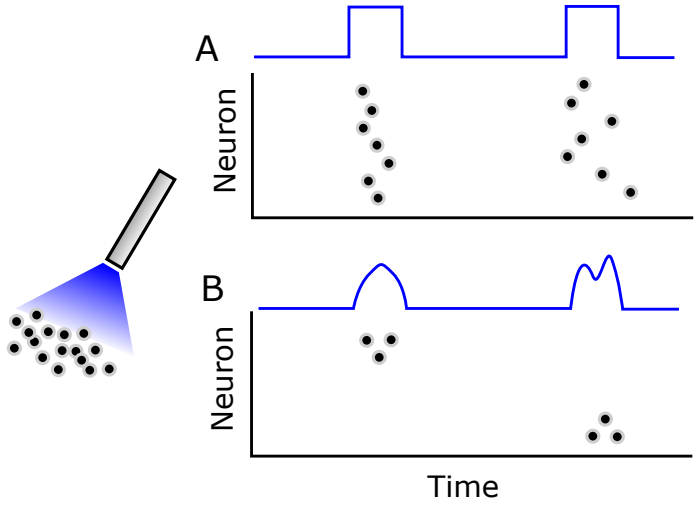

Figure 1.1: Underactuated neurocontrol schema. Most neurostimulation modalities are underactuated, wherein a single stimulation source impinges on orders-of-magnitude greater numbers of neurons. (A) The use of such stimulation has historically been limited to perturbative paradigms, wherein pulse-type inputs are used to create bulk population responses without fine temporal structure. (B) Increasingly, experimentalists seek to induce more precise spiking patterns in specific subsets of the population, which may necessitate the design of nuanced stimulation waveforms.

populations, but potentially of specific neurons and the timing of their spikes. That is, it may now be possible to test the long-standing neural coding hypothesis that spike timing is crucial to information processing [12].

Currently, however, these hardware instantiations are typically used in perturbative paradigms wherein 'pulses' of input are used to alter neural firing in a bulk manner (see Figure 1.1) that does not control the precise timing of individual neuronal spikes. Formal control analysis or design in this context, while desired, is not well-studied [13]. Thus, there is a need for formal mathematical analysis regarding the fundamental limits of such stimulation, particularly as it pertains to the feasibility of inducing precisely timed spiking activity in neural populations (Figure 1.1).

1.1.1 Underactuation in Neurocontrol

A key challenge associated with neurocontrol is *underactuation*, wherein a small number of inputs (in many current implementations, a single input), impinges on an orders-of-magnitude greater number of neurons [14], as schematized in Figure 1.1. In other words, individual neurons are not addressed via independent inputs, but rather a common one. This challenge is ubiquitous across stimulation modalities and is, perhaps, the major constraint that has restricted the use of neurostimulation to the aforementioned perturbative paradigms. In the context of the oscillatory objectives discussed above, some progress has been made on solving control problems such as entrainment and synchronization in the presence of underactuation [15–18]. However, this issue is unresolved in the case of asynchronous timed spike control objectives, such as those we consider herein. Current and foreseeable neurostimulation technologies are likely to face the challenge of underactuation, especially for *in vivo* instantiations.

1.1.2 Neurocontrol Analysis and Design Approaches

Dynamical Systems Framework

A direct approach to understanding the control properties of spiking neuronal networks (as distinct from macro-scale networks at the level of brain regions) involves the use of dynamical-systems models, such as the simple integrate-and-fire neuron [14], or biophysical models involving voltage-gated conductance equations [19]. While basic control characterizations have been obtained in single neurons [20], the nonlinearity, discontinuity, and noise associated with the neuronal dynamics in question lead to issues of scalability in both control analysis

and design. Nevertheless, such dynamical systems analysis is fundamental to revealing basic mathematical limitations and insights regarding the control of biophysical neurons.

Probabilistic Framework

An alternative to dynamical systems approaches is to treat neurons are probabilistic spike-generating units, e.g., as Poisson-like processes. Indeed, point processes provide a systematic way to handle nonlinearity and inherent stochasticity within the dynamics through a time-varying rate function. Such models include the popular class of Point-Process Generalized Linear Models (PPGLMs) [21, 22], which have been used to model event-based phenomena in ecology [23, 24], telecommunications [25], and, in the present context, the spiking activity in neuronal networks. Here, each spike is understood as a timed binary event. Since they are readily fit to spiking data, PPGLMs have emerged as a powerful tool in the analysis of neural recordings [26] and further, in the control design problem. Absent data, PPGLMs can also be formulated *de novo* as mathematical models of neural activity that can capture some aspects of the network structure and dynamics (e.g., delays, refractory).

Prior Work

The control of neural activity has received substantial attention in the context of oscillations and synchronization, spurred in large part by interest in clinical brain stimulation for motor disorders [27, 28]. The objective in this class of neurocontrol problem is generally the forced splaying of neural phases (i.e., desynchronization), wherein neurons are typically modeled using phase oscillator formalisms (e.g., [17, 19, 29–33]). Alternatively, others have approached the problem of desynchronization from the perspective of physiological and instrumentation constraints, favoring methods involving strictly pulsatile stimulation [34–37]. Control analysis results have also been obtained in the context of synchronization of neural ensembles [15,

38]. In contrast, we consider herein the mathematical problem of asynchronous neurocontrol (i.e., control neural spiking without overt rhythmicity). In other words, forcing a neuron to spike but not necessarily periodically. The other key distinction of our work is that we consider a neuronal-level objective (i.e., spiking and spike timing) versus a population-level objective (i.e., synchronization or desynchronization). [14] provides an early formulation of this problem, with related works include : optimal control of single neuron [20], or control design of populations using statistical framework [39] for integrate-and-fire models.

1.2 Intrinsic Control in Sensory Processes

One of the foundational, persistent questions in neuroscience is how sensory networks mediate robust, efficient processing of afferent inputs. Recent evidence suggests that the stimulus-evoked responses of early olfactory neurons dichotomize into phasic and tonic temporal motifs [40]. However, the precise mechanisms by which these motifs are converted into actionable information (i.e., decoded) and, in particular, the advantages of having these different sets of temporal dynamics is not well understood. Here, we leverage our theory on control of integrative processes to perform a computational study that sheds light on the meaning of these different sensory-evoked responses. We consider a particular class of decoding schemes, based on the influential drift-diffusion class of sensory decoding models (drift diffusion model, DDM) [41], which are based on a simple, intuitive premise that sensory processing is based on integrated neural activity crossing 'detection' thresholds. Such a model amounts to a higher-level abstraction of the basic spiking dynamics discussed earlier. Previous work has shown that drift-diffusion models are highly predictive of coarse behavioral features such as reaction time and accuracy in well-constrained cognitive paradigms such as the two-alternative, forced choice task (2A-FCT) [42]. However, the neural basis of this type of integrative decoding remains poorly understood. Moreover, it is not known whether this

type of decoding is specific to high-level cognitive tasks, or whether it is innate to sensory processing across modality and scale. As we will later show, it turns out that within this framework, a combination of phasic and tonic responses is provably optimal for particular drift landscapes and is highly consistent with experimental observations of neural activity in early sensory networks.

1.3 Contributions

In this dissertation, we develop extrinsic control strategies with an objective of emitting desired activity from neural ensembles under dynamical systems and probabilistic modeling frameworks. It turns out that solving this problem enables an interesting investigation of not just extrinsic neurocontrol, but the aforementioned notion of intrinsic control of sensory processes. Thus, we also perform a theoretical study of intrinsic neural responses and, specifically, investigate the hypothesis that neurons may be producing near-optimal activity motifs towards enabling fast, efficient sensory detection. In turn, this theoretical study reveals several interesting control-theoretic nuances that arise for general threshold-hitting problems. Thus, this dissertation spans basic control theory, neural engineering and mathematical and computational neuroscience as depicted in Figure 1.2. Specifically, we provide:

1. The formal synthesis of time-optimal selective spiking solutions in pairs of Leaky Integrate-and-Fire (LIF) neurons in an underactuated setting. The synthesis involves application of the Pontryagin maximum principle, but with several non-trivial caveats due to the selectivity specification, which leads to state constraints. We prove that the optimal solution in this case involves use of the so-called boundary control, associated with the state constraints. We also highlight the the role of system parameters in determining overall controllability of the network [43, 44].

2. The development of design methods for timed patterns of spikes. We derive greedy and regularization based approaches that can provide near-perfect construction of patterns under specified conditions for pairs and eventually populations of neurons. We also evaluate the performance of our control design when the system is subjected to noise and disturbances [44, 45].

3. A control analysis for PPGLMs that approximates, in essence, the reachable set of binary patterns for a given model. A relativistic notion of control viability that allows comparison between PPGLMs and validation of the proposed framework, showing its ability to reveal salient control properties of spiking networks [46].

4. The instantiation of the developed theory for the purposes of designing external neurostimulation on fitted PPGLMs and for underlying dynamical models of neuron [46, 47].

5. Characterization of experimental neural response for sensory detection tasks in early olfactory systems. Analysis of the 'optimal' response with respect to robust time-efficient detection objectives under DDM variants as detector models. Configuration of a competitive network architecture capable of producing these response motifs.

6. A theoretical study to investigate the makeup of the optimal evidence for decision problems in threshold-based models. Discussion of the non-intuitive features in the optimal solution or the lack thereof.

The remainder of the dissertation is organized as follows. In Chapter 2, we present solutions for the asynchronous neurocontrol problem for a dynamical systems-based model (LIF) for pairs and populations of neurons. Next, in Chapter 3, we approach similar problems within a statistical framework, namely PPGLM, to first introduce a controllability-like notion for systems traversing in binary space, and second, to create a design strategy for inducing

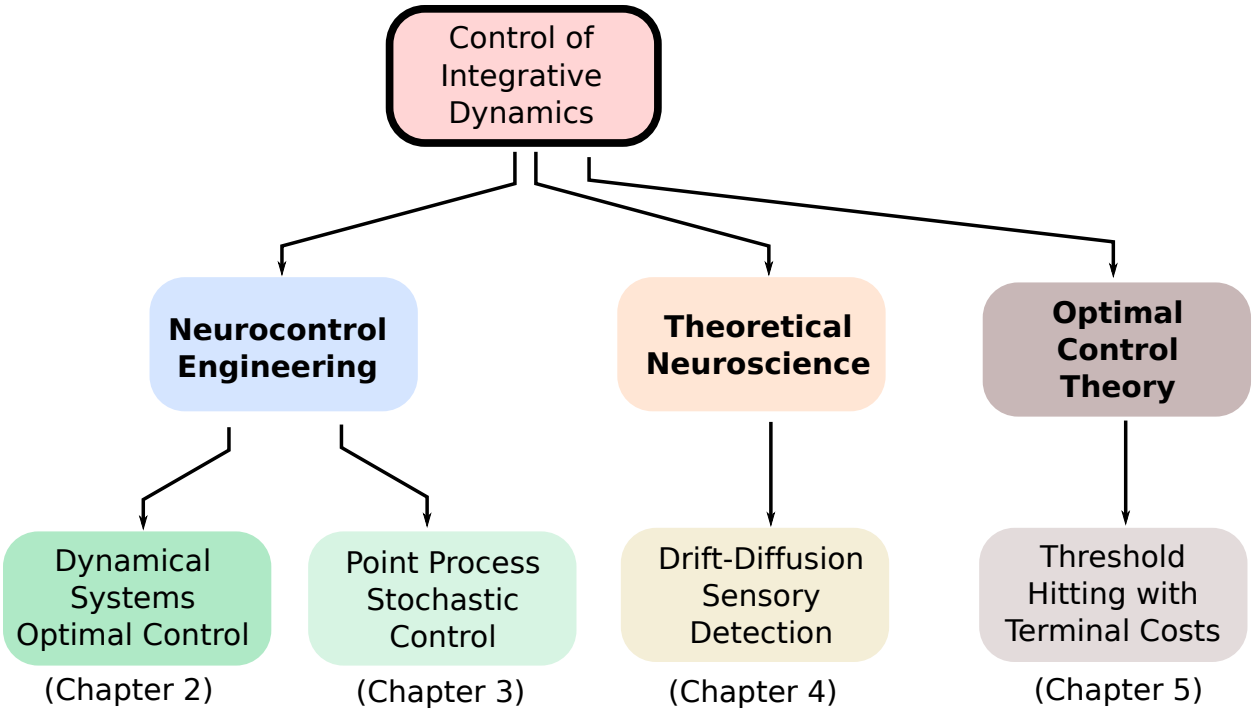

Figure 1.2: Overview of the dissertation

desired activity patterns in the underlying neural ensemble modeled by the PPGLM. Chapter 4 analyzes experimental data from locust olfactory neurons to understand how neurons intrinsically control themselves for sensory detection tasks. In Chapter 5, we formulate the optimal decision problem for a compromised objective between time and accuracy and discuss the peculiarities in the ensuing solution - the 'optimal evidence'. Finally, in Chapter 6 we highlight the key conclusions derived from our results and discuss their significance.

Chapter 2

Neurocontrol I: Dynamical Systems Framework

In this chapter we address the problem of time-optimal control of spiking in Leaky Integrate-and-Fire (LIF) neurons [48], where the desired spiking is selective, that is, certain neurons spike while others remain silent. Our presentation and discussion on fundamental optimal control analysis and design work toward the overall goal of understanding the limits of neurocontrol.

2.1 Background & Methods

2.1.1 Definitions: Spike Sequence and Pattern Control

We begin by formally defining the notions of spike sequences and patterns, which will facilitate our approach to spike timing control:

Definition 1 (Spike Sequence)**.** *In a population of C neurons, an K-spike sequence is a vector*

$$\Sigma_S = [\sigma_1, \sigma_2, ..., \sigma_K], \tag{2.1}$$

where $\sigma_k \in \{1, 2, ..., C\}$ indicates the neuron which produces the k^{th} spike in the sequence.

Definition 2 (Spike Pattern)**.** *In a population of C neurons, an K-spike pattern is a sequence with timing, i.e.,*

$$\Sigma_P = [(\sigma_1, t_1), (\sigma_2, t_2), ..., (\sigma_K, t_K)], \tag{2.2}$$

where $\sigma_k \in \{1, 2, ..., C\}$ indicates the neuron which produces the k^{th} spike at time $t_k > 0$, where $t_1 < t_2 < ... < t_K$.

2.1.2 Model Formulation

We proceed with the model formulation, starting with the base LIF model and then adding synaptic coupling between neurons.

Base Model

The leaky leaky integrate-and-fire neuron is a well-established model in computational neuroscience [1, 49]. The circuit of this model is shown in Figure 2.1 where a capacitor $\mathcal{C}$ and resistance R (modeling the capacitive and resistive properties of the cell membrane) are in parallel, with $u(t)$ being the external stimulus. Denoting the membrane potential as $v(t)$, the charge deposited on the capacitor is $q = \mathcal{C}v$ and therefore the current is given by $I_{\mathcal{C}} = \mathcal{C}\frac{dv}{dt}$, leading to the linear dynamics

$$\mathcal{C}\frac{dv(t)}{dt} = \frac{V_{rest} - v(t)}{R} + \beta u(t) + I_{syn}, \tag{2.3}$$

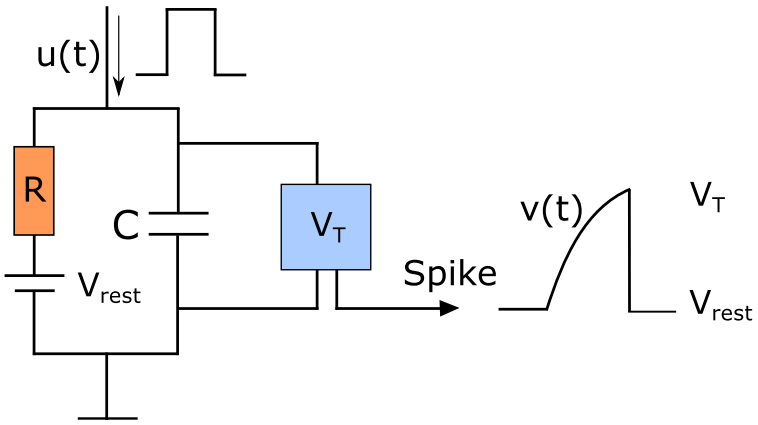

Figure 2.1: The LIF circuit. The membrane potential rises under the stimulus $u(t)$ until it hits the threshold V_T, at this point $v(t)$ is artificially reset to V_{rest} and a spike is said to be generated. We also show a cartoon of the possible voltage trace of the neuron under a rectangular pulse input.

where V_{rest} is the resting potential and $\kappa = R\mathcal{C}$ is the membrane time constant. Here, I_{syn} denotes synaptic input entering from other neurons. We also introduce a parameter β that encapsulates the effectiveness of the external input $u(t)$ for each neuron.

Spike generation: In this model, a spike is said to be generated at time t_s if the membrane potential reaches a predetermined threshold voltage V_T. Upon emitting a spike, the membrane potential is reset to V_{rest}. Thus, spike generation is governed by a discontinuous resetting rule:

$$v(t_s^-) = V_T \rightarrow v(t_s^+) = V_{rest} \tag{2.4}$$

Model normalization: In what follows, we will assume $V_{rest} = 0$. This normalizing assumption is not restrictive, since it can be readily achieved by a simple translation in the coordinate system, i.e., $v \leftarrow (v - V_{rest})$, $V_T \leftarrow (V_T - V_{rest})$.

Synaptic Coupling

We build an approximate model of synaptic coupling based on the standard formulations in [49]. Key to this formulation is the notion of impulsive coupling, wherein the major effect of I_{syn} occurs during a brief time window following an afferent spike (i.e., a spike from another neuron). Following a reduction of continuous synaptic models (see Appendix A.1), we formulate I_{syn} as

$$I_{syn}(t) = \rho_{syn}(t) \sum_{t_s \in \mathcal{T}} \delta(t - t_s), \tag{2.5}$$

where $\mathcal{T}$ denotes the set of all afferent spike times and $\rho_{syn}(t)$ is a synaptic constant that depends on the specific parameters of the neuron. If all neurons remain below the threshold, then $I_{syn} \equiv 0$.

Thus, the effect of a synaptic event on the postsynaptic neuron can be understood as an instantaneous rise in voltage that occurs only when a neighboring, connected neuron fires a spike. Knowing this rise can allow us to insulate neurons from each other in the spike control problem, formulated in the next section.

2.1.3 Problem Formulation: Minimum Time Selective Spiking

In this section, we start with three baseline problems pertaining to the design of $u(t)$ to create structured spiking patterns in populations of two LIF neurons of the form (2.3), and further study their extensions for neural populations. We first consider the problem of time-optimal sequence control, i.e., inducing target sequences with minimal temporal spacing between the beginning and end of the sequence. It turns out that this problem amounts to an analysis of *selective spiking*. We formulate a canonical version of this problem in two dimensions.

Problem 1. ***(P1: Pairwise time-optimal selective spiking with synaptic guard)*** *Consider two coupled LIF neurons of the form* (2.3)*:*

$$\begin{bmatrix} \dot{v}_1 \\ \dot{v}_2 \end{bmatrix} = \begin{bmatrix} -a_1 & 0 \\ 0 & -a_2 \end{bmatrix} \begin{bmatrix} v_1 \\ v_2 \end{bmatrix} + \begin{bmatrix} b_1 \\ b_2 \end{bmatrix} u + \begin{bmatrix} I_{syn_1} \\ I_{syn_2} \end{bmatrix} \tag{2.6}$$
$$\equiv f(\mathbf{v}, u, \mathbf{I}_{syn}) = \mathbf{A}\mathbf{v} + \mathbf{b}u + \mathbf{I}_{syn}$$

where $\mathbf{v} = [v_1\ v_2]^T$*,* $a_i = \frac{1}{R_i C_i}$*,* $b_i = \frac{\beta_i}{C_i}$*,* $a_i, b_i > 0$ *and* I_{syn_i} *are impulsive synaptic inputs of the form* (2.5) *for* $i = 1, 2$*. Find the control input* $u(t)$ *so that*

$$v_1(\tau) = V_T,\ v_2(t) \leq V_G < V_T, \forall t \in [0, \tau] \tag{2.7}$$

with arbitrary initial condition $\mathbf{v}(0) \in \mathcal{G}$ *where*

$$\mathcal{G} = \{(v_1, v_2) : 0 \leq v_1 \leq V_T, 0 \leq v_2 \leq V_G\}. \tag{2.8}$$

and $u(t)$ *solves the time-optimization*

$$\textit{minimize} \quad \mathbb{J}(u) = \int_0^\tau \mathrm{d}t \tag{2.9}$$

over all measurable functions u *that take values in the control set, where* $\mathcal{U}$ *is this set of admissible inputs.*

Taken together, (2.7)-(2.9) imply that Neuron 1 produces a spike before Neuron 2 and that under (2.7), the spike occurs in minimum time.

Functional decoupling of the network via guard V_G*:* The parameter V_G in (2.7), referred to as a synaptic guard, is key to selectivity. It ensures that Neuron 2 remains below threshold and,

further, is insulated from the synaptic effect due to the induced spike in Neuron 1, i.e.,

$$V_G < V_T - \bar{\rho}_{syn};\ \bar{\rho}_{syn} = \sup_t\ \rho_{syn}(t), \tag{2.10}$$

where $\rho_{syn}(t)$ is the synaptic contribution to the post-synaptic neuron (here, Neuron 2) and is derived in Appendix A.1. The guard, in essence, keeps the non-selected neuron sufficiently away from its own threshold so as not to produce an undesired, collateral spike. It is important to note that in solving (*P1*), it is sufficient to consider the dynamics in (2.6) as

$$\dot{\mathbf{v}} = f(\mathbf{v}, u, 0) \equiv f(\mathbf{v}, u) = \mathbf{A}\mathbf{v} + \mathbf{b}u, \tag{2.11}$$

since both neurons are below threshold for the duration of the synthesis. Despite this simplification in the dynamics, the selectivity/guard criterion (2.7) poses a key challenge. That is, it is not sufficient to simply fire Neuron 1 in minimum time, since doing so may in general cause Neuron 2 to fire an undesired spike. Mathematically, (2.7) functions as a state constraint that, as we will see, leads to several complications in the optimal synthesis.

If the problem has a solution for either choice of neuron labeling, then the population is said to be *pairwise feasible*. That is, either neuron can be made to spike selectively.

Problem 2. ***(P2: Pairwise time-optimal selective sequencing)*** *For the two neuron network in* (2.11)*, find the control input that achieves any K-spike target spike sequence Σ_S time optimally, i.e.,*

$$\underset{u\in\mathcal{U}}{\textit{minimize}}\quad \mathbb{J}(u) = \int_0^{\tau_1} \mathrm{d}t + \ldots + \int_{\tau_{K-1}}^{\tau_K} \mathrm{d}t \tag{2.12}$$

such that

$$\begin{aligned} &v_{\sigma_k}(\tau_k) = V_T,\ v_{\hat{\sigma}_k}(t) \leq V_G,\ \forall\, t \in [\tau_{k-1}, \tau_k], \\ &\mathbf{v}(0) \in \mathcal{G},\ \hat{\sigma}_k = \Omega \backslash \sigma_k \ \ \textit{where}\ \Omega = \{1, 2\}, \\ &k = 1, \ldots, K, \textit{and}\ \tau_0 = 0. \end{aligned} \tag{2.13}$$

The key complication here is the non-differentiability of the value function within the dynamic programming, as well as the spike discontinuity (2.4).

Problem 3. ***(P3: Pairwise time-optimal selective patterning)*** *Considering the same model in* (2.11)*, find the control which induces the spiking in the two neurons according to the times specified in the target pattern Σ_P, constrained by the underlying sequence. Mathematically,*

$$\underset{u \in \mathcal{U}}{\textit{minimize}} \quad \mathbb{J}(u) = \sum_{k=1}^{K} \left((t_k - t_{k-1}) - \int_{\tau_{k-1}}^{\tau_k} \mathrm{d}t \right)^2 \tag{2.14}$$

with the same constraints as described in (2.13) *and $t_0 = \tau_0 = 0$. Note that t_k are the desired spike times, and τ_k are the actual spike times.*

Next, we study three more problems pertaining to the design of $u(t)$ to create precise spiking in populations of LIF neurons. For a population of C neurons with $\mathbf{I}_{syn} = \mathbf{0}$ (2.6) can be rewritten as,

$$\begin{bmatrix} \dot{v}_1 \\ \vdots \\ \dot{v}_C \end{bmatrix} = \begin{bmatrix} -a_1 & \ldots & 0 \\ & \ddots & \\ 0 & \ldots & -a_C \end{bmatrix} \begin{bmatrix} v_1 \\ \vdots \\ v_C \end{bmatrix} + \begin{bmatrix} b_1 \\ \vdots \\ b_C \end{bmatrix} u = f(\mathbf{v}, u) = \mathbf{A}\mathbf{v} + \mathbf{b}u \tag{2.15}$$

Problem 4. ***(P4: Regularized Time-optimal selective spiking in Populations)*** *The selective spiking problem P1 becomes intractable for higher dimensions and we formulate a regularized version of the problem, adding a terminal cost which is a function of the voltages of the neurons except the target neuron. Without loss of generality for a target spike in Neuron*

1 in a population of C neurons, we can set up the following regularized time optimal problem:

$$\begin{aligned} \underset{u\in\mathcal{U}}{\textit{minimize}} \quad & \mathbb{J}(u) = \int_0^\tau \mathrm{d}t + \frac{1}{2}\gamma\,(\boldsymbol{\omega}\mathbf{v}(\tau))^T\boldsymbol{\omega}\,\mathbf{v}(\tau) \\ \textit{s.t.} \quad & v_1(\tau) = V_T \end{aligned} \tag{2.16}$$

where $\boldsymbol{\omega} = [0\ \omega_2 \dots\ \omega_C]$, $\omega_c \geq 0$, $\forall\, c = 2 \dots C$, the admissible set $\mathcal{U} = [\mathrm{U}_1, \mathrm{U}_2]$ and γ is the regularization constant.

In higher dimensions, the number of possible candidates for the control increases with the dimension of the system, making the problem challenging to solve analytically. We have provided a numerical approach to obtain the solution for $C > 2$.

Problem 5. ***(P5: Regularized Minimum Time-Energy selective spiking in Populations)*** *Along with the selectivity, if we want to minimize the energy of the control $u(t)$, we can add one more term in the integral of the objective. Without loss of generality for a target spike in Neuron 1 in a population of C neurons, we formulate the following regularized minimum time- energy optimal control problem:*

$$\begin{aligned} \underset{u\in\mathcal{U}}{\textit{minimize}} \quad & \mathbb{J}(u) = \int_0^\tau (1 + \frac{1}{2}\varrho u^2)\mathrm{d}t + \frac{1}{2}\gamma\,(\boldsymbol{\omega}\mathbf{v}(\tau))^T\boldsymbol{\omega}\mathbf{v}(\tau) \\ \textit{s.t.} \quad & v_1(\tau) = V_T \end{aligned} \tag{2.17}$$

where ϱ is the second regularization constant for the trade-off between the time and energy in the objective and the admissible set $\mathcal{U} = \mathbb{R}$. We follow the same numerical approach to solve this problem as P4.

Problem 6. ***(P6: Regularized Minimum Energy Timed selective spiking in Populations)*** *For a timed spiking problem, we can modify P5 to minimize the difference between achieved and target time τ_d for a desired spike along with the energy of the control $u(t)$. So without loss of generality for a target spike in Neuron 1 at $t = \tau_d$ in a population of C*

neurons, we formulate the following problem with the regularization on the terminal states of the unintended neurons:

$$\begin{aligned} \underset{u\in\mathbb{R}}{\textit{minimize}} \quad & \mathbb{J}(u) = \frac{1}{2}\int_0^\tau \varrho u^2 \mathrm{d}t + \frac{1}{2}\Big(\gamma\left(\boldsymbol{\omega}\mathbf{v}(\tau)\right)^T \boldsymbol{\omega}\mathbf{v}(\tau) + (\tau_d - \tau)^2\Big) \\ \textit{s.t.} \quad & v_1(\tau) = V_T. \end{aligned} \tag{2.18}$$

Ultimately, we will use the solution of *P6* to construct a one step greedy control for multi-spike timed spike sequences or patterns.

2.2 Minimum Time Selective Spiking

We consider the minimum-time selective spiking problem *P1*. We assume, without loss of generality, that the neurons are labeled so that the objective is to fire Neuron 1. It turns out that the solution to this problem depends on the ratio (see Appendix A.1.1)

$$\vartheta_1 = \frac{b_1 a_2}{b_2 a_1}, \tag{2.19}$$

which we treat in two separate cases corresponding to $\vartheta_1 \lessgtr \frac{V_T}{V_G}$.

As we will show in the following sections, for $\vartheta_1 > \frac{V_T}{V_G}$, i.e., Case 1, selective spiking can always be accomplished. However, if $\vartheta_1 \leq \frac{V_T}{V_G}$, i.e., Case 2, a solution may not exist and pairwise feasibility is not guaranteed.

2.2.1 Selective Spiking, Case 1: $\vartheta_1 > \frac{V_T}{V_G}$

Proposition 1. *Consider the two neuron network* (2.11)*, where*

$$\vartheta_1 > \frac{V_T}{V_G}. \tag{2.20}$$

Assume that the set of admissible controls $\mathcal{U}$ *forms a box constraint of the form* $\mathcal{U} = [0, \mathrm{U}]$*, and we take as given the initial conditions* $v_i(0) < V_G$*,* $i = 1, 2$*. The time optimal feedback control* $u^* \in \mathcal{U}$ *for the selective spiking problem P1 for Neuron 1 is given by*

$$u^* = \begin{cases} \mathrm{U} & \text{for } v_2 < V_G, \\ u_{arc} & \text{for } v_2 = V_G, \end{cases} \tag{2.21}$$

where $u_{arc} = \frac{a_2}{b_2} V_G$ *is the unique control that keeps* $v_2(t) = V_G$ *invariant. Moreover, such a control always exists. Thus, optimal controls are either given by a constant control at maximum value,* $u^*(t) \equiv \mathrm{U}$*, if the state space constraint does not become active or, if the corresponding trajectory meets the state space constraint, optimal controls are a concatenation of a segment for the maximum control until the state constraint is reached followed by a constant boundary control* $u^*(t) = u_{arc}$ *until the terminal value* $v_1 = V_T$ *is reached.*

Proof*:* Necessary conditions for optimality for problem *P1* are given by the Pontryagin maximum principle. In the presence of state space constraints, these take a rather complicated form (the multipliers associated with the state space constraint are measures). The problem considered here, however, is simpler, and instead of analyzing those conditions, we shall define a synthesis of extremal controlled trajectories through a direct construction, and then verify the optimality of the synthesis. In particular, there is no need to consider possible degeneracies

that in principle are allowed by necessary conditions for optimality (e.g., abnormal extremals, etc.).

Synthesis Construction: We want to solve the optimal control problem *P1* on the set $\mathcal{G}$ in (2.8). We first treat the problem in the absence of the state constraint and define the Hamiltonian function as

$$\mathcal{H}(\boldsymbol{\lambda}, \mathbf{v}, u) = 1 + \boldsymbol{\lambda}\, f(\mathbf{v}, u) = 1 + \boldsymbol{\lambda}(\mathbf{A}\mathbf{v} + \mathbf{b}u). \tag{2.22}$$

According to the maximum principle, as long as no state space constraints are active, the multiplier $\boldsymbol{\lambda}$ is a solution to the adjoint equation

$$\dot{\boldsymbol{\lambda}}(t) = -\boldsymbol{\lambda}(t)\mathbf{A} \tag{2.23}$$

and the optimal control minimizes the Hamiltonian over the control set $[0, \mathrm{U}]$. The solutions of (2.23) are of the form

$$\lambda_1(t) = d_1 \mathrm{e}^{a_1 t}, \quad \lambda_2(t) = d_2 \mathrm{e}^{a_2 t} \tag{2.24}$$

for some constants d_1 and d_2, and thus we have

$$u^*_{NoGuard}(t) = \begin{cases} \mathrm{U} & \text{if } \Phi(t) < 0 \\ \\ 0 & \text{if } \Phi(t) > 0 \end{cases} \tag{2.25}$$

with

$$\Phi(t) = b_1\lambda_1(t) + b_2\lambda_2(t) \tag{2.26}$$

as the switching function. The terminal constraint is defined by

$$\psi(\tau, \mathbf{v}) = v_1(\tau) - V_T, \tag{2.27}$$

and the transversality condition [50, Section 2.2] of the maximum principle implies that $\boldsymbol{\lambda}(\tau) = [\nu \quad 0]$ where ν is some multiplier. This gives us $d_2 = 0$, and thus the switching function has a constant sign in the absence of the guard constraint. Hence the optimal control is simply a BANG, i.e., the maximal input.

With the state constraint (the guard), there can be switching in the optimal control, and we need to consider two subcases: trajectories that do or do not hit the boundary $v_2 = V_G$. For $\mathbf{A}$ with real eigenvalues, the optimal controls of linear single input control systems are BANG-BANG with at most $C - 1$ switchings (where C is the dimension of the system, here $C = 2$) [50], and we must have $u > 0$ at the spike time (otherwise $\mathbf{v}$ would be decaying). We thus consider controls only of the form

$$u = \begin{cases} 0 & \text{for } t \leq \hat{t} \text{ where } v_1(\hat{t}) < V_T, \\ \mathrm{U} & \text{for } \hat{t} < t \leq \tau. \end{cases} \tag{2.28}$$

These define a smooth flow of extremal controlled trajectories as long as the state space constraint is not violated. If the extremals hit the state constraint boundary, the control must switch to the boundary control, u_{arc}, that keeps the system from exceeding the constraint:

$$u_{arc} = \frac{a_2 V_G}{b_2}. \tag{2.29}$$

However, we need to verify whether this boundary control u_{arc} will eventually bring Neuron 1 to threshold. For $v_1 = V_T$ and $u = u_{arc}$ we have

$$\dot{v}_1 = -a_1 V_T + b_1 \frac{a_2 V_G}{b_2} > 0 \tag{2.30}$$

where the inequality holds by our assumption on ϑ_1. Now if (2.30) holds, then in fact $\dot{v}_1 > 0$ $\forall\, v_1 \in [0, V_T]$ under the boundary control, and v_1 will eventually reach threshold.

Thus for appropriate initial conditions, applying the maximal input $u(t) = \mathrm{U}$ produces a spike in Neuron 1 without hitting the Neuron 2 guard. For the remaining initial conditions, we construct a control that applies maximal input until the guard is reached, and then drops to u_{arc} until v_1 hits threshold. Note that we do not need to employ the zero control in (2.28), so we may take $\hat{t} = 0$ (the possibility of additional switching will arise in the next section under the alternative case for ϑ_1). Thus the control (2.21) will produce a spike in Neuron 1 without inducing a spike in Neuron 2, across all initial conditions. This concludes the synthesis construction.

***Proof of Optimality**:* The optimality of this control follows from regular synthesis-type sufficient conditions for optimality, and we briefly outline the reasoning. The value or cost-to-go function of this synthesis is continuous, but not differentiable on the curve that separates initial states for which the trajectory includes a boundary segment from those that do not. The curve Γ that separates these two regions is defined by the set of initial conditions that hit the final condition $\mathbf{v}(\tau) = [V_T\ V_G]^T$ under the BANG control $u(t) = \mathrm{U}$. To find this curve, we first explicitly compute the time for v_1 to hit threshold,

$$\tau = \frac{1}{a_1} \log \left(\frac{{}^{b_1}\!/_{a_1}\mathrm{U} - v_1(0)}{{}^{b_1}\!/_{a_1}\mathrm{U} - V_T} \right) \equiv \frac{1}{a_1} \log \left(E(v_1(0))^{-1} \right) \tag{2.31}$$

where for convenience we define

$$E(v) = \frac{{}^{b_1}\!/_{a_1}\mathrm{U} - V_T}{{}^{b_1}\!/_{a_1}\mathrm{U} - v}. \tag{2.32}$$

We then eliminate τ by solving explicitly for $v_2(t)$ with the final condition $v_2(\tau) = V_G$

$$V_G = E(v_1(0))^{\frac{a_2}{a_1}} v_2(0) + \frac{b_2}{a_2}\mathrm{U}\left(1 - E(v_1(0))^{\frac{a_2}{a_1}}\right), \tag{2.33}$$

to find the separatrix as

$$\Gamma = \left\{\mathbf{v} \in \mathcal{G} : E(v_1)^{\frac{a_2}{a_1}} v_2 + \frac{b_2}{a_2}\mathrm{U}\left(1 - E(v_1)^{\frac{a_2}{a_1}}\right) - V_G = 0\right\}. \tag{2.34}$$

We define the region Γ_- as bounded between Γ and $v_1 = V_T$ inclusive, and the region $\Gamma_+ = \mathcal{G} \setminus \Gamma_-$. Thus, Γ_+ includes all initial conditions whose trajectories include a boundary arc, while initial conditions in Γ_- can be driven to threshold directly at maximum input.

The value function corresponding to this synthesis is

$$\mathcal{V} = \begin{cases} \mathcal{V}_-(\mathbf{v}) & \text{for } \mathbf{v} \in \Gamma_-, \\ \mathcal{V}_+(\mathbf{v}) & \text{for } \mathbf{v} \in \Gamma_+. \end{cases} \tag{2.35}$$

For trajectories without a boundary arc, the value is just the spike time under maximal input, calculated as in (2.31),

$$\mathcal{V}_-(\mathbf{v}) = \frac{1}{a_1}\log(E(v_1)^{-1}). \tag{2.36}$$

The calculation of the value $\mathcal{V}_+(\mathbf{v})$ involves two steps: the time t_g for Neuron 2 to reach the guard voltage, plus the time t_{th} for Neuron 1 to attain the threshold V_T under the boundary arc control. By direct calculation,

$$\mathcal{V}_+(\mathbf{v}) = t_g + t_{th} = \frac{1}{a_2}\log\left(\frac{{}^{b_2}\!/_{a_2}\mathrm{U} - v_2}{{}^{b_2}\!/_{a_2}\mathrm{U} - V_G}\right) + \frac{1}{a_1}\log\left(\frac{{}^{b_1}\!/_{a_1}u_{arc} - v_1(t_g)}{{}^{b_1}\!/_{a_1}u_{arc} - V_T}\right) \tag{2.37}$$

where

$$v_1(t_g) = \left(\frac{{}^{b_2}\!/_{a_2}\mathrm{U} - V_G}{{}^{b_2}\!/_{a_2}\mathrm{U} - v_2}\right)^{\frac{a_1}{a_2}} v_1 + \frac{b_1}{a_1}\mathrm{U}\left(1 - \left(\frac{{}^{b_2}\!/_{a_2}\mathrm{U} - V_G}{{}^{b_2}\!/_{a_2}\mathrm{U} - v_2}\right)^{\frac{a_1}{a_2}}\right) \tag{2.38}$$

is the Neuron 1 voltage at the time t_g, that is, when the trajectory hits the Neuron 2 guard.

It is clear from the construction that $\mathcal{V}$ is continuously differentiable in the interior of $\mathcal{G}$ away from the curve Γ. We now show that on Γ, $\mathcal{V}$ remains continuous, but is no longer differentiable. Substituting v_2 from (2.34) into (2.38) yields

$$v_1(t_g) = \frac{V_T - {}^{b_1}\!/_{a_1}\mathrm{U}}{v_1 - {}^{b_1}\!/_{a_1}\mathrm{U}} v_1 + \frac{b_1}{a_1}\mathrm{U}\left(1 - \frac{V_T - {}^{b_1}\!/_{a_1}\mathrm{U}}{v_1 - {}^{b_1}\!/_{a_1}\mathrm{U}}\right) = V_T. \tag{2.39}$$

Hence (2.37) reduces to

$$\mathcal{V}_+(\mathbf{v}) = t_g = \frac{1}{a_2}\log\left(\frac{v_2 - {}^{b_2}\!/_{a_2}\mathrm{U}}{V_G - {}^{b_2}\!/_{a_2}\mathrm{U}}\right). \tag{2.40}$$

Substituting v_2 once again in (2.40), it follows that

$$\mathcal{V}_+(\mathbf{v}) = \frac{1}{a_1}\log(E(v_1)) = \mathcal{V}_-(\mathbf{v}). \tag{2.41}$$

However,

$$\frac{\partial \mathcal{V}_+}{\partial v_2}_{\restriction\Gamma} \neq \frac{\partial \mathcal{V}_-}{\partial v_2}_{\restriction\Gamma} = 0, \tag{2.42}$$

so that $\mathcal{V}$ is not continuously differentiable.

All controlled trajectories in the synthesis are extremals, and away from Γ the value function $\mathcal{V}$ satisfies the Hamilton-Jacobi-Bellman equation for the unconstrained optimal control problem,

$$\frac{\partial \mathcal{V}(t,\mathbf{v})}{\partial t} + \frac{\partial \mathcal{V}(t,\mathbf{v})}{\partial \mathbf{v}} f(t,\mathbf{v},u^*) + L(t,\mathbf{v},u^*) = 0 \tag{2.43}$$

where L is the Lagrangian of the problem (for time optimal control problems, as in our case, $L = 1$).

This conclusion follows from the method of characteristics (e.g., see [50]), but can also directly be verified using the explicit formulas derived above. That $\mathcal{V}$ is not differentiable on Γ does not invalidate the proof of optimality, although the standard optimality argument based on dynamic programming (e.g., [50] Theorem 5.2.1) does not apply. Here, we need to invoke regular synthesis constructions as they are described in [50, Section 6.3]. Since trajectories do not return from the state space constraint into the interior of the state space, these arguments could, for example, be undertaken by redefining the state space constraint as a second terminal manifold, along with a penalty term that gives the time along the boundary control until $v_1 = V_T$. Alternatively, the constructions in [51], where a regular synthesis argument has been generalized to problems with order 1 state space constraints, could be modified to apply to cases when the state space constraint is active at the terminal time. Either way, straightforward modifications of regular synthesis type arguments give the optimality of the above field of extremals. □

Example 1. *We demonstrate minimum spike time control in an example of* (2.11) *with the following parameters:*

$$\begin{aligned} &R_1 = 0.5\ G\Omega,\ R_2 = 0.33\ G\Omega \\ &\mathcal{C}_1 = 300\ pF,\ \mathcal{C}_2 = 300\ pF \\ &V_T = 30\ mV,\ V_G = 27\ mV \\ &\mathrm{U} = 2.5\ nA,\ \beta_1 = 1,\ \beta_2 = 1.2. \end{aligned} \tag{2.44}$$

Note that these are idealized parameters used for illustrative purposes only, although with biologically plausible units. Here, the condition $\vartheta_1 > \frac{V_T}{V_G}$ is satisfied, and we can apply the above proposition to induce a spike in Neuron 1 in minimal time. Figure 3(a) shows the state space under this construction.

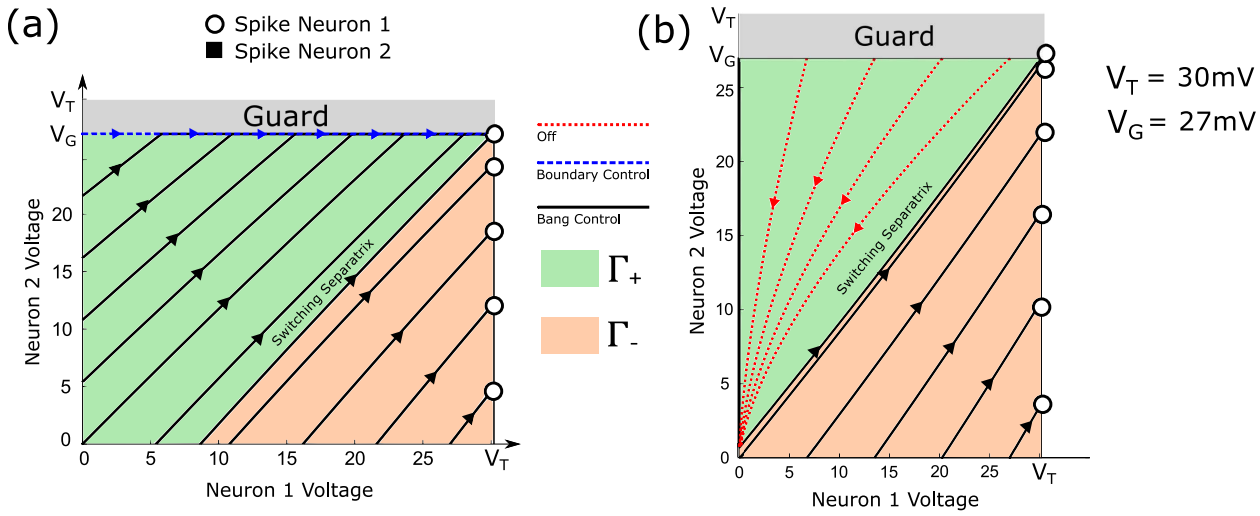

Figure 2.2: (a) State trajectories for selective spiking of Neuron 1 under Case 1 for several initial conditions. Trajectories either reach threshold under maximal input, or reach the guard under maximal input and then follow the boundary under a lower constant input until Neuron 1 reaches threshold. (b) State trajectories for selective spiking under Case 2 for several initial conditions. For those trajectories that do not reach Neuron 1 threshold (before hitting the guard) under maximal input, the input is zero until the trajectory decays to the switching separatrix, and then bangs high until Neuron 1 spikes.

2.2.2 Selective Spiking, Case 2: $\vartheta_1 \leq \frac{V_T}{V_G}$

We now consider the case of eliciting a spike in Neuron 1 when $\vartheta_1 \leq \frac{V_T}{V_G}$. We have shown in the previous section that for Case 1, a control solution always exists. It will turn out that not all parameters allow a solution in Case 2, so this case reveals the conditions for pairwise feasibility of sequences while providing the minimum time spiking solution when it exists.

One might expect the solution in Case 2 to be qualitatively similar to Case 1, but in fact there are no longer increasing trajectories that ride along the guard boundary: under the boundary control ($u_{arc} = \frac{a_2 V_G}{b_2}$), we find $\dot{v}_1 < 0$ at $v_1 = V_T$. That is, along the guard, $v_1(t)$ does not rise beyond a certain limit and fails to reach the threshold V_T. Instead, we have,

Proposition 2. *Consider the two neuron network* (2.11)*, where* $\vartheta_1 \leq \frac{V_T}{V_G}$*. Assume that the set of admissible controls is a box constraint* $\mathcal{U} = [0, \mathrm{U}]$*. The time optimal control* $u^* \in \mathcal{U}$ *for*

the selective spiking problem P1 for Neuron 1, if such a solution exists, is

$$u^* = \begin{cases} 0 & \textit{for } \mathbf{v} \in \Gamma_+, \\ \mathrm{U} & \textit{for } \mathbf{v} \in \Gamma_-. \end{cases} \tag{2.45}$$

with $\Gamma_\pm$ defined as above.

***Proof**:* We follow a similar analysis to the previous case, but identify the differences in the optimal control structure from the solution in Section 2.2.1. Again, our approach is to define a synthesis of extremal controlled trajectories, prove their optimality, and finally give conditions for the existence of a solution for all $\mathbf{v} \in \mathcal{G}$.

Synthesis Construction: The Hamiltonian and multiplier are similar to (2.22) and (2.24). The minimum condition similarly results in (2.25) with the conclusion that the optimal control is simply BANG at $u^*(t) = \mathrm{U}$ for trajectories that do not hit the guard under this control. Similar to (2.33), there again exists a curve Γ that separates such initial conditions from those requiring switching, given by (2.34). Note that there is no boundary segment in this case as u_{arc} cannot drive the voltage of Neuron 1 up to threshold along the state constraint boundary (see Appendix A.1.1), and thus we are led to consider controls only of the form

$$u = \begin{cases} 0 & \text{for } t < \hat{t} \text{ where } v_1(\hat{t}) < V_T, \\ \mathrm{U} & \text{for } \hat{t} \le t \le \tau. \end{cases} \tag{2.46}$$

in the interior of $\mathcal{G}$, and $\hat{t} = 0$ is allowed. *This concludes the synthesis construction.*

***Proof of Optimality**:* The value function for the region Γ_- equals the time taken by Neuron 1 to reach the threshold V_T under the constant control U, and takes the same form as (2.36). For $\mathbf{v} \in \Gamma_+$, the value function is calculated assuming that the control is turned off for an

interval $[0, \hat{t}]$, during which the system decays from the initial condition $\mathbf{v}(0) = [v_1\ v_2]^T$ to a point $\mathbf{v}(\hat{t}) = [\hat{v}_1\ \hat{v}_2]^T$ on the curve Γ. At this time the control switches to the maximum value U, and the corresponding trajectory follows the curve until the terminal condition $\mathbf{v}(\tau) = [V_T\ V_G]^T$ is reached. This gives

$$\mathcal{V}_+(\mathbf{v}) = \hat{t} + t_{th} = \frac{1}{a_1}\log\left(\frac{v_1}{\hat{v}_1}\right) - \frac{1}{a_1}\log(E(\hat{v}_1)) \tag{2.47}$$

where

$$\begin{gathered} \hat{v}_2 = \left(\frac{\hat{v}_1}{v_1}\right)^{\frac{a_2}{a_1}} v_2 \quad \text{and} \\ \left(E(\hat{v}_1)\frac{\hat{v}_1}{v_1}\right)^{\frac{a_2}{a_1}} v_2 + \frac{b_2}{a_2}\mathrm{U}\left(1 - E(\hat{v}_1)^{\frac{a_2}{a_1}}\right) - V_G = 0 \end{gathered} \tag{2.48}$$

using the fact that $[\hat{v}_1\ \hat{v}_2]^T$ lies on Γ. Here we cannot get an explicit expression for $\mathcal{V}_+$ in terms of the initial condition $[v_1\ v_2]^T$ because of the transcendental form of (2.48).

Note that for this synthesis the state space constraint does not become active. It is clear from the construction that the corresponding values satisfy the Hamilton-Jacobi-Bellman equation away from Γ. However, this problem is a nonstandard one in that the value function may no longer be continuous on Γ, with the only exception at $v_1 = 0$, i.e.,

$$\mathcal{V}_+(\mathbf{v}) = \mathcal{V}_-(\mathbf{v}), \quad \text{for } \mathbf{v} \in \Gamma \text{ such that } v_1 = 0. \tag{2.49}$$

In general, there may exist a unique point on the curve Γ (in our problem with $u = 0$) where the vector field $\dot{\mathbf{v}} = \mathbf{A}\mathbf{v}$ is tangent to Γ while pointing in the opposite direction. As a result, $\dot{\mathbf{v}} = \mathbf{A}\mathbf{v}$ points into the region Γ_+ and into the region Γ_-, above and below this point respectively. This generates a loss of small-time local controllability that causes the value function to become discontinuous along Γ above this point. For, if the initial condition lies to the right of Γ_+ above this point, then optimal trajectories must decay below the

point in order to reach the terminal manifold. We see this in Figure 2.2(b) (also described below), where the OFF segment in the extremal cannot simply converge to the separatrix Γ, no matter how close it is to Γ. This issue of controllability makes the value function discontinuous. The value is still lower semi-continuous on the full state space. In fact, the value of this synthesis satisfies Sussmann's weak continuity requirement (Definition 6.3.3 [50]). While the discontinuity of the value impedes on the application of most HJB-type sufficient conditions for optimality, this is not the case for regular synthesis type constructions , and the optimality of the synthesis follows from Theorem 6.3.3 in [50]. □

Existence of Solution: However, the control approach in (2.46) will fail if trajectories starting in Γ_+ do not in fact hit the separatrix at some time during the initial off-control. A necessary and sufficient condition for trajectories to hit the separatrix is that Γ intersects the positive v_2 axis. When this condition holds and $\mathbf{v}(0)$ lies above Γ, then there must be a time $\hat{t}$ where the trajectory hits Γ under $u = 0$. Conversely, suppose Γ does not intersect the positive v_2 axis. The slope of Γ, considering v_2 as a function of v_1, must be less than the slope of the decaying trajectory for there to be an intersection (ignoring the degenerate parameter choice for which tangency is possible). Taking the ratios $\dot{v}_2/\dot{v}_1$ for $u = 0$ and $u = \mathrm{U}$ (recalling that Γ is itself a solution with maximal input), and rearranging the result, shows the slope condition can be met only if $v_2 > \vartheta_1 v_1$. However, by our assumption $\vartheta_1 \leq V_T/V_G$, no point on Γ meets this inequality (the curve lies entirely below the line from the origin to $[V_T\ V_G]^T$). In fact, since $\dot{v}_i$, $i = 1, 2$, is monotonic in u, it follows that there is no admissible control that can push a solution across Γ, so that the latter serves as a barrier to Neuron 1's threshold for all initial conditions in Γ_+ (at least, without first crossing the Neuron 2 guard). So in this case, selective spiking of Neuron 1 is not possible.

Thus, the condition for the existence of a time-optimal solution for selective spiking of Neuron 1 is that the v_2 intercept of Γ is positive, which occurs when

$$\left(1 - \frac{a_1 V_T}{b_1 \mathrm{U}}\right)^{a_2} > \left(1 - \frac{a_2 V_G}{b_2 \mathrm{U}}\right)^{a_1}. \tag{2.50}$$

Example 2. *We use the same parameter values as in* (2.44) *but swap the roles of Neuron 1 and Neuron 2, i.e.,*

$$\begin{aligned} &R_2 = 0.5\ G\Omega,\ R_1 = 0.33\ G\Omega \\ &\mathcal{C}_2 = 300\ pF,\ \mathcal{C}_1 = 300\ pF \\ &V_T = 30\ mV,\ V_G = 27\ mV \\ &\mathrm{U} = 2.5\ nA,\ \beta_2 = 1,\ \beta_1 = 1.2. \end{aligned} \tag{2.51}$$

Now, $\vartheta_1 \leq V_T/V_G$. Moreover, condition (2.50) *holds so that the switching separatrix intersects the positive v_2 axis. Thus, a time-optimal solution for selectively spiking Neuron 1 always exists. Figure 2.2(b) shows example trajectories.*

2.2.3 Geometric Interpretation of Cases and Pairwise Feasibility

Thus far in our discussion we assume, without loss of generality, that a selective spike is desired in Neuron 1. Now for pairwise feasibility, i.e., to analyze when time-optimal selective spiking of either neuron is possible (from any initial condition), both neurons must be associated with either Case 1 or Case 2. To do this, we introduce

$$\vartheta_2 = \frac{b_2 a_1}{b_1 a_2} = \frac{1}{\vartheta_1}. \tag{2.52}$$

We associate Neuron 1 with ϑ_1 and Neuron 2 with ϑ_2 to determine the Case (Section 2.2.1, 2.2.2) to which these neurons belong. We say Neuron 1 is Case 1 or 2 when $\vartheta_1 > \frac{V_T}{V_G}$ or

$\vartheta_1 \leq \frac{V_T}{V_G}$, respectively, and similarly for Neuron 2 with the same inequality relation on ϑ_2. Since we have $V_T > V_G$, this allows for three possible scenarios,

1. $\vartheta_1 > \frac{V_T}{V_G}$, $\vartheta_2 < \frac{V_T}{V_G}$: Neuron 1 is Case 1 and with ϑ_2 being the reciprocal of ϑ_1 we have Neuron 2 is Case 2.

2. $\vartheta_1 < \frac{V_T}{V_G}$, $\vartheta_2 > \frac{V_T}{V_G}$: Neuron 1 is Case 2 and Neuron 2 is Case 1 and the structure of the solution is identical to the previous scenario.

3. $\vartheta_1 \leq \frac{V_T}{V_G}$, $\vartheta_2 \leq \frac{V_T}{V_G}$: Both Neurons are Case 2 and this happens when $\frac{V_G}{V_T} \leq \vartheta_{1,2} \leq \frac{V_T}{V_G}$.

As we will show in the following sections, for one of the neurons belonging to Case 1, pairwise selective spiking can be accomplished. However, if $\vartheta_{1,2} \leq \frac{V_T}{V_G}$, i.e., both neurons are Case 2, a solution may not exist and pairwise feasibility is not guaranteed.

To provide an additional geometric interpretation (see Appendix A.1.1) of these conditions, we introduce the quasistatic equilibrium line

$$\mathbf{v}(\infty) := \{(v_1, v_2) | b_2 a_1 v_1 = b_1 a_2 v_2\}, \tag{2.53}$$

which defines the set of points for which $\dot{\mathbf{v}} = \mathbf{0}$ (for each $u \in \mathcal{U}$).

In a pair of neurons, two possible parametrization scenarios can be encountered:

Neuron 1 and 2 correspond to different cases

Here we discuss the pairwise feasibility for when Neuron 1 is Case 1 and Neuron 2 is Case 2. It is important to note that the result extends to the reverse scenario, i.e. Neuron 1 is Case 2 and Neuron 2 is Case 1.

Here, the line of quasi-static equilibrium in (2.53) intersects the line $v_1 = V_T$ before it intersects $v_2 = V_G$. Thus, Neuron 1 can always increase along the Neuron 2 guard boundary. Conversely, Neuron 2 cannot increase along the Neuron 1 guard beyond the point of intersection between $\mathbf{v}(\infty)$ and $v_1 = V_G$. As we showed above, in this case selective spiking of Neuron 1 is always possible. Thus, pairwise feasibility reduces to the condition (2.50) modulo a swapping of labels. Specifically,

Lemma 1. *Consider the two neuron network* (2.11)*, where Neuron 1 satisfies Case 1 and Neuron 2 satisfies Case 2. Then, the network is pairwise feasible if and only if*

$$\left(1 - \frac{a_2 V_T}{b_2 \mathrm{U}}\right)^{a_1} \geq \left(1 - \frac{a_1 V_G}{b_1 \mathrm{U}}\right)^{a_2}. \tag{2.54}$$

Proof: The proof follows immediately from Proposition 2 and (2.50), with a swapping of labels. □

Thus, it follows that if (2.54) does not hold, a time-optimal solution for Neuron 2 does not exist (for all initial conditions), and thus the neurons are not pairwise feasible.

Neuron 1 is Case 2; Neuron 2 is Case 2

If both neurons are Case 2, then pairwise feasibility would necessitate (2.54) holding to within a swapping of labels (i.e., so that either neuron can be selectively spiked). Clearly, this is impossible (see Appendix A.1.1) except for the limiting case when $V_G = V_T$, i.e., the neurons are not guarded. In such a scenario, the optimal solution may produce simultaneous spiking of both neurons depending on the initial condition.

2.3 Minimum Time Sequence Control

We now use the above results to analyze longer pairwise spiking sequences Σ_S to solve the problem *P2*. Based on the results of the previous section for pairwise feasibility, i.e., to allow all possible spike sequences for two neurons, we make the following assumption hereon.

Assumption 1. *The pair of neurons are parameterized such that Neuron 1 satisfies Case 1, Neuron 2 satisfies Case 2, and Lemma 1 holds.*

This assumption ensures that the selective spiking solutions for the two neurons are given by Proposition 1 and 2, respectively.

We now analyze all the possible length 2 sequences, i.e., $[1,1]$, $[1,2]$, $[2,1]$ and $[2,2]$ and recognize how we can use the basic characterizations developed in Section 2.2.1, 2.2.2 to synthesize a time optimal strategy for these sequences. We employ a dynamic programming approach where, using the time-optimal solution for the second spike in neuron i, we define a terminal cost and then solve the resulting optimal control problem for the first spike in neuron j, $i, j \in \{1, 2\}$. While the optimal synthesis for some of these sequences can be generalized from the solution of *P1*, we shall see that for the target sequence $[2,1]$, no time optimal control solution may exist.

2.3.1 Synthesis of all 2 spike sequences

Without loss of generality, consider the spike sequence $\Sigma_S = [1,1]$ that we want to achieve in minimum time. We will use the concept of dynamic programming to solve the following

problem.

$$\begin{aligned} \min \quad & \mathbb{J}(u) = \int_0^{\tau_1} \mathrm{d}t + \int_{\tau_1}^{\tau_2} \mathrm{d}t \\ \text{s.t.} \quad & \dot{\mathbf{v}} = f(\mathbf{v}, u) = \mathbf{A}\mathbf{v} + \mathbf{b}u \\ & 0 \leq u(t) \leq \mathrm{U} \\ & v_1(\tau_1) = V_T,\ v_1({\tau_1}^+) = 0 \\ & v_1(\tau_2) = V_T,\ v_2(t) \leq V_G \ \text{ for } t \in [\tau_1, \tau_2] \end{aligned} \tag{2.55}$$

We will start from the last spike, Neuron 1, for this example and solve the minimum time problem *P1* for all the initial condition for Neuron 2, namely $v_2 \in [0, V_G]$, $v_1 = 0$, and use the solution of *P1* as the terminal cost $\varphi(\mathbf{v}(\tau_1))$ for the previous spike, Neuron 1 again, in our case. So we will solve the following optimal control problem

$$\begin{aligned} \min \quad & \mathbb{J}(u) = \int_0^{\tau_1} \mathrm{d}t + \varphi(v_2(\tau_1)) \\ \text{s.t.} \quad & \dot{\mathbf{v}} = f(\mathbf{v}, u) = \mathbf{A}\mathbf{v} + \mathbf{b}u \\ & 0 \leq u(t) \leq \mathrm{U} \\ & v_1(\tau_1) = V_T,\ v_2(t) \leq V_G \ \text{ for } t \in [0, \tau_1] \end{aligned} \tag{2.56}$$

Now we will seek synthesis for all possible two spike sequences using (2.56).

Spike sequence [1,1]

The optimal synthesis for the sequence $\Sigma_S = [1, 1]$ is given in Figure 2.3(a). We highlight the solution of *P1* for Neuron 1 on the top left, the terminal cost $\varphi(v_2(\tau_1))$ in the middle, and in the bottom, we show the solution of (2.56). On the right, we construct the complete synthesis for the whole sequence.

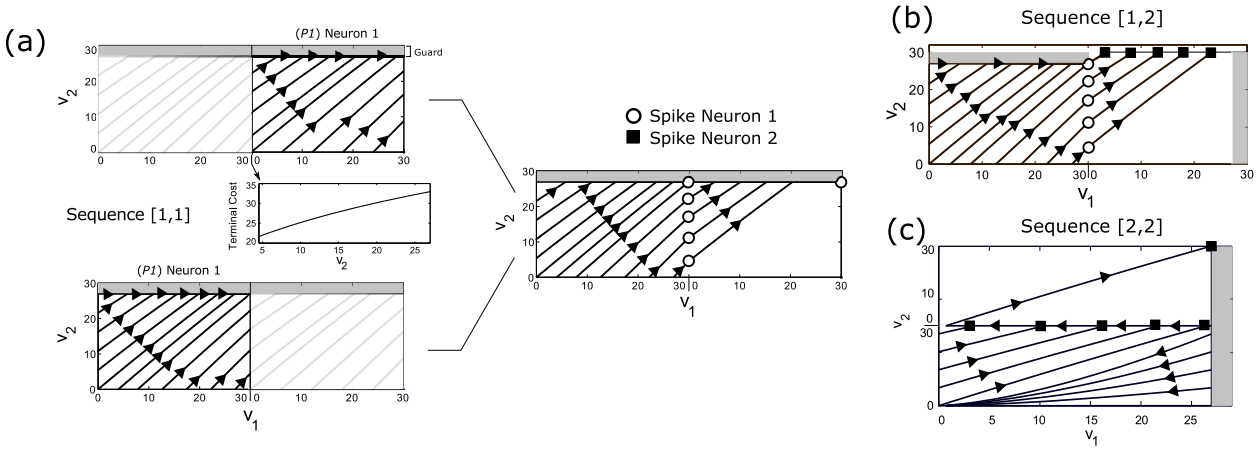

Figure 2.3: Optimal Synthesis for Sequences $[1,1]$,$[1,2]$ and $[2,2]$ is shown in (a) (b) (c) for the nominal parameters (2.44). In these depictions, the state space is repeated to indicate the reset condition. (a) Synthesis for $[1,1]$, showing both parts of the dynamic programming. The terminal cost is increasing and differentiable. The optimal trajectories from several initial conditions are shown. (b) Optimal trajectories for sequence $[1,2]$. (c) Optimal trajectories for sequence $[2,2]$. In this case, all initial conditions collapse onto a single manifold associated with the second spike.

Given an arbitrary initial condition $[v_1\ v_2]^T$, the time-optimal solution of the first part without any terminal cost (i.e., $\varphi(v_2(\tau_1)) \equiv 0$, given by Proposition 1) has the property that, among all admissible controls, it leads to the smallest possible value for the terminal state $v_2(\tau_1)$. Since the function $\varphi(v_2(\tau_1))$ is strictly increasing, this is then also the optimal solution for the combined problem, and thus allows us to simply concatenate two solutions of *P1* for Neuron 1. Overall, the optimal control is simply given by the BANG control U until v_2 reaches the guard, after which the boundary control is used exactly as in the single spike problem.

Spike sequence [1,2]

However, such monotonicity arguments do not work in the other cases. Figure 2.3(b) shows the synthesis of optimal controlled trajectories for the sequence $\Sigma_S = [1,2]$. The terminal cost $\varphi(v_2(\tau_1))$ is calculated as the value function from the solution of *P1* for Neuron 2 and is a strictly decreasing function of v_2 (since the higher the voltage v_2, the lower the time to

induce a spike in Neuron 2). Thus, in principle, it might be possible for the solution of the first part to deviate from the solution of *P1* for Neuron 1 if the loss in doing so would be made up by the gain in the penalty function $\varphi(v_2(\tau_1))$ at the terminal point. Consider the switching function

$$\Phi(t) = \lambda_1 b_1 + \lambda_2 b_2 \tag{2.57}$$

If there is a switching at $t = \hat{t}$, then we have

$$\begin{aligned} \Phi(\hat{t}) &= \lambda_1(\hat{t}) b_1 + \lambda_2(\hat{t}) b_2 = 0 \\ \lambda_1(\hat{t}) b_1 &= -\lambda_2(\hat{t}) b_2 \end{aligned} \tag{2.58}$$

Also, for a switching structure OFF-BANG we must have

$$\dot{\Phi}(\hat{t}) < 0. \tag{2.59}$$

Now using (2.58) for computing the derivative of the switching function

$$\dot{\Phi}(\hat{t}) = \lambda_2(\hat{t}) b_2 (a_2 - a_1). \tag{2.60}$$

From the non-triviality [50, Section 2.2] and transversality conditions

$$\lambda_2(\tau_1) = \frac{\partial \varphi(v_2(\tau_1))}{\partial v_2} < 0, \tag{2.61}$$

since the terminal cost is a decreasing function of v_2. Also, we have previously derived that the adjoint variables are solutions of linear homogeneous differential equations which do not change sign in $t \in [0, \tau_1]$. So we have $\lambda_2(\hat{t}) < 0$, as well. Using these and assuming $a_2 < a_1$, from (2.60) we get

$$\dot{\Phi}(\hat{t}) > 0. \tag{2.62}$$

This violates the necessary condition in (2.59) for an OFF-BANG switching. Note that for the case $a_1 < a_2$, OFF-BANG switching cannot be ruled out using this argument, and the synthesis has to be constructed by direct computation. In our example with the parameters from (2.44), it turns out that the optimal solution is simply BANG/BANG-BOUNDARY (2.21), i.e., the terminal cost $\varphi(v_2)$ has no effect on the solution of (2.56). Thus the time optimal synthesis for $\Sigma_S = [1, 2]$ is a combination of the individual synthesis for Neurons 1 and 2.

Spike sequence [2,2]

Similar controllability properties also allow us to give a short solution for the sequence $\Sigma_S = [2, 2]$. The optimal synthesis is shown in Figure 2.3(c). In this case, the terminal cost $\varphi(v_1(\tau_1))$ is a function of v_1 and it is also strictly increasing in v_1 (since the higher the value of v_1, the higher the time to ensure selective spiking in Neuron 2). From the analysis of transversality condition and the switching function like in the previous sequence (2.59), we can show that OFF-BANG is optimal for the first spike in Neuron 2 with $a_1 < a_2$, and sub-optimal for $a_2 < a_1$ if there exists a switching. Indeed, for the first Neuron 2 spike and initial conditions under the separatrix, the optimal control is OFF-BANG. But for initial conditions on the v_2 axis, the optimal control is simply BANG. In the example, the overall construction is achieved by concatenating the solutions of *P1* for Neuron 2 vertically. Since Neuron 2 is reset to 0 after firing, the initial condition for the second problem is given by $[v_1(\tau_1)\ 0]^T$.

Spike sequence [2,1]

Proposition 3. *Under Assumption 1, no time optimal control solution exists in general for a target sequence* Σ_S *containing the sub-sequence* $[2, 1]$.

Proof: The synthesis is more involved for this sequence. The terminal cost for the first Neuron 2 spike is the value function from (2.35) with $v_2 = 0$, i.e.,

$$\varphi(v_1(\tau_1)) = \mathcal{V}(\mathbf{v})|_{v_2=0}, \tag{2.63}$$

which is a decreasing function in v_1, and $\varphi(v_1(\tau_1))$ is not differentiable with respect to v_1 for some $v_1 = v_{nd}$ where $v_{nd} \in [0, V_G]$ (as shown in the bottom left of Figure 2.4). Note that for any initial condition at the origin or on the v_1 axis to the left of the separatrix, OFF-BANG cannot lead to optimality, and for those cases, the extremals will be generated by $u^*(t) = \mathrm{U}$, $\forall\, t \in [0, \tau_1]$. Also, to the right of the separatrix OFF-BANG will be the optimal policy as it is the only viable option in the presence of state constraints. So we can conclude that if there is indeed a switching to the left of the separatrix, then there must exist a v_s with $v_s \in (0, V_G]$, such that for $\mathbf{v}(0) = \{(v_1, v_2) : v_1 = 0, v_2 \in (v_s, V_G)\}$, the optimal policy will be OFF-BANG whereas for $\mathbf{v}(0) = \{(v_1, v_2) : v_1 = 0, v_2 \in [0, v_s]\}$, the optimal control is BANG. Now we will calculate this voltage v_s which acts as an onset for the change in optimal policy. Considering the switching at $t = \hat{t}$, we have $v_2(\hat{t}) = v_s$ and

$$\Phi(\hat{t}) = \lambda_1(\hat{t})b_1 + \lambda_2(\hat{t})b_2 = 0. \tag{2.64}$$

Since the Hamiltonian vanishes identically for our problem, we get,

$$\mathcal{H}(\hat{t}) = 1 - a_2 v_s \lambda_2(\hat{t}) = 0. \tag{2.65}$$

Also, from the transversality condition with $\lambda_0 = 1$ we have

$$\lambda_1(\tau_1) = \frac{\partial \varphi(v_1(\tau_1))}{\partial v_1}, \tag{2.66}$$

which is known. Since we reach the threshold V_T from v_s using the BANG control, from (2.31)

$$\tau_1 - \hat{t} = \frac{1}{a_2} \log\left(\frac{v_s - \frac{b_2}{a_2}\mathrm{U}}{V_T - \frac{b_2}{a_2}\mathrm{U}} \right) \tag{2.67}$$

Using the fact that the adjoint variables satisfy linear homogeneous differential equations, we can write

$$\lambda_1(\hat{t}) = \frac{\partial \varphi(v_1(\tau_1))}{\partial v_1} \left(\frac{v_s - \frac{b_2}{a_2}\mathrm{U}}{V_T - \frac{b_2}{a_2}\mathrm{U}} \right)^{-\frac{a_1}{a_2}} \tag{2.68}$$

From (2.64)-(2.68), we can solve for v_s with

$$1 + \frac{a_2 v_s b_1}{b_2} \frac{\partial \varphi(v_1(\tau_1))}{\partial v_1} \left(\frac{v_s - \frac{b_2}{a_2}\mathrm{U}}{V_T - \frac{b_2}{a_2}\mathrm{U}} \right)^{-\frac{a_1}{a_2}} = 0 \tag{2.69}$$

If such a v_s exists, the construction may be much more complicated with the possible presence of a 'cut-locus' type phenomenon, and we leave a detailed analysis of such a problem for future work. In our case, the terminal cost decreases with a rapid rate for $v_1 \in [0, v_{nd}]$ and abruptly changes to a much smaller slope for $v_1 \in (v_{nd}, V_G]$ (See Figure 2.4) due to the nature of the value functions on either side of separatrix $\mathcal{V}-$, $\mathcal{V}+$ in (2.36), (2.37). This results in a field of extremals trying to converge to the point v_{nd}, even when the monotonicity of the value function is not affected by the loss of differentiability (see top left in Figure 2.4). We calculate the set of initial conditions for which this point can be attained, specifically $\mathbf{v}_c = \{(v_1, v_2) : v_1 = 0, v_2 \in [v_c, V_G]\}$, where v_c denotes the highest point on v_2 axis from which $[V_T \; v_{nd}]^T$ can be reached via BANG control. This voltage v_c and the set $\mathbf{v}_c$ are shown in the right panel of Figure 2.4. Now, the optimal control problem for $\mathbf{v}(0) \in \mathbf{v}_c$ simply reduces to

$$\begin{aligned} \min \quad & \mathbb{J}(u) = \int_0^{\tau_1} \mathrm{d}t \\ \text{s.t.} \quad & u(t) \in \mathcal{U} \end{aligned} \tag{2.70}$$

with the terminal constraint $\mathbf{v}(\tau_1) = [v_{nd}\ V_T]^T$ and state constraints $v_1(t) \leq V_G$, $v_2(t) \leq V_T$. This is similar to the selective spiking problem of Neuron 1, and indeed the best control is a combination of BANG and boundary control as in (2.21)

$$u^* = \begin{cases} \text{U} & \text{for } t \leq t_c \text{ where } v_2(t_c) = V_T \\ u_{arc} & \text{for } t_c < t \leq \tau_1 \text{ where } v_1(\tau_1) = v_{nd}. \end{cases} \tag{2.71}$$

But this implies that Neuron 2 maintains the voltage (V_T), even after the spike is emitted, which violates our assumption that the neurons are reset instantaneously after reaching V_T, as described in (2.4). So the synthesis $\mathcal{S}^*$ corresponding to (2.71) is excluded from the admissible set of extremals purely out of the physical constraints imposed on the system. This resembles the classical problem of finding surfaces of minimum revolution [50], where the Goldschmidt extremal (see Chapter 5) cannot be attained because of C^1 (continuously differentiable once) assumption on the extremals. Thus, any synthesis $\mathcal{S}$ for (2.70) will be sub-optimal to $\mathcal{S}^*$. For simplicity, we have picked a synthesis such that

$$u_{sub} = u(\mathbf{v}(0)) \text{ for } t \in [0, \tau_1], \tag{2.72}$$

i.e., a constant control which varies depending on the initial condition shown in Figure 2.4. For the set of initial conditions

$$\mathbf{v}(0) = \{(v_1, v_2)\ :\ v_1 = 0,\ 0 \leq v_2 < v_c\} \cup \{(v_1, v_2)\ :\ 0 \leq v_1 < V_G,\ v_2 = 0\}, \tag{2.73}$$

the optimal synthesis remains the same as the solution of *P1* for Neuron 2. □

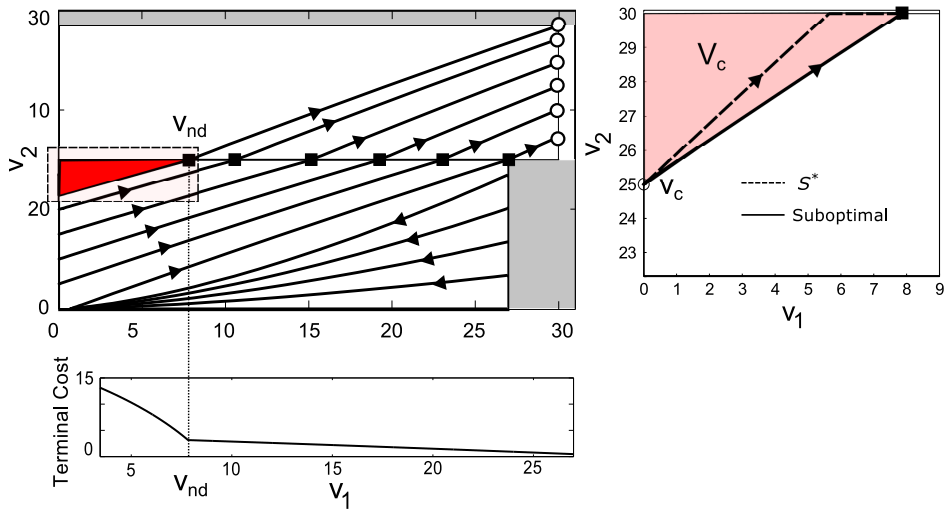

Figure 2.4: A possible suboptimal synthesis is shown for the sequence $\Sigma_S = [2, 1]$. Note that the value function for the last spike, i.e. Neuron 1, plotted in the bottom panel, is not differentiable with respect to v_1. This is added as the terminal cost for the optimum control problem for the first spike in Neuron 2. In the right panel, the actual optimal solution and a constant control suboptimal synthesis proposed in (2.72) is shown.

2.3.2 Greedy Designs for Sequences with Arbitrary Length

From our analysis of the 2-spike sequences in the previous section, we can design the time optimal control for any Σ_S of K spikes ($K \geq 2$) without the subsequence $[2, 1]$. In addition if we assume $a_2 < a_1$, it can be shown using an inductive argument that the overall synthesis can be constructed from the solutions of individual selective spiking problems in Propositions 1 and 2.

In general, for a Σ_S with the subsequence $[2, 1]$, to illustrate the complexities of sequence control, it is instructive to consider the 4-spike sequence, $\Sigma_S = [1, 2, 1, 1]$. In this case, the target sequence contains a $[2, 1]$ event, meaning that any solution will be suboptimal. In this case, a dynamic programming approach that interleaves the interpolation control (2.72) can yield such a solution. However, from a practical perspective, pursuing this design approach

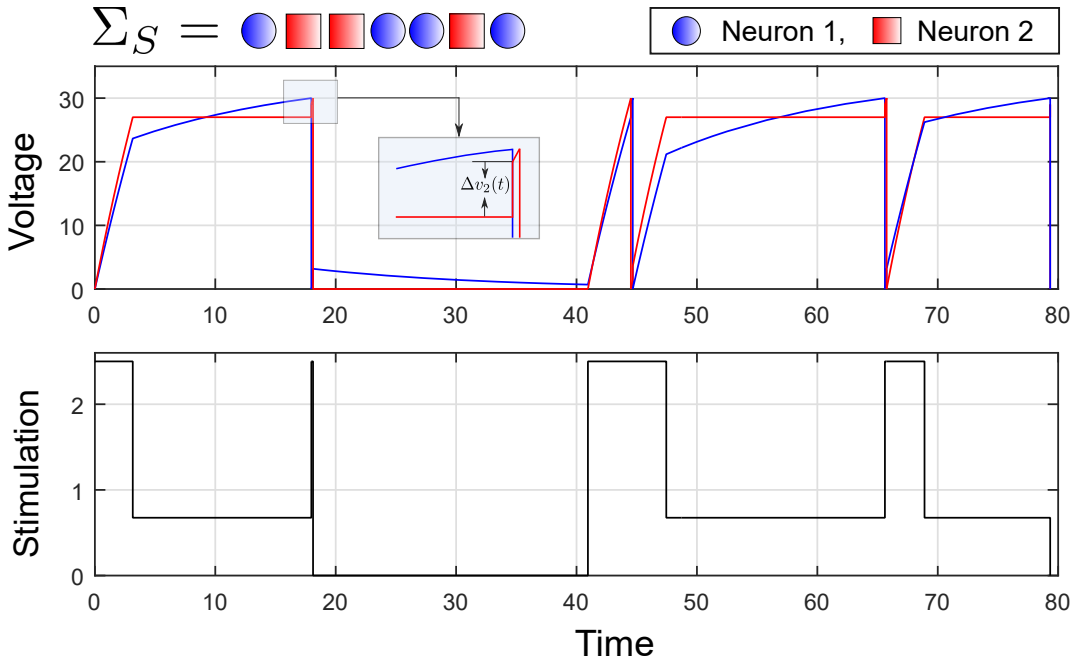

Figure 2.5: Simulation example of the greedy algorithm for *P2* for a target sequence $\Sigma_S = [1, 2, 2, 1, 1, 2, 1]$ with the nominal parameters in (2.44). The inset shows the synaptic contribution $\Delta v_2(t) = 2mV$, to Neuron 2 due to the first spike in Neuron 1.

for long sequences is difficult as it requires computing the location of non differentiability in the value functions of all $[2, 1]$ events.

Thus, we argue that from a design perspective, a simple greedy approach where we minimize the time for each spike in Σ_S progressively, constitutes an acceptable, tractable approximation. In Figure 2.5, we show the solution of the greedy controller for an arbitrary spike sequence Σ_S.

Decoupling the network for longer sequences

In applying the greedy approach, it is important to note that the synaptic contribution from the spiking neuron can carry the voltage of the other neuron in the network over the synaptic guard V_G. Thus, we cannot readily apply the solution of *P1* for the following spike in the

sequence (pattern), as the initial condition may violate the state constraint in (2.8) for *P1*. Here, we propose strategies to eventually utilize Proposition 1, 2 for the greedy design.

1. First, if the initial condition after any spike in the sequence (pattern), at $t = \tau_1$, is not within the relevant state space $\mathcal{G}$, we can apply $u = 0$ until $t = t'$, $t' > \tau_1$, such that $\mathbf{v}(t') \in \mathcal{G}$. Then, we can apply the solution of *P1* to induce the target spike.

2. Alternatively, we can modify the guard V_G of the non-target neuron at each step of the greedy design, depending on the number of consecutive spikes in the target neuron in the sequence (pattern), e.g., if $\Sigma_S = [1, 1, 2, 2, 2]$, then we can set the guard voltage for Neuron 2 at $V_G(\sigma_1) < V_T - 2\bar{\rho}_{syn}$ for the first spike and $V_G(\sigma_2) < V_T - \bar{\rho}_{syn}$ for the second spike. Thus, the relevant state space for the first and second spike will be modified to $\mathcal{G}(\sigma_1) = [0, V_T] \times [0, V_G(\sigma_1)]$ and $\mathcal{G}(\sigma_2) = [0, V_T] \times [0, V_G(\sigma_2)]$, respectively. This ensures that whatever the contribution is from the presynaptic neuron (in this case, Neuron 1), we start in the relevant state space for the next spike in the sequence (pattern). Once the target neuron changes to $\sigma_3 = 2$, the guard voltage for Neuron 1 is determined by the number of consecutive spikes in Neuron 2 (3 in this example), i.e., $V_G(\sigma_3) < V_T - 3\bar{\rho}_{syn}$ and so on. Note that by successively reducing the guard voltage, the selective spiking problem may become infeasible as discussed in Section 2.2.3.

3. Finally, we can combine the above two approaches to develop an algorithm where we can use (2) until the problem is infeasible. At this point, we go back to (1) and add an off time before implementing the solution of *P1*.

In our examples of sequence and pattern control, we have used the first approach in developing the greedy design (see Figure 2.5, 2.6).

2.4 Fixed-time Selective Spiking and Spike Patterns

We now move to the problem of controlling timed spike patterns, i.e., *P3*. It is intuitive that a basic necessary condition in this case is that the desired spike time exceeds the minimum selective spiking time, i.e., the solution to *P1*.

Specifically, suppose that we want to achieve the target pattern $\Sigma_P = [(1, t_1)]$, i.e., a spike in Neuron 1 at time t_1. The cost function in *P3* (2.14) reduces to

$$\mathbb{J}(u) = \left(t_1 - \int_0^{\tau_1} \mathrm{d}t \right)^2 \tag{2.74}$$

(subject to the selectivity constraint in (2.7)). Here, τ_1 denotes the achieved spike time and $\bar{\tau}_1$ is the solution of *P1* for an arbitrary initial condition $\mathbf{v}(0)$. If $\bar{\tau}_1 \geq t_1$, then evidently that is our best option and the solution of (2.74) and *P1* are the same, i.e. $\tau_1 = \bar{\tau}_1$.

For the other case, i.e. $\bar{\tau}_1 < t_1$, contingent on controllability, a control must exist such that $\tau_1 = t_1$. If such a condition is met, then in general there may be multiple solutions to the pattern control problem. Herein, we consider one simple strategy involving the introduction of an off time $\hat{t}$ to the optimal control solution of *P1* such that

$$\hat{t} + \tau_1^r = t_1 \tag{2.75}$$

where τ_1^r is the solution of the time optimal control *P1*, for the initial condition $\mathbf{v}(\hat{t})$. We noted earlier that the initial conditions for the selective spiking problem nominally lie on either the v_1 or v_2 axis, under the assumption that one of the neurons has just produced a spike. In this case, feasibility of (2.75) reduces to understanding those initial conditions that generate specific values of τ_1^r.

2.4.1 Off-time Insertion for Pattern Control

We characterize the relationship between τ_1^r and initial conditions via the notion of a Λ-Controllable set.

Definition 3 (Λ- Controllable set)**.** *Without loss of generality, the Λ-controllable set $\zeta(\Lambda)$ of Neuron 1 is the set of initial conditions from which the selective spiking of Neuron 1 in P1 is achieved in time Λ, i.e.,*

$$\zeta_1(\Lambda) = \{(v_1, v_2) : \ \mathbf{v}(0) = [v_1 \ v_2]^T, \nexists \, t < \Lambda, \ s.t. \ v_1(t) = V_T, \ v_2(t) \leq V_G\} \tag{2.76}$$

The Λ-controllable sets for the system (2.11) are provided in Appendix A.2. Since we are interested in initial conditions along the v_1 and v_2 axes, we consider the functions

$$\begin{aligned} \omega_1 \ &: \ \Lambda \ \rightarrow \ v_1, \text{such that } (v_1, 0) \in \zeta_1(\Lambda) \\ \omega_2 \ &: \ \Lambda \ \rightarrow \ v_2, \text{such that } (0, v_2) \in \zeta_1(\Lambda), \end{aligned} \tag{2.77}$$

i.e., the intersection of the Λ-controllable sets with the axes.

Earlier, we noted that the value function for the selective spiking of both neurons remains continuous on both the v_1, v_2 axis (i.e., from (2.41), (2.49)). This fact, together with the derivation of the Λ-controllable sets in the Appendix, allows us to conclude that the functions (2.77) are continuous in Λ. Thus, we are able to ensure existence of the *off-time pattern control* from (2.75), i.e.,

$$u^p = \begin{cases} 0 & \text{for } t \in [0, \hat{t}], \\ u^* & \text{for } t \in (\hat{t}, t_1], \end{cases} \tag{2.78}$$

where u^* comes from Proposition 1 or 2. The computation of the off-time $\hat{t}$ is obtained directly from the Λ-controllable sets and is provided in Appendix A.3. Thus, an overall pattern control strategy can be formulated as:

$$\Pi^* = \begin{cases} u^* & \text{if } \bar{\tau}_1 \geq t_1, \\ u^p & \text{if } \bar{\tau}_1 < t_1. \end{cases} \tag{2.79}$$

2.4.2 Greedy Designs for Control of Long Patterns

We now consider the synthesis and design of the general pattern control problem *P3*. To begin, we consider the dynamic programming strategy studied in (2.56) but for *P3*. It turns out that the same issues pertaining to non-differentiability of the value function in *P2* persist in this case. To illustrate this, consider the 2-spike target pattern $\Sigma_P = [(1, t_1), (1, t_2)]$. Starting from the last spike $\sigma_2 = 1$, we solve

$$\mathbb{J}(u) = \left((t_2 - t_1) - \int_{\tau_1}^{\tau_2} \mathrm{d}t \right)^2, \tag{2.80}$$

with the terminal and state constraints, and use the value function of (2.80) as the terminal cost to the following optimal control problem

$$\mathbb{J}(u) = \left(t_1 - \int_0^{\tau_1} \mathrm{d}t \right)^2 + \varphi(v_2(\tau_1)). \tag{2.81}$$

Let us denote the solution of *P1* for the second spike from initial condition $\mathbf{v}(0) = [0\ v_2]^T$, by $\bar{\tau}$. Then, depending on v_2, the terminal cost in (2.81) takes the following form,

$$\varphi(v_2) = \begin{cases} 0 & \text{for } v_2, \text{ s.t. } \bar{\tau} \leq (t_2 - t_1), \\ ((t_2 - t_1) - \bar{\tau})^2 & \text{for } v_2, \text{ s.t. } \bar{\tau} > (t_2 - t_1). \end{cases} \tag{2.82}$$

Thus, similar complications as referenced in Section 2.3.2 regarding non-differentiability arise here, and once again we consider implementation of a straightforward greedy strategy for pattern control involving (2.79). In Figure 2.6, we show an example of this greedy algorithm for an arbitrary pattern

$$\Sigma_P = [(1, 20), (2, 30), (2, 70), (1, 95), (1, 115), (2, 120), (1, 130)], \tag{2.83}$$

with the same spike sequence as in Figure 2.5.

2.4.3 Performance of Greedy Design under Disturbance and Noise

In this section, we analyze the robustness of the greedy design when the coupled LIF network in (2.3) is subjected to noise and disturbances. Here we consider two types of uncertainties :

1. Incoming synaptic contributions of the pulse coupled form discussed in Section 2.1.2, from other neurons.

2. Noise in the dynamics of the membrane voltage of the neurons in (2.3) (process noise) and in measurement of these voltages (measurement noise). Note that in implementing the greedy controller in (2.79), we repeatedly apply Proposition 1, 2, which are feedback control, i.e., measurement is implicit.

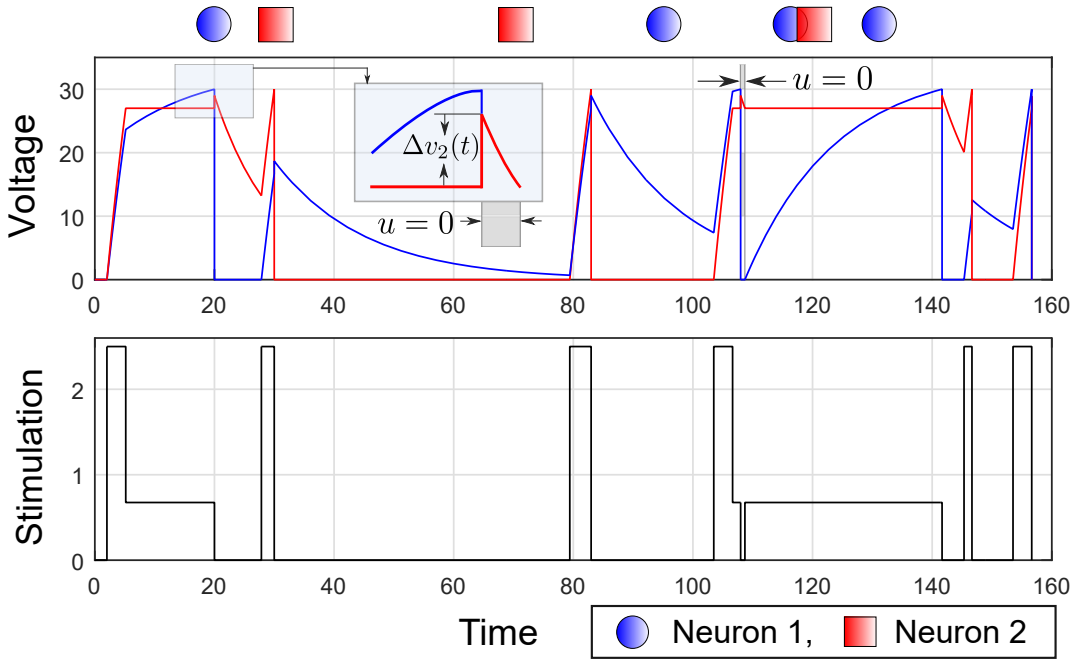

Figure 2.6: Simulation example of the greedy algorithm discussed in Section 2.4.2 for *P3* for a target pattern Σ_P in (2.83) with the nominal parameters in (2.44). Similar to Figure 2.5, we show the synaptic contribution $\Delta v_2(t) = 2mV$, to Neuron 2. We also explicitly indicate the off-time ($u = 0$) after the first (inset) and fourth spike in Neuron 1, as part of the decoupling strategy discussed in Section 2.3.2.

In Figure 2.7(A), we show one realization of the voltage and control waveforms for $d = 150$ incoming spikes over the control horizon for the same Σ_P used in the example of Figure 2.6. To illustrate the effect of these disturbances on the control strategy, in Figure 2.7(D) we plot the average Victor-Purpura (VP) metric [52, 53] between the achieved and target spike trains as we vary the number of incoming spikes d over 50 trials. In each trial, we randomly select the arrival times of the spikes, the contribution and target of the synapse between the two neuron indices. The VP metric is a measure of synchrony between two spike patterns that involves three basic operations: adding or deleting any spike with cost 1, moving any spike with cost κ_1 per unit time, and renaming any index of the spike with cost κ_2. Here, a lower VP distance corresponds to better control performance. We observe that with higher disturbance, represented by d, the controller performs reasonably well with gradual degradation in the achieved patterns.

Next, we consider additive Gaussian noise both during the evolution of the membrane voltage and in measurement. Thus the linear model in (2.11) is modified to

$$\begin{aligned} \dot{\mathbf{v}}(t) &= \mathbf{A}\mathbf{v}(t) + \mathbf{b}u(t) + \mathbf{e}_1(t) \\ \mathbf{y}(t) &= \mathbf{C}\mathbf{v}(t) + \mathbf{e}_2(t), \end{aligned} \tag{2.84}$$

where the measurement vector $\mathbf{y}$ is a linear readout of the neuron voltages through a randomly selected matrix $\mathbf{C}$, which is full rank. $\mathbf{e}_1(t)$, $\mathbf{e}_2(t)$ follow multivariate Gaussian distribution with $\mathbf{e}_1(t) \sim \mathbb{N}(\mathbf{0}, \boldsymbol{\mathcal{W}}_1)$, $\mathbf{e}_2(t) \sim \mathbb{N}(\mathbf{0}, \boldsymbol{\mathcal{W}}_2)$ and $\boldsymbol{\mathcal{W}}_1$, $\boldsymbol{\mathcal{W}}_2$ are the constant covariance matrices of the form $\boldsymbol{\mathcal{W}}_1 = \eta_1^2\,\mathbb{I}$, $\boldsymbol{\mathcal{W}}_2 = \eta_2^2\,\mathbb{I}$, $\mathbb{I}$ is the identity matrix. Here, we compute the voltage estimates of the two neurons at each time step by means of a Kalman Filter [54] and employ the feedback strategy in (2.79) based on these estimates. In Figure 2.7 (B,C), we plot the pattern control solutions for the same Σ_P used in the example of Figure 2.6, for smaller $(\eta_1 = 0.1, \eta_2 = 1)$ and higher $(\eta_1 = 1, \eta_2 = 10)$ process and measurement variance. We observe

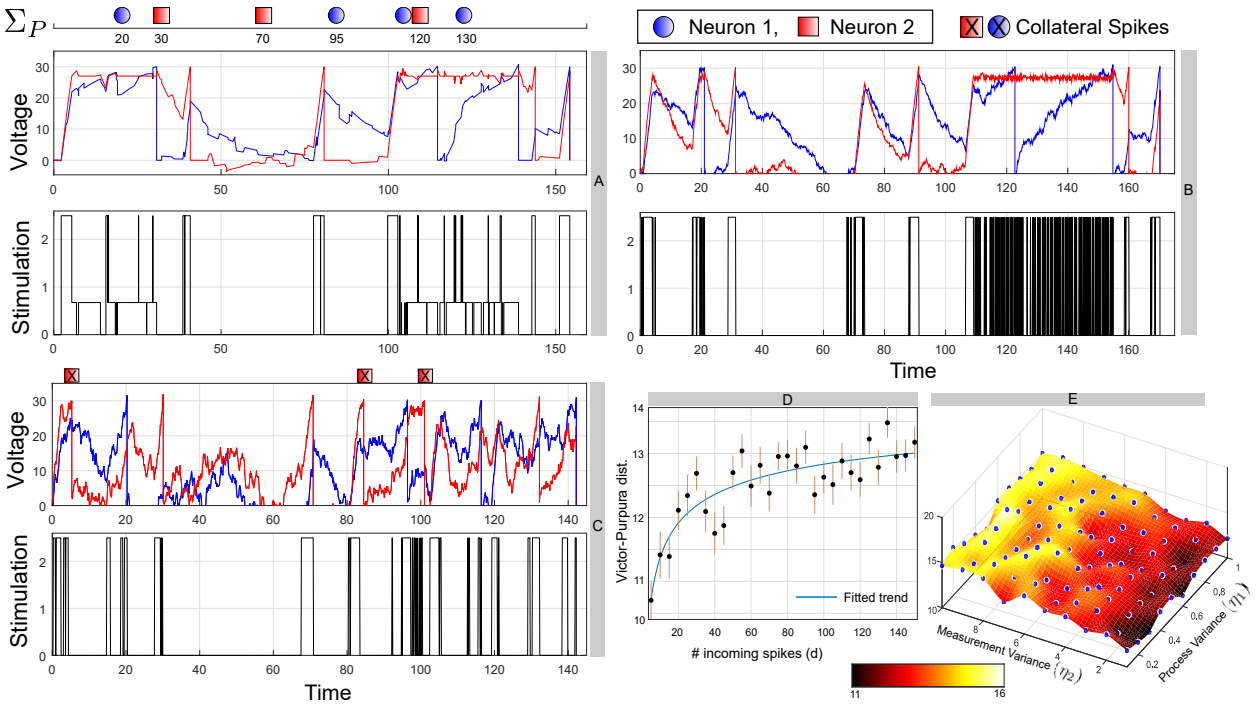

Figure 2.7: Induced voltage waveforms in the two neurons for Σ_P using the greedy design and the control under incoming synapses (A) and process, measurement noise (B for higher variance and C for lower variance). (D) Performance analysis of the controller in terms of VP distance with parameters $\kappa_1 = 1$, $\kappa_2 = 1.5$ against number of incoming spikes d as measure of disturbance. (E) Surface plot fitted to the simulation data of average VP metric (same κ_1, κ_2) vs the process and measurement noise variances, in the course of solving the pattern control problem for Σ_P in (2.83) over different trials.

that the controller's ability to induce the target spike train is not compromised substantially, although with higher levels of noise, spurious spikes are generated, as indicated in panel (C). However, the noisy dynamics in (2.84) can result in a high frequency of switching in the control (B,C, bottom panel), especially during the boundary arc, i.e, the non-target neuron is to be held at guard V_G. Panel (E) shows the performance of the greedy design with respect to the average VP metric between Σ_P and achieved patterns over 50 different trials, as we change the level of noise during the evolution and measurement phase.

2.5 Selective Spiking in Populations

2.5.1 Regularized Time Optimal Selective Spiking in a Population

Proposition 4. *The solution to the C neuron regularized selective spiking problem P4 is BANG-BANG with at most $C-1$ switchings.*

Proof. Necessary conditions for optimality for problem *P4* are given by the Pontryagin maximum principle. the Hamiltonian, adjoint and terminal constraint follows from (2.22), (2.23), (2.27). From the transversality condition we have

$$\boldsymbol{\lambda}(\tau) = \gamma\, \mathbf{W}\mathbf{v}(\tau) + [\nu\, 0 \cdots 0]^T, \qquad \mathcal{H}(\tau) = 0 \tag{2.85}$$

where $\mathbf{W} = \boldsymbol{\omega}^T\boldsymbol{\omega}$. Now from the solution of the multiplier as in (2.24), the switching function is given by

$$\Phi(t) = \mathbf{b}^T\boldsymbol{\lambda}(t) = \sum_{c=1}^{C} b_c\, d_c\, \mathrm{e}^{a_c t}. \tag{2.86}$$

Note that the presence of the regularization term does not change the form of the switching function. So the optimal control will be

$$u^*(t) = \begin{cases} \mathrm{U}_2 & \text{if } \Phi(t) < 0 \\ \mathrm{U}_1 & \text{if } \Phi(t) > 0. \end{cases} \tag{2.87}$$

The value of the regularization parameter γ determines any possible switchings in the optimal control. The switching function is a nontrivial exponential polynomial (i.e., the polynomial co-efficients are constant with zero degree) and can be shown to have at most $C-1$ zeros [50]. Thus, the optimal control is BANG-BANG with a maximum of $C-1$ switchings.

Note that for a multi-input system, i.e.,

$$\dot{\mathbf{v}} = \mathbf{A}\mathbf{v} + \sum_{s=1}^{S} \mathbf{b}_s u_s, \tag{2.88}$$

where $S =$ no. of independent inputs and $\mathbf{b}_s \in \mathbb{R}^C$ is the $\mathbf{b}$ matrix in (2.6) for the s^{th} input u_s, the switching function for each input takes the same form as in (2.86), and the same result (i.e., Proposition 4) holds. □

Proposition 5. *The solution to the C neuron minimum time-energy regularized selective spiking problem P5 is given by sum of exponential kernels,*

$$u^*(t) = -\frac{1}{\varrho} \sum_{c=1}^{C} b_c \, d_c \, \mathrm{e}^{a_c t}. \tag{2.89}$$

Proof: The Hamiltonian in this case will be given by

$$\mathcal{H}(\boldsymbol{\lambda}, \mathbf{v}, u) = 1 + \frac{1}{2}\varrho u^2 + \boldsymbol{\lambda}(\mathbf{A}\mathbf{v} + \mathbf{b}u). \tag{2.90}$$

From the Maximum principle, the optimal control minimizes the Hamiltonian over the admissible set $\mathcal{U}$, such that

$$u^*(t) = -\frac{1}{\varrho} \, \boldsymbol{\lambda}\mathbf{b}. \tag{2.91}$$

Since the multipliers follow the same adjoint dynamics as in (2.23), we can simplify (2.91) to get (2.89). □

From the terminal constraint (2.27) and transversality conditions derived in (2.85), we can solve for c_i's which determine our optimal control for problem *P5*.

2.5.2 Numerical Approach

In this section, we discuss the numerical procedure adopted to solve the problems *P4* and *P5*. Note that in problem *P4*, since there are $C-1$ possible switchings, it is difficult to ascertain the optimal control like in *P1*. This restricts the use of the terminal constraint on the target neuron (i.e., $v_1(\tau) = V_T$). Thus, we have proposed a numerical approach to obtain an approximate optimal solution. We first discretize the system and take two extreme time points, the first one (τ_1) corresponding to the pure minimum time solution i.e., $\gamma = 0$ and the other end point (τ_2) corresponding to an arbitrarily high time. Now we solve the following convex program for τ_r, $r = 1, 2$. Note that for *P5* the quadratic energy term is added to the objective and the box constraint on the input is removed.

$$\begin{aligned} \underset{\hat{u},\hat{\mathbf{v}}}{\text{minimize}} \quad & \frac{1}{2}\gamma\, \hat{\mathbf{v}}(I)^T \mathbf{W}\, \hat{\mathbf{v}}(I) \\ \text{s.t.} \quad & \hat{v}_1(I) = V_T, \hat{\mathbf{v}}(1) = \mathbf{v}(0) \\ & \hat{\mathbf{v}}(i+1) = \mathbf{A}_d\, \hat{\mathbf{v}}(i) + \mathbf{b}_d\, \hat{u}(i) \\ & \mathrm{U}_1 \leq \hat{u}_i \leq \mathrm{U}_2, \forall\, i = 1, \ldots, I-1 \end{aligned} \tag{2.92}$$

where $I = \left\lceil \frac{\tau_r}{\Delta} \right\rceil$, Δ denotes forward Euler discretization step, $\mathbf{A}_d = (\mathbb{I}_C + \mathbf{A}\Delta)$, $\mathbb{I}_C$ is the C-dimensional identity matrix and $\mathbf{b}_d = \mathbf{b}\Delta$. From these solutions, we use the bisection algorithm to revise the end points iteratively until some ϵ tolerance is reached. If the problem is well behaved as in the case of *P4*, *P5*, this algorithm should be a reasonable approximation of the optimal solution. We run this algorithm several times by changing τ_1, τ_2 to ensure the solution is not stuck in a local minima if such a minima exists.

2.5.3 Examples

Here we display the numerical results for *P4*-*P5* for $C = 7$, $S = 2$ and random parametrization for the resistance and capacitance with gaussian spread. We also remove the non-negativity constraint from the set of admissible inputs as assumed in *P1*-*P3*.

$$\begin{aligned} &\mathbb{E}[R] = 0.5\ G\Omega, \sigma[R] = .05\ G\Omega, \mathbb{E}[\mathcal{C}] = 300\ pF \\ &\sigma[\mathcal{C}] = 2\ pF, V_T = 30\ mV, \beta = 2, \boldsymbol{\omega} = [0\ 1 \ldots 1] \\ &\mathrm{U}_1 = -2.5\ nA, \mathrm{U}_2 = 2.5\ nA\ (\text{for } P4) \end{aligned} \tag{2.93}$$

In Figure 2.8-2.9, we plot the solution of *P4*, *P5* respectively and demonstrate the effect of regularization for the selective spiking problem. In the left panel of both figures ($\gamma = 0$), along with the intended spikes in Neuron 1, we observe collateral spiking in the population. In the right panel of the figures ($\gamma \neq 0$), we see that selectivity is improved by adding regularization. We have used CVX [55] with MATLAB interface for the numerical solution of problems *P4*, *P5* [1].

As we are only penalizing the terminal states of the unintended neurons, it is important to note that a high γ may lead to a scenario where the threshold is violated at an intermediate point along the state trajectory. Thus, over-regularization deteriorates the selective performance of these formulations.

2.5.4 Regularized Timed Selective Spiking in a Population

Proposition 6. *The C neuron regularized minimum energy timed selective spiking problem P6, can be constructed as a two point boundary value problem.*

[1] Note *P5* can be also formulated as a two point boundary value problem

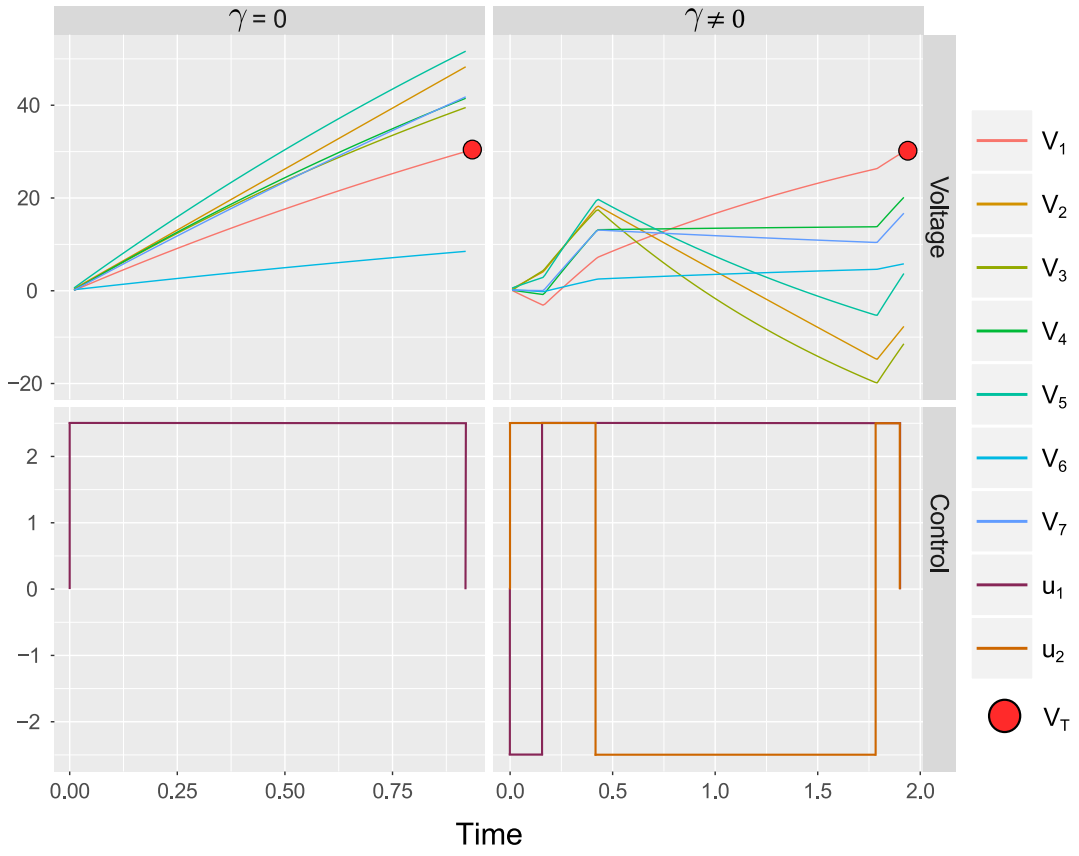

Figure 2.8: (Left:) The solution of problem *P4* with no regularization on the terminal states ($\gamma = 0$). The optimal controls are simply BANG (as expected) and there are 5 collateral spikes in addition to Neuron 1. (Right:) Voltage trajectories and controls are shown for the regularized problem with ($\gamma = {}^{\cdot 2}/_{V_T}$). No collateral spike is generated and the controls are BANG-BANG with 1 and 2 switches, respectively.

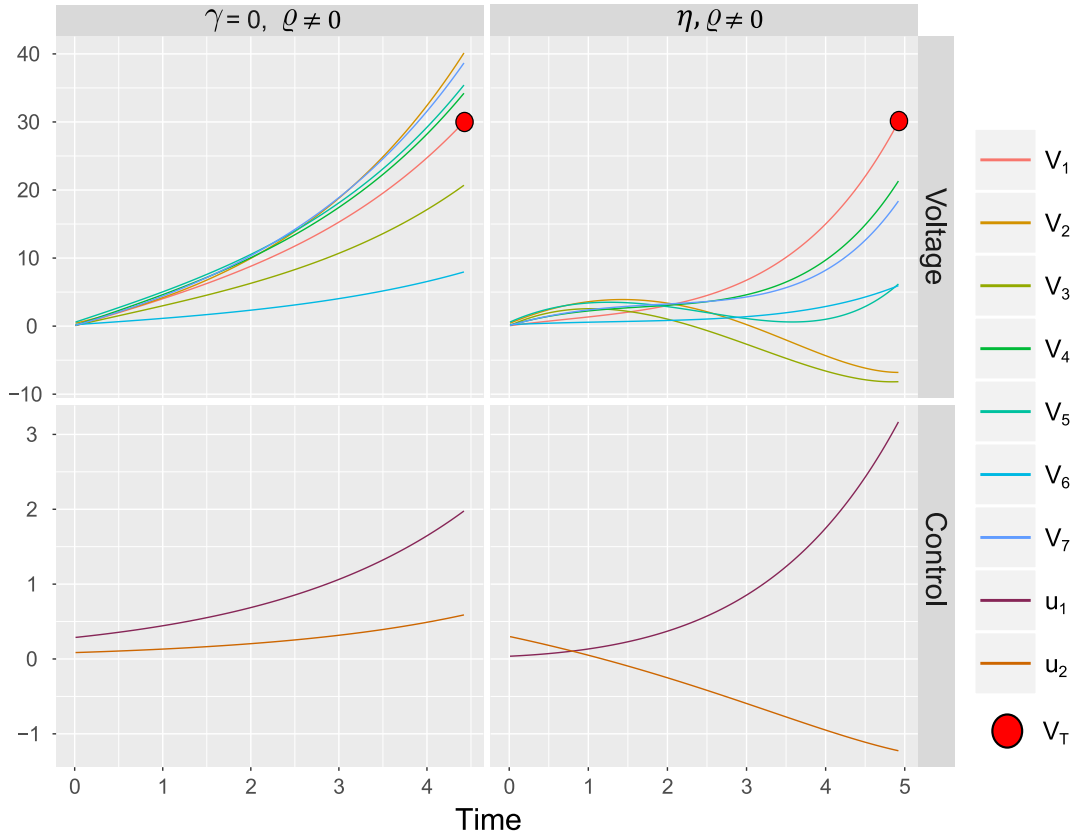

Figure 2.9: (Left:) The voltage trajectories and controls are shown as a function of time with no regularization on the terminal states ($\gamma = 0, \varrho = .1$) in *P5*. In this case, 4 collateral spikes are induced along with Neuron 1. (Right:) Voltage trajectories and controls are shown for the regularized problem with ($\gamma = {}^{5}/_{V_T}, \varrho = .1$). In this case, too, the selective spiking in Neuron 1 is ensured. Note that for both the cases $\gamma = 0, \gamma = {}^{5}/_{V_T}$, the optimal controls take the form of exponential kernels.

Proof: The Hamiltonian for this problem is

$$\mathcal{H}(\boldsymbol{\lambda}, \mathbf{v}, u) = \frac{1}{2}\varrho u^2 + \boldsymbol{\lambda}(\mathbf{A}\mathbf{v} + \mathbf{b}u). \tag{2.94}$$

From necessary conditions of optimality, we have (2.91) and the terminal constraints on the adjoint variables given by (2.85). From the transversality condition on the Hamiltonian, we have

$$\mathcal{H}(\tau) - (\tau_d - \tau) = 0. \tag{2.95}$$

For this problem we first re-scale the time $\bar{\tau} = {}^{t}/_{\tau}$ such that $\bar{\tau} \in [0, 1]$ to give a fixed endpoint problem. Adding τ to the augmented state vector we have

$$\mathbf{y} = [\mathbf{v}^T \ \boldsymbol{\lambda} \ \tau]^T \in \mathbb{R}^{2C+1} \tag{2.96}$$

and the state derivatives will be modified as $\frac{\mathrm{d}\mathbf{y}}{\mathrm{d}\bar{\tau}} = \tau \frac{\mathrm{d}\mathbf{y}}{\mathrm{d}t}$. Now we have a two point boundary value problem with the nonlinear differential equation

$$\dot{\mathbf{y}} = y(2C+1) \begin{bmatrix} \mathbf{A} & -\frac{1}{\varrho}\mathbf{b}\mathbf{b}^T & 0 \\ \mathbf{0} & -\mathbf{A} & 0 \\ \mathbf{0} & \mathbf{0} & 0 \end{bmatrix} \mathbf{y} \tag{2.97}$$

and boundary conditions (2.85), (2.95) for the time rescaled system

$$\begin{aligned} &\mathbf{y}_v(0) = \mathbf{y}_0 \ \text{ (given)}, \ \ y_1(1) = V_T \\ &\mathbf{y}_{adj}(1) = \gamma \, \mathbf{W}\mathbf{y}_v(1) + [\nu \, 0 \cdots 0]^T \\ &\mathbf{y}_{adj}^T(1)\mathbf{A}\mathbf{y}_v(1) - \frac{1}{2\varrho}\mathbf{y}_{adj}^T(1)\mathbf{b}\mathbf{b}^T\mathbf{y}_{adj}(1) - (\tau_d - y_t) = 0 \end{aligned} \tag{2.98}$$

where for convenience of presentation we denote $\mathbf{y}_v = \mathbf{y}_{1,\ldots,C} = \mathbf{v}$, $\mathbf{y}_{adj} = \mathbf{y}_{C+1,\ldots,2C} = \boldsymbol{\lambda}^T$, $\mathbf{y}_t = y_{2C+1} = \tau$. □

2.5.5 One Step Greedy Pattern Control

Until now, we have focused our discussion on single spike events. In this section, we present a one step greedy algorithm for the control design of multi-spike patterns using *P6*. Here we repeatedly solve *P6* to minimize the difference between the target and achieved spike time for the desired spike, ascertained by any target spike pattern Σ_P where for the k^{th} spike the target time τ_d^k is determined by $\tau_d^k = t_k - t_{k-1}$, $k = 1, \ldots, K$, $t_0 = 0$. In Figure 2.10, we show an example of this strategy for a population with $C = 5$ neurons parametrized as in (2.93), $S = 2$ inputs, and a randomly selected 10-spike target pattern $\Sigma_P = [(3, 16.8), (4, 44.2), (1, 52.4), (2, 87.5), (1, 88.6), (1, 115.4), (1, 132.1), (2, 154.4), (2, 160), (3, 168)]$. We plot the resulting voltage traces (top panel) and the control waveform (bottom panel) from successive application of *P6*. Note that because of the regularized formulation in (2.18), we induce collateral firing in Neuron 1 before the second spike. We have used the MATLAB solver **bvp4c** [56] for the numerical solution of the two point boundary value problem in *P6*.

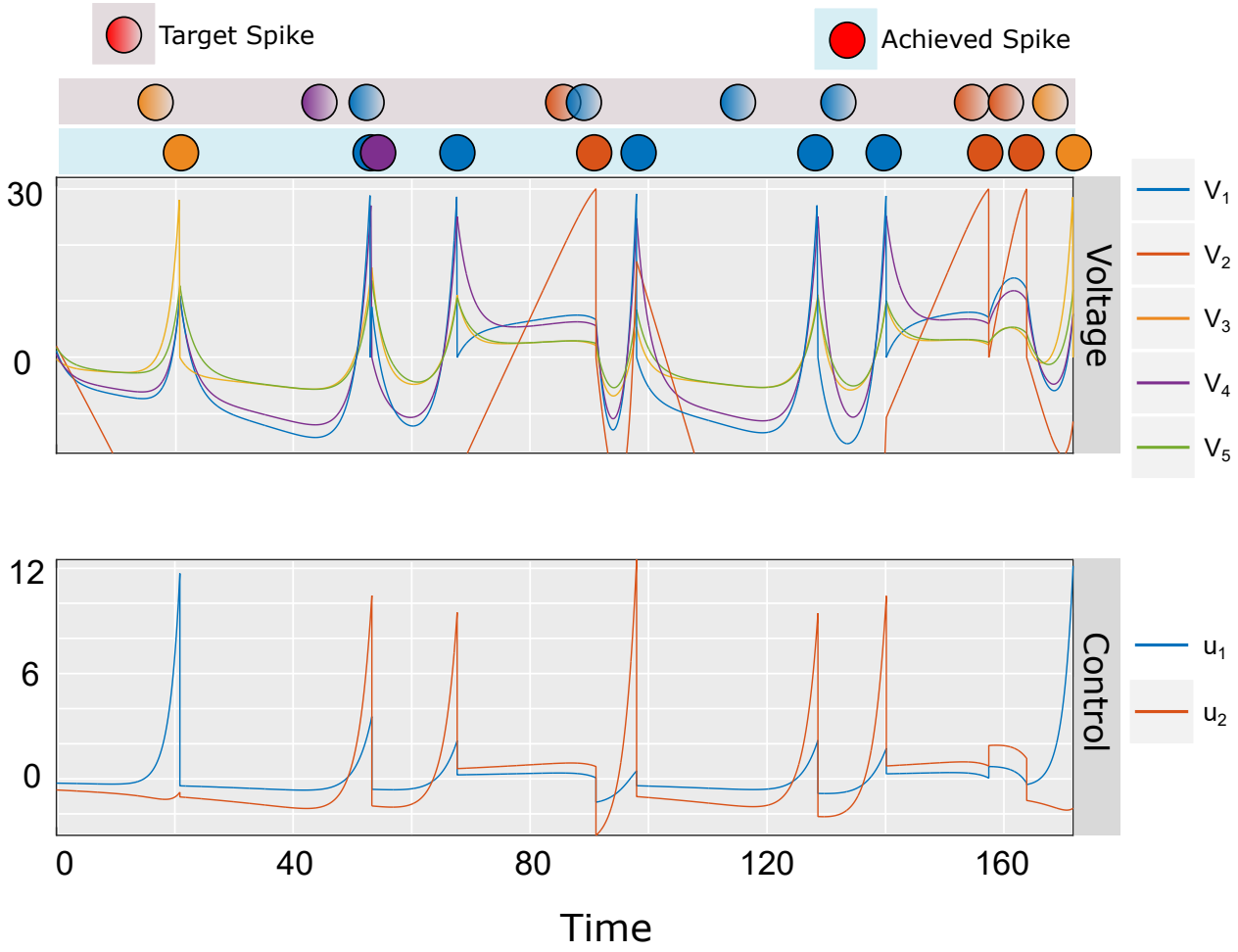

Figure 2.10: Circles in the Top two rows: Target and achieved spikes placed at corresponding times, color coded to represent neuron indices. (Top Panel): Neuron voltages excited by the one step greedy design. (Bottom Panel): Optimized control generated stepwise for each spike in Σ_P.

2.6 Discussions

Here we have studied an optimal control treatment of the neurocontrol problem for LIF dynamics. Instead of adopting classical controllability methods, we analyzed these problems in the context of neural systems - i.e, can any desired spike pattern be induced through exogenous stimulation? We have ascertained that in pairs of neurons, a minimum amount of heterogeneity in the parameters is critical to achieving different spike patterns. We illustrated that even in the case of two neurons, an optimal control solution may not be achievable; but through greedy algorithm, numerical optimization, and regularization, we can obtain efficient results both in pairs and networks of neurons. That said, the next question is how to broaden these results when the neuronal dynamics is non-linear and stochastic? The consensus in the neuroscience community is that neural spiking is inherently noisy, and in the next chapter we address these issues by formulating the neurocontrol problem in a stochastic setting.

Chapter 3

Neurocontrol II: Probabilistic Framework

Recently, the problem of extrinsic neurocontrol has been formulated for the class of statistical models [39], namely PPGLM, where the rate of neural spiking (assumed to follow Poisson distribution) is fitted using Generalized Linear Model. In the Poisson class of random processes, the rate function associated with a neuron governs its probability of producing a spike at any moment in time. Thus, in a statistical model, neuronal spikes are described as binary events in a particular output realization. As of yet, no methods for basic control analysis have been developed for these models. Such analysis is needed in order to provide baseline characterizations such as establishing whether or not a design objective is feasible. For instance, it would be vacuous to attempt a design on a system that is not yet theoretically controllable. The goal of this chapter is to bridge this gap by providing a set of quantitative metrics, based on dynamic optimization, that assay the control properties of a statistical neural model to enable basic characterizations (e.g., given two PPGLMs, which is 'more controllable') and, eventually, the problem of input design.

3.1 Preliminaries

In this section we first demonstrate the intuition behind using a PPGLM to model the spiking activity in neurons and then proceed to develop the probabilistic descriptions of patterns of activity in these neurons.

3.1.1 Notation

A point process is an integer-valued stochastic process that models the occurrence of isolated events in time and space, e.g., neural spiking. The inhomogeneous Poisson process is one such example that can capture temporal dependencies via a time-varying rate/intensity function [57]. Generalized Linear Models (GLMs) provide a regression framework to model output variables $\mathbf{Y}$ with respect to the input/explanatory variables $\mathbf{X}$. GLMs assume that a transformation of the conditional mean of $\mathbf{Y}$ is a linear function of $\mathbf{X}$, i.e.,

$$g(\mathbb{E}(\mathbf{Y}|\mathbf{X})) = \mathbf{X}\boldsymbol{\beta} \tag{3.1}$$

where $g(.)$ is the link function and $\boldsymbol{\beta}$ is a vector of unknown parameters. Combining point processes with GLMs, i.e., modeling the rate function of neurons by a GLM, results in a PPGLM, the primary object of study in this chapter.

Throughout this dissertation, events and spikes are used synonymously. Most mathematical notation is standard. The continuous time univariate and multivariate point processes are indicated by $N(t)$ and $\mathbf{N}(t)$, $t \in \mathbb{R}^+$ respectively, whereas $N_{t'}$ and $\mathbf{N}_{t'}$, $t' \in \mathbb{N}$ denote their discrete counterpart. In a univariate discrete process, N_i, the value of discrete process at the i-th window, is a scalar. For a multivariate discrete process, $\mathbf{N}_i$ is a vector of all variables at

the i-th window and $N_{c,i}$ is a scalar that represents the value of the c-th variable in the i-th time bin. We follow the same notation for the associated difference processes.

3.1.2 Model Description (Exclusive Event Point Process)

We first consider a univariate inhomogeneous Poisson process $N(t)$ with the intensity (event rate) function $\lambda(t|H(t))$, where $H(t)$ denotes the history of the process along with other covariates, i.e.,

$$\lambda(t|H(t)) = \lim_{\Delta \to 0} \frac{\Pr[N(t+\Delta) - N(t) = 1|H(t)]}{\Delta}. \tag{3.2}$$

We divide the total time window under consideration, $[0, T]$, into I intervals such that $\Delta = {}^{T}/_{I}$ and denote the discrete process as $N_i \equiv N(i\Delta)$ and $H_i \equiv H(i\Delta)$, $i = 1, ..., I$. This yields the difference process

$$\delta N_i = N_i - N_{i-1} = N(i\Delta) - N((i-1)\Delta). \tag{3.3}$$

We make the key assumption that $\Delta \ll 1$ ($\Delta \neq 0$), resulting in $\delta N_i \in \mathbb{B}$, where $\mathbb{B} := \{0, 1\}$. We separate the conditional intensity (3.2) into components related to the background activity, spiking history over Q lags, and S independent extrinsic control inputs $\mathbf{U} \in \mathbb{R}^{S \times I}$, up to P previous instances via the log-link model

$$\lambda_i \equiv \lambda(i\Delta \mid \mathbf{X}, H_i) = \exp(\beta_0 + \sum_{q=1}^{Q} \beta_q \, \delta N_{i-q} + \sum_{s=1}^{S} \sum_{p=0}^{P} \gamma_p^s \, u_{s,i-p}) = \exp(\boldsymbol{\theta}^T \mathbf{x}_i). \tag{3.4}$$

The parameter set is given by $\boldsymbol{\theta} = [\beta_0 \dots \gamma_P^S]^T \in \mathbb{R}^F$, $F = 1 + Q + (P+1)S$ and the co-variate matrix $\mathbf{X} \in \mathbb{R}^{F \times I}$ with the i-th column $\mathbf{x}_i$ as

$$\mathbf{x}_i = [1 \; \delta N_{i-1} \dots \delta N_{i-Q} \; u_{1,i} \dots u_{S,i-P}]^T, \tag{3.5}$$

$\forall i = 1 \ldots I.$

The joint likelihood of a particular realization of $N(t)$ with k spikes over the I intervals, conditioned on $\mathbf{X}$, follows the form detailed in [58]

$$\Pr(\mathbf{N}|\mathbf{X}) = \exp\left(\sum_{c=1}^{C}\sum_{i=1}^{I} \delta N_{c,i} \log(\lambda_{c,i}\Delta) - \lambda_{c,i}\Delta\right) + o(\Delta^k). \tag{3.6}$$

where any function $f(x) \in o(h(x))$ implies that $\lim_{x\to 0} \frac{f(x)}{h(x)} \to 0$. We extend this model for the C-variate process $\mathbf{N}(t)$ as in [59] and the log-likelihood for small Δ can be written as

$$L(\mathbf{N}|\mathbf{X}) \equiv \log(\Pr(\mathbf{N}|\mathbf{X})) = \sum_{c=1}^{C}\sum_{i=1}^{I}\left(\delta N_{c,i} \log(\lambda_{c,i}\Delta) - \lambda_{c,i}\Delta\right), \tag{3.7}$$

where

$$\lambda_{c,i} = \exp(\beta_0^c + \sum_{c'=1}^{C}\sum_{q=1}^{Q} \beta_q^{c',c}\, \delta N_{i-q} + \sum_{s=1}^{S}\sum_{p=0}^{P} \gamma_p^s\, u_{s,i-p}).$$

In terms of neural spiking, this set of co-variates captures:

1. any baseline activity in the network, via the bias term $(\beta_0^c)_{c=1}^C$;
2. refractory periods following a spike in the c-th neuron, via the self process history $(\beta_q^{c,c})_{q=1}^Q$;
3. afferent excitation or inhibition from other neurons, via the network spiking history $(\beta_q^{c,c'})_{c'=1,c'\neq c}^C$;
4. temporal dynamics (e.g., exponentially decaying) of the excitation or inhibition from other neurons, via additional history terms $(\beta_q^{c,c'})_{c'=1,q=1}^{C,Q}$; and
5. effect of any extrinsic stimulation and the integrative nature in which the neurons process such information, via the current stimulus and the history terms $(\gamma_p^{p,s})_{p=0,s=1}^{P,S}$.

However, more detailed biophysical dynamics associated with sub-threshold membrane potential and particular ion channels are outside the explanatory power of this model.

3.1.3 Model Description (Simultaneous Event Point Process)

The model described in (3.2)–(3.7), albeit useful in many contexts, is limited because it excludes multiple neurons producing simultaneous spiking events. Thus, we also consider a second model, a discrete-time, multinomial generalized linear model of a simultaneous event multivariate point process (SEMPP) [60, 61]. The coincidence of spiking events (simultaneous events) from different neurons in the interval Δ, is handled by projecting the system onto higher dimensions such that only a single kind of event can occur at any interval.

Briefly, for a C-dimensional inhomogeneous Poisson process $\mathbf{N}(t)$, a new $M = 2^C - 1$ dimensional marked point process $\mathbf{N}^*(t)$ is defined such that at any interval, there is at most one non-zero bit. The conditional intensity function for this marked point process $\mathbf{N}^*(t)$ is defined as $\lambda^*_m(t|H(t))$, $m = 1, ..., M$, similar to (3.2) where $H(t)$ denotes the history of the process along with other covariates.

Once again with $\Delta = {}^{T}/_{I} \ll 1$ ($\Delta \neq 0$) over the time window $[0, T]$, we denote the discrete process as $N_{c,i}$ for $c = 1 \dots C$ which yields the difference process $\delta N_{c,i}$ (for the multivariate point process), $\delta N^*_{m,i} \in \mathbb{B}$ (for the marked point process) similar to (3.3). In matrix representation we can write

$$\delta \mathbf{N} = \mathbf{D}\mathbf{N}, \tag{3.8}$$

where $\mathbf{D} \in \mathbb{R}^{I \times I}$ transforms $\mathbf{N}$ to its difference process $\delta \mathbf{N}$ (similarly for the marked process $\mathbf{N}^*$). Here a logistic-link function is used to relate the co-variates with the rate of the process,

$$\log \frac{\lambda^*_{m,i}\Delta}{1-\lambda^g_i\Delta} = \beta^m_0 + \sum_{c=1}^{C}\sum_{q=1}^{Q}\beta^{m,c}_q\,\delta N_{c,i-q} + \sum_{s=1}^{S}\sum_{p=0}^{P}\gamma^{m,s}_p\,u_{s,i-p} = \boldsymbol{\theta}^T_m\mathbf{x}_i, \tag{3.9}$$

where $\lambda^g_i = \sum_{m=1}^{M}\lambda^*_{m,i}$ is the conditional intensity for the discrete ground process [62] $N^g_{t'}$ at $t' = i$. $\boldsymbol{\theta}_m$ is the m-th row of the parameter matrix $\Theta \in \mathbb{R}^{M\times F}$ with

$$F = 1 + QC + (P+1)S \tag{3.10}$$

co-variates at each interval. Θ reflects the dependence of the intensity function on the co-variates $\mathbf{X} \in \mathbb{R}^{F\times I}$. The log-likelihood for the marked point process conditioned on the co-variates $\mathbf{X}$, is given by

$$L(\mathbf{N}^*|\mathbf{X}) = \log(\Pr(\mathbf{N}^*|\mathbf{X})) = \sum_{i=1}^{I}\sum_{m=1}^{M}\delta N^*_{m,i}\boldsymbol{\theta}^T_m\mathbf{x}_i - \sum_{i=1}^{I}\log\left(1+\sum_{m=1}^{M}\exp(\boldsymbol{\theta}^T_m\mathbf{x}_i)\right). \tag{3.11}$$

In the analysis that follows, we work with both the likelihood models in (3.7), (3.11). Much of the analysis that follows will be based on characterizing how the number of events (spikes) in a target realization impacts these likelihoods. We specifically consider the spike count $\Psi : \mathbb{R}^{C\times I} \to \mathbb{R}$,

$$\Psi(\delta\mathbf{N}) = \Psi(\mathbf{ND}) = \mathbf{b}^T\delta\mathbf{N}\mathbf{1}_I = \sum_{c=1}^{C}\sum_{i=1}^{I} b_c\,\delta N_{c,i}, \tag{3.12}$$

as the number of events in the realization. For the exclusive event process $\mathbf{b} = \mathbf{1}_C \in \mathbb{R}^C$ and (3.12) reduces to

$$\Psi(\delta\mathbf{N}) = \sum_{c=1}^{C}\sum_{i=1}^{I}\delta N_{c,i}. \tag{3.13}$$

For SEMPP, $\mathbf{b} \in \mathbb{R}^M$ contains the number of events associated with each dimension of the projected point process, e.g., for $C = 3$, the projected dimension is $M = 7$ and

$$\mathbf{b} = [1\,1\,2\,1\,2\,2\,3]^T, \tag{3.14}$$

corresponding to all possible combinations, i.e., three 1-spike events, three 2-spike events and one 3-spike event.

3.2 Control Analysis of Statistical Spiking Models

In this section based on the likelihood models developed above we approach the question of controllability in spiking networks from a probabilistic standpoint. In particular we identify spike count as a key marker that relates to the probability of achieving any spike pattern as a function of extrinsic control.

3.2.1 ϵ-Controllability for PPGLMs

We first consider an analogue to the classical notion of controllability. As a statistical model, any such notion must involve the likelihood of particular realizations, heretofore referred to as *target patterns*. As such, we first consider the following candidate:

Definition 4 ($\epsilon-$Controllability for PPGLMs)**.** *A PPGLM is $\epsilon-$controllable if, for all $\epsilon > 0$, there exists an input $\mathbf{U}$ such that any realization $\mathbf{N}(t)$ of the PPGLM can attain a log-likelihood satisfying*

$$-\epsilon \leq L(\mathbf{N} \mid \mathbf{U}) \leq 0. \tag{3.15}$$

Despite its intuitive appeal, the following highlights that the notion of $\epsilon-$controllability is too strong to be of practical utility in the desired context.

Lemma 2. *The PPGLM described in* (3.7), (3.11) *is not* $\epsilon-$ *controllable, even if the energy of the input* $\mathbf{U}$ *is unconstrained.*

Proof: The proof is given in Appendix B.1, and hinges on the fact that the likelihood function is in fact strictly concave in $\mathbf{U}$. □

The Lemma establishes that allowing $\mathbf{U}$ to assume arbitrarily large energy confers no advantage in controlling the PPGLM. This is conceptually different from classical control analysis, where allowing progressively larger energy (in general) improves the overall range of trajectories that can be induced. Two points should be considered when interpreting this result. First, our analysis focuses on at most one event in each time bin. With increasing energy, one may increase the likelihood on *an* event, but not necessary a single one. Second, in a coupled network scenario, applying a large input in order to target a spike in a particular neuron will have collateral effects elsewhere in the network. However, clearly some *minimum* energy is required in order to maximize the likelihood of given realizations.

3.2.2 Event Count as a Surrogate for Pattern Complexity

As a consequence of Lemma 2, we seek a characterization that examines the complexity of the realizations (spike patterns) that can be induced. Below, we establish that the spike count, i.e. simply the number of spikes contained in a particular realization (i.e. (3.12)), can serve as an informative marker in this regard.

Lemma 3. *For a PPGLM of the form* (3.4)–(3.7) *with infinitesimally small interval* ($\Delta \ll 1$), *the maximum likelihood of any realization decreases with respect to number of events.*

Proof: The proof is given in Appendix B.2. □

Lemma 3 is most easily understood in a *fully actuated* scenario wherein each neuron receives its own, independent control input. In this case, it is straightforward to show that the control can be designed to negate any effect of process history. Consider the likelihood model of (3.7) with $S = C$ along with $P = 0$ and $\gamma_0^{c,s} = 0$ for $c \neq s$, i.e., $\boldsymbol{\gamma}_0$, which reflects how the current input affects all the processes, is a C-dimensional vector. Since here the probability of an event is independent at each time and other input indices, we can analyze the likelihood for each i and c separately, i.e.,

$$\max_{\mathbf{U}\in\mathbb{R}^{C\times I}} \; L(\mathbf{N} \mid \mathbf{U}) = \sum_{i=1}^{I}\sum_{c=1}^{C} \max_{u_{c,i}\in\mathbb{R}} \; L(N_{c,i} \mid u_{c,i}) = \sum_{i=1}^{I}\sum_{c=1}^{C} \max_{u_{c,i}\in\mathbb{R}} \; L_{c,i}, \tag{3.16}$$

where

$$L_{c,i} \equiv L(N_{c,i} \mid \mathbf{u}_i) = \delta N_{c,i}\,(\boldsymbol{\theta}_c^T \mathbf{x}_i + \log\Delta) - \Delta\exp(\boldsymbol{\theta}_c^T \mathbf{x}_i). \tag{3.17}$$

For $\delta N_{c,i} = 0$, (3.17) reduces to

$$L_{c,i} = -\Delta\exp(\boldsymbol{\theta}_c^T \mathbf{x}_i) = -\Delta\exp(r_{c,i} + \gamma_0^c\, u_{c,i}). \tag{3.18}$$

We observe that given any $\epsilon' > 0$,

$$L_{c,i}(\delta N_{c,i} = 0 \mid u) \geq -\epsilon' \;\text{ when } u \leq u_{c,i}^*, \tag{3.19}$$

where $u_{c,i}^* = \frac{1}{\gamma_0^c}(\log(\frac{\epsilon'}{\Delta}) - r_{c,i})$, assuming $\gamma_0^c > 0$. In other words, for the pattern consisting of all zeros, the likelihood indeed can be made arbitrarily close to one (for the fully actuated case). We now show that the addition of any spike to the pattern results in likelihood degradation.

Specifically, for $\delta N_{c,i} = 1$, we can maximize the indexed likelihood as

$$L_{c,i}(\delta N_{c,i} = 1 \mid u^*_{c,i}) = -1 \text{ with } u^*_{c,i} = -\frac{1}{\gamma_0^c}(\log\Delta + r_{c,i}). \tag{3.20}$$

Since the maximum likelihood of each $L_{c,i}$ is fully determined by the input $u_{c,i}$, we can design an extrinsic control $\mathbf{u}^*$ using (3.19), (3.20) that maximizes the likelihood for the whole realization, i.e. from (3.16)

$$\begin{aligned} L(\mathbf{N}|\mathbf{U}^*) &= \sum_{\delta N_{c,i}=0} L_{c,i}(\delta N_{c,i} = 0|\mathbf{U}^*) + \sum_{\delta N_{c,i}=1} L_{c,i}(\delta N_{c,i} = 1|\mathbf{U}^*) \\ &= -(CI - \Psi(\delta\mathbf{N}))\epsilon' - \Psi(\delta\mathbf{N}) \end{aligned} \tag{3.21}$$

Now for unconstrained inputs we have

$$\lim_{\epsilon'\to 0} L(\mathbf{N} \mid \mathbf{U}^*) \approx -\Psi(\delta\mathbf{N}), \tag{3.22}$$

i.e., the maximum likelihood decreases with the number of events $\Psi(\delta\mathbf{N})$ in any realization $\mathbf{N}$ of the process $\mathbf{N}(t)$.

A similar analysis can be carried out for the fully actuated SEMPP model, wherein we can treat marked process independently and use (3.16) to maximize the likelihood over the whole realization. In this case, the likelihood at the c-th process, i-th time index is

$$L_{c,i} \equiv L(N_{c,i} \mid \mathbf{u}_i) = \delta N_{c,i}\, \gamma\, u_{c,i} - \log(1 + \exp(\gamma' u_{c,i})). \tag{3.23}$$

Since the inputs are unconstrained, the total contribution from the co-variates can be reformulated in terms of only two parameters γ, γ' $\forall\, c, i$. Also note that we have removed the asterisk indicating the marked point process since analyzing each process independently in one dimension means, $\delta N^*_{c,i} = \delta N_{c,i}$. For $\delta N_{c,i} = 0$, we can achieve probability approximately

close to one and can obtain a similar version of (3.19). When $\delta N_{c,i} = 1$, the maximum is attained at

$$L_{c,i}(\delta N_{c,i} = 1 \mid u^*_{c,i}) = \varphi(\gamma, \gamma') \text{ with } u^*_{c,i} = \frac{1}{\gamma'}\log(\frac{\gamma}{\gamma' - \gamma}), \tag{3.24}$$

where

$$\varphi(\gamma, \gamma') = \log\left(\frac{\gamma^{\frac{\gamma}{\gamma'}}}{\gamma'(\gamma' - \gamma)^{\frac{\gamma}{\gamma'}-1}}\right) < 0. \tag{3.25}$$

The likelihood maximization in (3.24) is independent of each c, i and similar to (3.21), we have

$$L(\mathbf{N}|\mathbf{u}^*) \approx \Psi(\delta\mathbf{N})\varphi(\gamma, \gamma'). \tag{3.26}$$

Thus, from our analysis of both the likelihood models (3.7), (3.11), we can conclude that in terms of likelihood, increasing the number of spikes in a pattern results in likelihood degradation, which can be interpreted as greater control difficulty.

3.2.3 Estimation of Complexity-based Viable Sets

Clearly, there are many factors in addition to spike count that determine the likelihood of a particular realization of a considered PPGLM. Indeed, not all patterns with the same spike count will generate the same likelihood. Accepting this limitation (see also Section 3.5), we will leverage the result of the previous section to form a tractable, accurate assay for the control properties of a PPGLM in terms of spike count. We proceed first by introducing the notion of a viable pattern set, which is analogous to the reachable set for a classical control system.

Definition 5 (ρ-Viable Pattern Set)**.** *Consider an arbitrary M-dimensional PPGLM defined over I intervals. Given a likelihood threshold ρ, the ρ-Viable Pattern Set, $\mathcal{N}(\rho\,; C, I, \mathcal{U})$, is*

the set of patterns defined as

$$\mathcal{N}(\rho\,; C, I, \mathcal{U}) = \{\mathbf{N} \in \mathbb{R}^{C\times I} \mid \exists\, \mathbf{U} \in \mathcal{U} \text{ s.t. } \Pr(\mathbf{N} \mid \mathbf{U}) \geq \rho\}, \tag{3.27}$$

where $\mathcal{U}$ denotes the set of admissible inputs.

It follows from Lemma 3 that, in general, $\mathcal{N}(\rho\,; C, I, \mathcal{U})$ includes all patterns with a spike count less than or equal to some maximally viable count, $\mu \leq CI$. We can thus formulate a relativistic analysis as follows.

Definition 6 ((μ, ρ)-Viability)**.** *For a likelihood threshold ρ and spike count μ, the PPGLM* (3.4)–(3.7)*, is (μ, ρ)-viable if $\exists\ \mathbf{U} \in \mathcal{U}$ such that*

$$\mathcal{N}(\rho\,; C, I, \mathcal{U}) \supset \mathcal{N}_\mu(C, I), \tag{3.28}$$

where $\mathcal{N}_\mu(C, I)$ denotes the set of all patterns with spike counts of μ or less, i.e., $\forall\, \mathbf{N} \in \mathcal{N}_\mu(C, I)$, we have

$$\Psi(\delta\mathbf{N}) = \mathbf{b}^T \delta\mathbf{N}\, \mathbf{1} \leq \mu \tag{3.29}$$

where $\delta\mathbf{N} \in \mathbb{B}^{C\times I}$ is the difference process corresponding to $\mathbf{N}$.

The key problem is now to obtain the maximally viable count, μ, for a given ρ. This amounts to a joint optimization problem for the spike count, $\Psi(\delta\mathbf{N})$, and control $\mathbf{U}$. Since the difference process imposes the constraint

$$\delta N_{c,i} = \{0, 1\},\ \ \forall\, c, i, \tag{3.30}$$

this optimization is a Nonlinear Mixed Integer program. To make this tractable, we relax the integer constraint and introduce a new variable χ, such that

$$\chi_{c,i} \in [0,1], \ \forall\, c,i. \tag{3.31}$$

This allows us to define a relaxed viability notion as follows.

Definition 7 (Relaxed maximally viable spike count)**.** *The relaxed maximally viable spike count μ_r is defined as*

$$\mu_r = \Psi(\chi) \tag{3.32}$$

and can be calculated from the solution of the following program,

$$\begin{aligned} \underset{\mathbf{U},\chi}{\textit{maximize}} \quad & \Psi(\chi) \\ \textit{subject to} \quad & L(\chi \mid \mathbf{U}) \geq \log(\rho) \\ & u_{s,i} \in \mathcal{U}, \ \forall\, s,i \\ & 0 \leq \chi_{c,i} \leq 1 \quad \forall\, c,i. \end{aligned} \tag{3.33}$$

While this optimization is still non-convex, we show below that numerical evaluation of the pairs (μ_r, ρ) leads to accurate, informative characterization of PPGLMs.

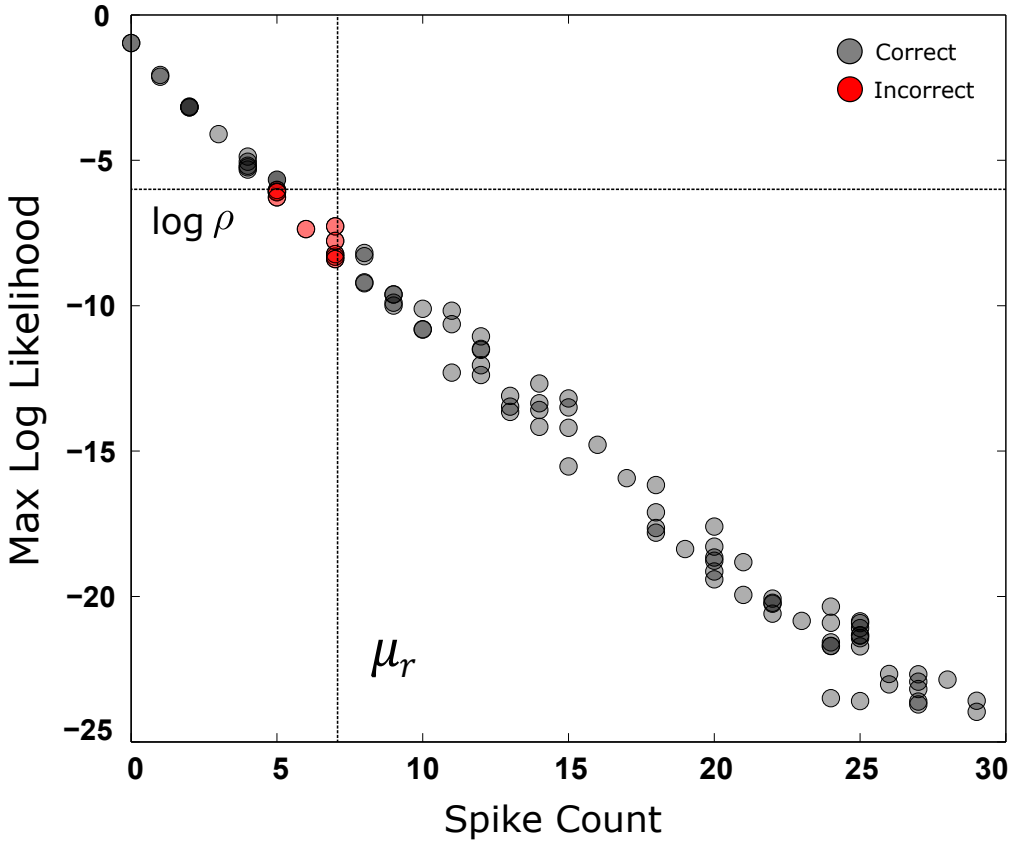

Figure 3.1: Accuracy of the relaxed maximally viable spike count (μ_r). The maximum likelihood is computed for 100 random realizations and compared to the predicted thresholds from the (μ_r, ρ)-controllability calculation ($\rho = 10^{-6}$).

3.3 Validation of the Analysis Framework

Here through numerical simulations we verify how relaxed maximally viable spike count affects the probability of achieving any pattern.

3.3.1 (μ_r, ρ)-Viability is Accurate

Figure 3.1 demonstrates the veracity of the relaxation in (3.33). We consider PPGLMs with randomly selected parameters Θ for $C = 3$ neurons, $Q = 6$ lags and $I = 10$ time bins. The inputs are constrained via $\mathcal{U} = [-5, 5]$. We solve (3.33) numerically[2] for the likelihood in (3.7) and find the relaxed maximum spike count $\mu_r = 7.08$ for $\rho = 10^{-6}$, $\Delta = 0.1$ and one independent input, i.e., $S = 1$. Then, the maximum likelihood is calculated individually for 100 random patterns and compared to the results of the (μ_r, ρ) optimization. Only 8/100 patterns are misclassified (spike counts that are below μ_r but nevertheless whose likelihoods do not exceed ρ). Patterns whose spike counts exceed μ_r are always classified correctly in this example.

3.3.2 (μ_r, ρ)-Viability Enables Salient Comparison of PPGLMs

Based on our formulation of (μ, ρ)-viability, if $\mu_r^1 > \mu_r^2$,

$$\left|\mathcal{N}^1(\rho)\right| > \left|\mathcal{N}^2(\rho)\right| \tag{3.34}$$

where $|.|$ denotes the cardinality of a set. We demonstrate the utility of the viability analysis via an example, where we show how the analysis can disassociate PPGLMs with

[2]We used a random sampling procedure over the initial conditions of our solver to ensure convergence to a robust local maximizer.

symmetric and asymmetric connectivity (see Figure 3.2A). We consider PPGLMs with the same structure, input constraint and window length as in the previous example and a fixed reference parametrization (essentially, the connectivity between units) $\Theta = \sigma \times \Theta_r$, where Θ_r is the base parameter. Two observations are of note in Figure 3.2B. First, a small amount of connectivity (via the scaling parameter $\sigma \in [0, 1]$) is advantageous for control, beyond which viability decreases monotonically. This numerical inference can, in fact, be substantiated via a formal analysis:

Lemma 4. *For a PPGLM modeling Exclusive or Simultaneous Event Processes with likelihoods defined in* (3.7), (3.11) *and connectivity defined via the parameters* $\beta_q^{m,c}$, $\forall\, q, m, c$ *($M = C$ for the log-link model), the likelihood of any given pattern is strictly concave with respect to the network connectivity parameters.*

Proof: The proof is contained in Appendix B.3, and is a variation of the proof of Lemma 2. □

The second observation is that an asymmetric topology is, in general, more viable than a symmetric topology, consistent with studies of similar 3-neuron motifs using dynamical systems models and Lie bracket-based controllability analysis [63].

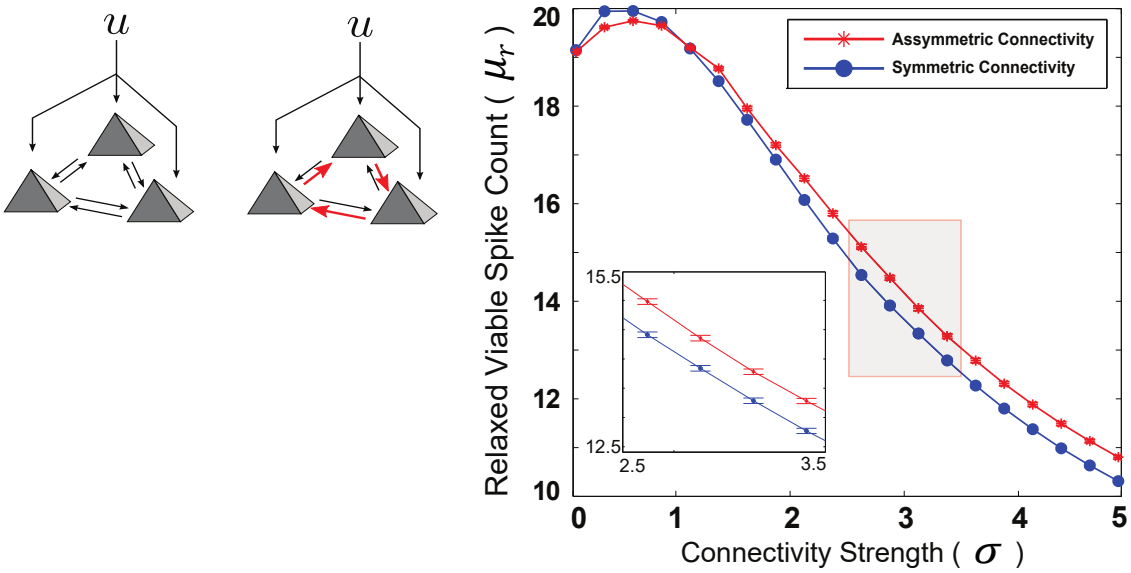

Figure 3.2: Symmetric and Asymmetric 3-neuron motifs. (B) μ_r vs. Connectivity weight σ for $\rho = 10^{-10}$.

3.4 Control Design of Statistical Spiking Models

The previous section focused on the development of the analytical framework for PPGLMs based on optimization. Along with this analysis, it is natural to also consider the overt design of an exogenous control input $\mathbf{U}^*$ to induce a specific target spiking pattern $\mathbf{N}_T$ with highest probability.

3.4.1 Control Design with Maximum Likelihood Estimation

Considering a cost function $\mathbb{J} : \mathbb{R}^{C\times I} \times \mathbb{R}^{C\times I} \to \mathbb{R}$, that accepts two patterns and returns a real number denoting how dissimilar they are, we can formulate the following optimization problem,

$$\mathbf{U}^* = \arg\min_{\mathbf{U}\in\mathcal{U}} \langle \mathbb{J}(\mathbf{N}, \mathbf{N}_T)\rangle_{\Pr(\mathbf{N}|\mathbf{U})} = \arg\min_{\mathbf{U}\in\mathcal{U}} \sum \mathbb{J}(\mathbf{N}, \mathbf{N}_T)\Pr(\mathbf{N}|\mathbf{U}), \tag{3.35}$$

where the sum is over all possible spike patterns $\mathbf{N}$. For a delta cost function $\mathbb{J}(\mathbf{N}, \mathbf{N}_T) = -\delta(\mathbf{N}, \mathbf{N}_T)$ as proposed in [39] we can rewrite (3.35) as

$$\mathbf{U}^* = \arg\min_{\mathbf{U}\in\mathcal{U}} - \Pr(\mathbf{N}_T|\mathbf{U}) = \arg\min_{\mathbf{U}\in\mathcal{U}} - \log\Pr(\mathbf{N}_T|\mathbf{U}) = \arg\min_{\mathbf{U}\in\mathcal{U}} - L(\mathbf{N}_T|\mathbf{U}). \tag{3.36}$$

Thus, the delta cost function reduces (3.35) to a maximum likelihood estimation (MLE) problem.

Proposition 7. *The maximum likelihood estimation problem of finding the extrinsic control* $\mathbf{U}^*$ *for the likelihood defined in* (3.7) *and* (3.11)*, under an energy constraint on the control, is convex.*

Proof: In Lemma 2, we have established that the likelihoods presented in (3.7) and (3.11) are strictly concave with respect to the extrinsic control $\mathbf{U}$, which makes (3.36) convex. □

Here, in addition to the delta cost function, we also studied a jittered cost function which encompasses K different patterns, structurally close (in terms of an appropriate metric) to the target pattern $\mathbf{N}_T$. In this case, the problem is:

$$\mathbf{U}^* = \arg\min_{\mathbf{U}\in\mathcal{U}} - \sum_{k=1}^{K} \omega_k \Pr(\mathbf{N}_k|\mathbf{U}) = \arg\min_{\mathbf{U}\in\mathcal{U}} - \sum_{k=1}^{K} \omega_k \, L(\mathbf{N}_k|\mathbf{U}) \tag{3.37}$$

where $\omega_k > 0$ denotes the weights assigned to the jittered patterns according to their similarity to the target pattern $\mathbf{N}_T$ with

$$\omega_k = \max\{\omega_1, \ldots, \omega_K\} \text{ when } \mathbf{N}_k = \mathbf{N}_T. \tag{3.38}$$

Figure 3.3 demonstrates a possible weighting strategy as a function of jitter in timing of spikes and in neurons, for a target pattern $\mathbf{N}_T$. The origin in the plane, indicating $\mathbf{N}_T$, gets

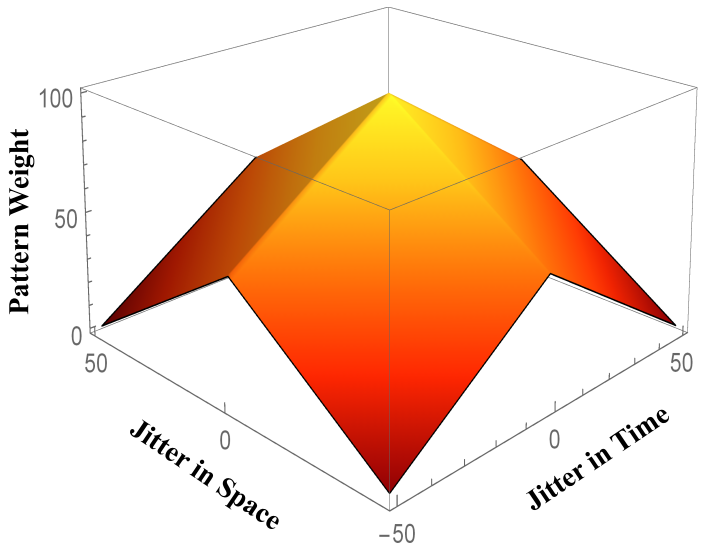

Figure 3.3: A schematic for assigning weights (ω_k) to the jittered cost function in (3.37). The target pattern $\mathbf{N}_T$ denoted as $(0, 0)$, in the middle, is given the most importance, whereas patterns with disturbance both in time and space (of neurons), progressively get lower weights.

the highest weight and the jittered patterns are weighted according to their proximity to $\mathbf{N}_T$.

Note that any constraint on energy (quadratic form) will not alter the convexity of the program. Also, any regularization in the cost in terms of energy effectively makes the problem a maximum *a posteriori* (MAP) estimation problem.

3.4.2 Analysis and MLE Design Example

Verification of the Controllability Analysis

Here we validate our controllability analysis results on a randomly parametrized PPGLM model equipped with a log-link function (3.4). First we solve for maximally viable spike count μ_r, (3.33) with $C = S = 4$, $\rho = 10^{-8}$, $\Delta = 0.01$ and $\mathcal{U} = [-10, 10]$. Then for some randomly chosen (μ_r, ρ)-viable pattern $\mathbf{N}_T$ (using (3.28) and (3.29)) shown in Figure 3.4 (top panel),

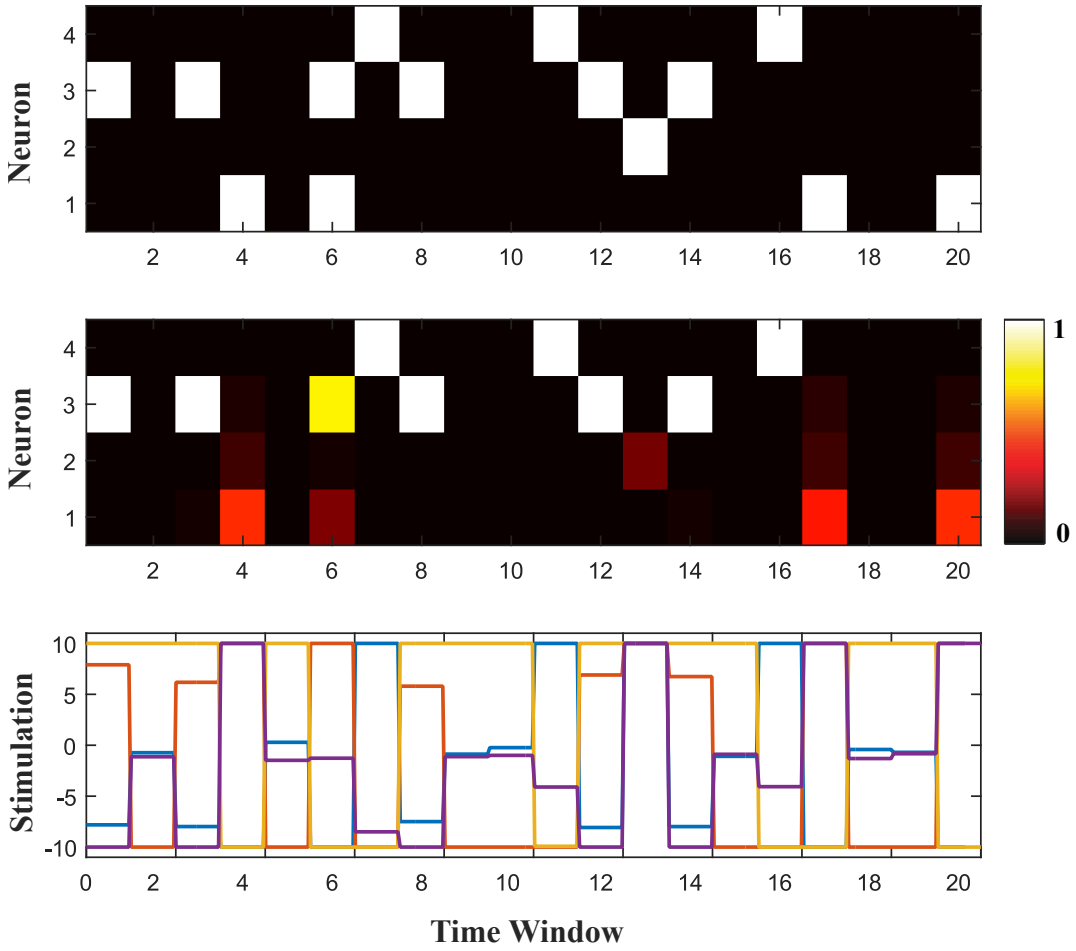

Figure 3.4: Validation of (μ, ρ)- viability. Top panel : A random pattern $\mathbf{N}_T$ with $\Psi(\delta\mathbf{N}_T) < \mu_r$ where μ_r is the solution of (3.33) for randomly chosen Θ. Middle panel : Achieved pattern in terms of probability of spiking in each window, with $\mathbf{U}^*$ from (3.36) and Bottom Panel : The optimized control $\mathbf{U}^*$ from the MLE problem.

we calculate $\mathbf{U}^*$ from the MLE problem in (3.36). In the middle and bottom panel of Figure 3.4 we plot the probability of spike in each window ($\lambda_{c,i}\Delta$) and the corresponding extrinsic control input $u_{s,i}\ \forall\, c, s, i$ from the maximization solution. We also observe that indeed the pattern $\mathbf{N}_T$ is ρ-viable (3.27). We note that in this example, the low probability of spiking in Neuron 1 is due to the presence of large excitatory connectivity between Neuron 1 and 2. Thus, the MLE solution biases the resultant pattern in order to avoid spurious spiking in Neuron 2.

Seven neuron coupled PPGLM network

We have thus far given two different formulations for the problem of controlling spike patterns in neural populations. Here we considered a 7 neuron, coupled PPGLM network for the fully actuated case i.e. $S = C = 7$ and solved (3.36), (3.37) for a target pattern, the letter '**W**' (see Figure 3.5). In Figure 3.5, we plotted the average realization, simulated from the solution of two different objectives in (3.36),(3.37) respectively. We achieved the target almost perfectly for the delta cost function, with the jittered cost function yielding a noisier output. However we noted that for the jittered objective, we obtained an energy efficient control.

PPGLM Control of Underlying Stochastic Integrate and Fire (INF) model

Finally, in this section we illustrate that our design strategy can be used indirectly to control dynamical systems models. Here we consider C coupled stochastic integrate and fire (INF) neurons of the form [49],

$$\begin{aligned} \frac{dv(t)}{dt} &= -\frac{1}{\tau_v}v(t) + \frac{1}{\mathcal{C}}(bu(t) + I_{syn}(t)) + \eta\, e(t) \\ I_{syn}(t) &= -g_{syn}(t)(v(t) - E_{syn}) \\ g_{syn}(t) &= \bar{g}\frac{(t-t_s)}{\tau_s}\exp\left(-\frac{(t-t_s)}{\tau_s}\right) \end{aligned} \tag{3.39}$$

where τ_v is the membrane time constant, $\mathcal{C}$ is the membrane capacitance, $e(t)$ is standard Gaussian white noise, η denotes the standard deviation of this noise, $u(t)$ is the extrinsic control input, b denotes the influence of the input on the neuron, $I_{syn}(t)$ is the synaptic current coming from a pre-synaptic neuron firing an action potential at time t_s, E_{syn} is the reversal potential of the synapse, $\bar{g}$ models the constant synaptic conductance and τ_s determines the decay of the synaptic current as time is elapsed from the incoming spike at t_s.

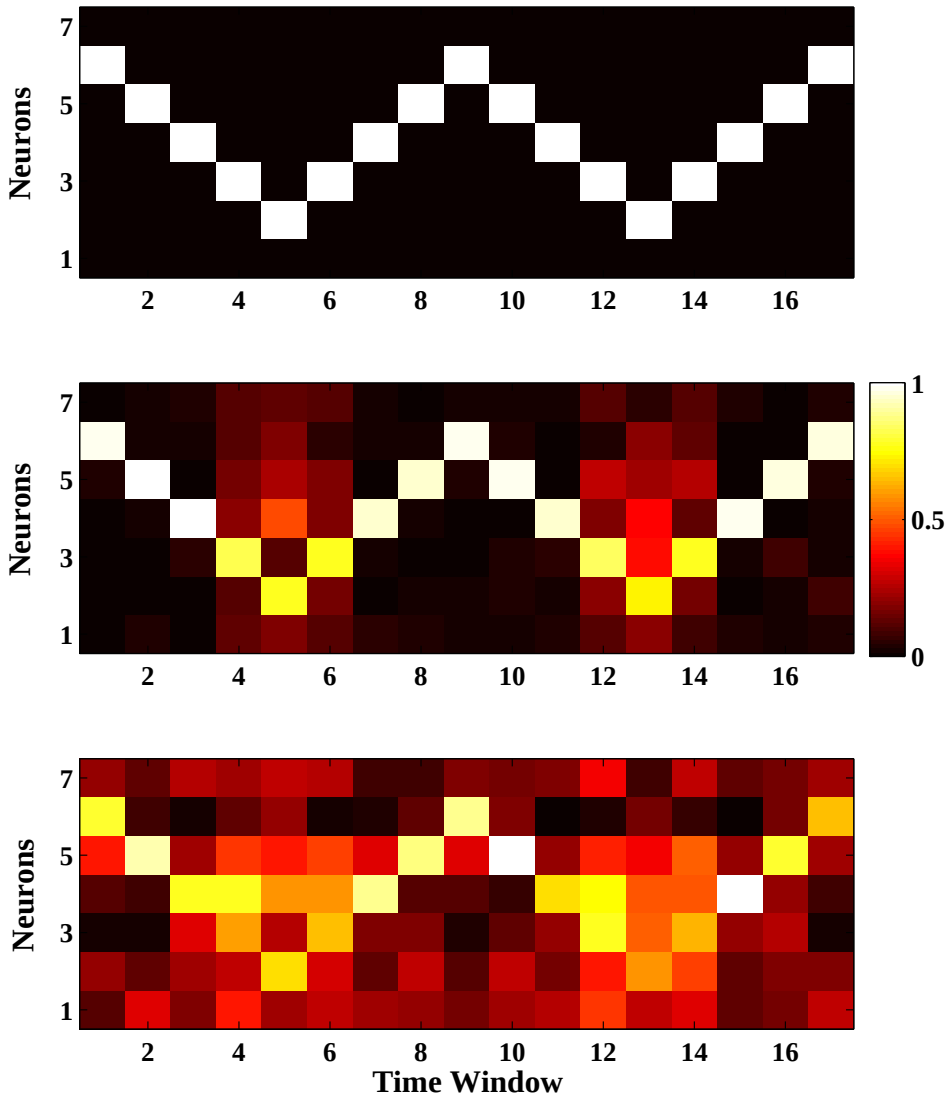

Figure 3.5: The solution of a jittered and delta cost function for a target pattern $\mathbf{N}_T$ = the letter "W" (top panel) in a population of $C = 7$ neurons. In the second panel, we solved the optimization problem (3.36) with $S = 7$ inputs and plotted the spike pattern averaged over several realizations. In the bottom panel, we solved the problem (3.37) with the same number of inputs and allowing spikes on either side of the target pattern with penalties. For this fully actuated case, we achieved the target spike train with high probability and the effect of adding jittered spikes is also very evident in the simulations.

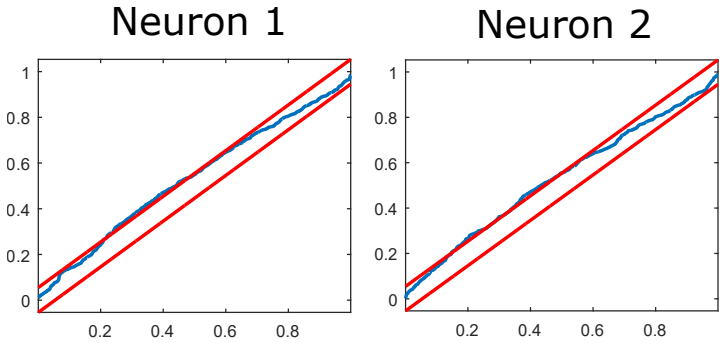

Figure 3.6: KS plots with 95% confidence bounds for goodness of fit assessment for a fully actuated two neuron INF network ($C = S = 2$) fitted using $Q = 3$ process history and $P = 5$ input history terms.

The model parameters for the neurons are given by

$$\begin{aligned} &\mathcal{C} = 10\ nF,\ \tau_v = 15\ ms,\ V_{rest} = -70\ mV, \\ &V_T = -50\ mV,\ E_{syn} = 70\ mV,\ \eta^2 = 2 \\ &\bar{g} \sim \mathbb{U}[0,1],\ \tau_s = 1\ ms,\ b \sim \mathbb{N}(0,1). \end{aligned} \tag{3.40}$$

Now, we determine the GLM model parameters Θ in a Monte Carlo fashion in $K_T = 500$ different trials. Exciting stochastic INF network with $\mathbf{U}(t)$ drawn from a Gaussian distribution such that $u_{s,i}(t) \sim \mathbb{N}(0, 50)\ \forall\, s, i$, produces spike patterns $\mathbf{N}_j$ for $j = 1 \ldots K_T$ and using these data we fit $\hat{\Theta}$ that best describes the training set. Conceptually, this is akin to a system identification step.

In Figure 3.7 we show the performance of the control $\mathbf{U}^*$, obtained from the delta objective, on the INF network for different cases of actuation (C neurons, S inputs). The covariate matrix $\mathbf{X}$ has three process lags ($Q = 3$) and input history ($P = 5$), selected based on the Akaike information criterion (AIC). Figure 3.6 shows the Kolmogorov-Smirnov (KS) goodness-of-fit test using time-rescaling theorem [64], which indicates that the model accurately reflects the data. With the hypothesis that the control inputs calculated from the PPGLM should also emit a spike train close to the target $\mathbf{N}_T$ (panel A) in the underlying dynamical model, we

stimulate the INF neurons with the same $\mathbf{U}^*$ (panel D). In panel B, C we show the generated spike pattern (averaged over several realizations) and one sample waveform, when the original stochastic INF neurons are excited by $\mathbf{U}^*$, and indeed we can see that the induced pattern is close to target $\mathbf{N}_T$. For validation of optimality of $\mathbf{U}^*$, in panel E we plot the achieved spike pattern for a randomly selected input. We observe that as underactuation becomes more prominent, the performance of $\mathbf{U}^*$ degrades. The simulation results were primarily generated using CVX with MATLAB interface.

Control Design for underlying Biophysical Models

To evaluate the utility of this design approach on a more complicated biophysical model, we further consider a network of diffusively coupled Fitzhugh-Nagumo (FN) neurons of the form [65]. Here the dynamics of the c-th neuron is given by

$$\begin{aligned} \frac{dv_c}{dt} &= v_c - \frac{v_c^3}{3} - w_c + bu(t) + \frac{\sigma_w}{C}\sum_{c'=1}^{C}(v_c - v_{c'}) + \eta\, e(t) \\ \tau\frac{dw_c}{dt} &= v_c + \bar{\alpha} - \bar{\beta} w_c, \end{aligned} \tag{3.41}$$

where v_c denotes the membrane potential, w_c the recovery variable, σ_w is the coupling strength, α, β, τ are system parameters and $u(t)$, $e(t)$ the extrinsic input and standard Gaussian white noise respectively as before in (3.39). In our simulations we have used

$$\begin{aligned} &\tau = 12.5,\ \bar{\alpha} = .7,\ \bar{\beta} = 0.8,\ \eta^2 = 0.5 \\ &\sigma_w \sim \mathbb{U}[0,1],\ b \sim \mathbb{N}(0,1). \end{aligned} \tag{3.42}$$

where $\mathbb{U}$ denotes uniform distribution. We use a spike detection algorithm that records a spike from simulated voltage for amplitudes higher than $V_T \sim 1\ mV$ [66] and refractory period of 2 ms. In Figure 3.8 we show the average achieved pattern and one voltage waveform (panel

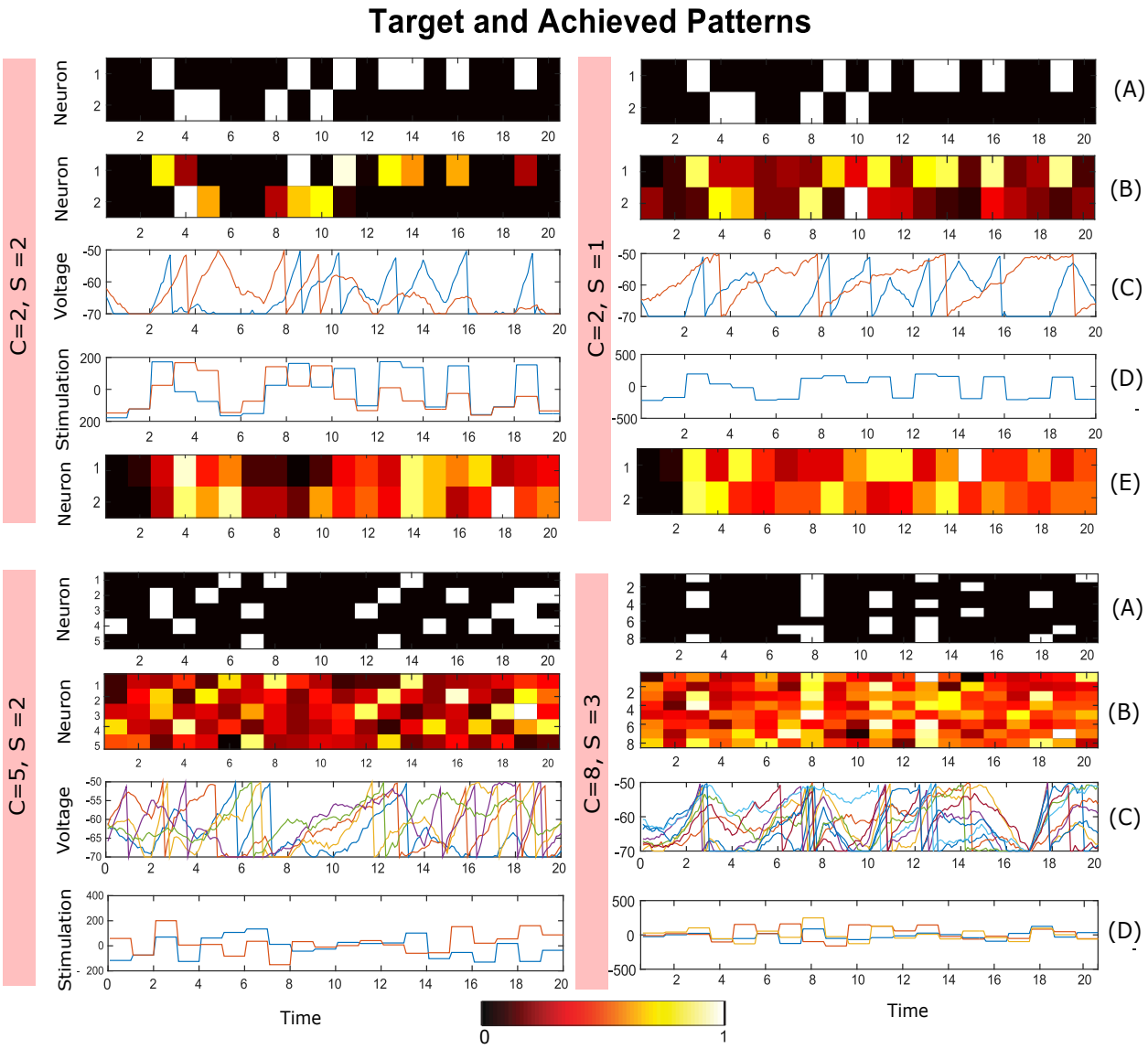

Figure 3.7: Control design for a C neuron coupled stochastic integrate and fire network. A : The target pattern for simulation study. B : The mean pattern over different realization for the INF neurons with the control $\mathbf{U}^*$. C: One realization of voltage traces for the two INF neurons under $\mathbf{U}^*$. D: The optimized input $\mathbf{U}^*$. E : The mean spiking pattern generated for a randomly selected $\mathbf{U}$ to validate optimality of $\mathbf{U}^*$.

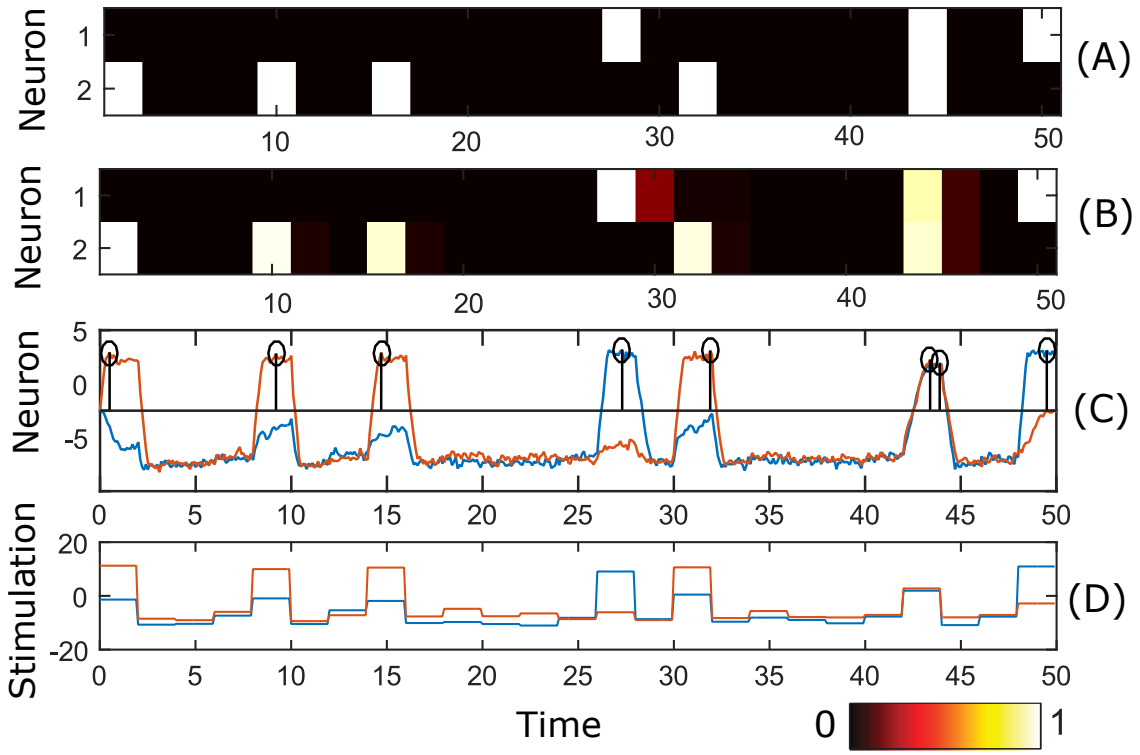

Figure 3.8: Control design for diffusively coupled FN neurons ($C = 2$). A: The target pattern $\mathbf{N}_T$ for the simulation. B: The average pattern over different realizations for the 2 neurons under $\mathbf{U}^*$. C: One realization of voltage traces for the 2 FN neurons under $\mathbf{U}^*$. The circled lines denote the detected spikes from the spike detection program. D: The optimized input $\mathbf{U}^*$.

B and C respectively) for a randomly selected target pattern (panel A) for a fully actuated ($C = S = 2$) network of FN neurons as in (3.41).

3.4.3 Analysis of Jittered Cost Function

We proceed with the jittered cost function by using the concept of gray coding [67]. In a gray code, two consecutive binary differs by only 1 bit. For example, consider the following target pattern in one dimension with $I = 4$, $\mathbf{N}_T = [0\ 1\ 1\ 1]$. Using a gray code, the two 'nearest' patterns are $\mathbf{N}_- = [0\ 1\ 1\ 0]$, $\mathbf{N}_+ = [0\ 1\ 0\ 1]$, compared to the normal binary sequence where the patterns on either side of $\mathbf{N}$, $\mathbf{N}_- = [0\ 1\ 1\ 0]$, $\mathbf{N}_+ = [1\ 0\ 0\ 0]$, may differ significantly

from the target pattern. So using the $\mathbf{N}_-$, $\mathbf{N}_+$ as the jittered patterns (over the neurons at each interval for a population) in (3.37), we can robustly achieve a pattern structurally close to $\mathbf{N}_T$.

Here, we select the ${}^{(K-1)}/_{2}$ (assuming K is odd) nearest (in terms of the gray code) patterns on either side of $\mathbf{N}_T$ and then transform them back to decimal equivalent to construct the marked point process. Note that the addition of these jittered patterns in the cost function does not alter the convexity of the program. Figure 3.9 illustrates the outcome of the optimal control problem with jittered cost function as compared with the dirac-delta function as a function of network size. The same number of inputs was considered in all cases ($S = 2$). We sampled 50 different target patterns from the binary space $\mathbb{B}^{C\times I}$, for number of neurons C $(= 3 \dots 8)$ and $I = 10$ time points, calculated the control $\mathbf{U}^*$ according to the two cost functions and plotted the average VP metric, along with the energy (Frobenius norm for $\mathbf{U}^*$) expended for the two cases.

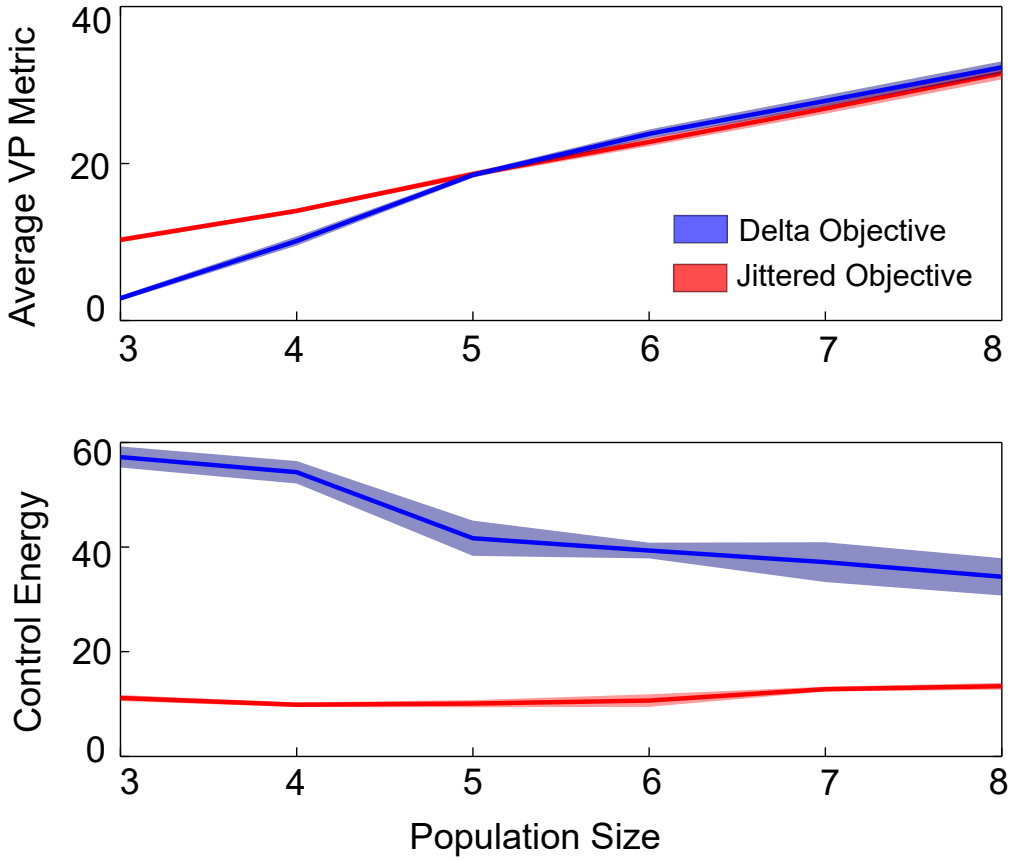

Figure 3.9: Performance comparison for jittered and delta cost function as objectives for (3.35). We plotted the VP metric and the controller energy used for a wide sample of patterns in a varying population of neurons with the same number of inputs for both cases. We see that the jittered cost program always produces an energy efficient control and as the population becomes underactuated (3.37) yields a comparable performance with respect to (3.36), in achieving the target spike pattern. This leads us to the conclusion that for controlling the spiking activity in an underactuated neural population, (3.37) is advantageous over (3.36).

3.5 Discussions

Here we have introduced a control analysis and design paradigm for statistical models of spiking networks. In the analysis framework, we show that the number of events in a realization of any PPGLM is a simple indicator of pattern viability in terms of likelihood. It is important to note the limitations in the proposed approach. Most notably, we focus here on evaluating the (relaxed) maximally viable spike count μ_r to investigate the space of patterns that can be achieved to within the probability threshold ρ. As mentioned, this framework does not distinguish between different patterns with the same count μ, and labels all of them to be viable for ρ if $\mu \leq \mu_r$. For an idealistic scenario, i.e. full actuation and unconstrained control inputs, we proved in (3.21), (3.26) that the event count solely dictates likelihood degradation. But with stringent energy constraints on the input and heavy underactuation, the process history and other co-variates also affect the likelihood so that dependence on $\Psi(\delta\mathbf{N})$ is not exclusive. The misclassified patterns in Figure 3.1 are attributed to this fact. Understanding this limitation, the aforementioned issue of non-convexity of (3.33) and the constraint relaxation (3.31), we posit that the framework is strong enough to reveal salient control properties in spiking networks. Our example highlighting concave dependence on connection strength, a fact that is analytically verifiable, demonstrates this utility.

Chapter 4

Intrinsic Control in Sensory Detection Tasks

In this chapter, we study integrative processing of sensory inputs in high-dimensional combinatorial detection spaces, as exemplified in olfaction [68, 69]. Rather than considering high-level cognitive tasks such as in the 2A-FCT, we are interested in studying simple detection and response to sensory stimuli. Simply stated, we seek to understand whether the early neural responses associated with such stimuli are consistent with a DDM-type threshold decoder; and further, how the underlying network may enable the realization of such responses.

Thus, our central premise is that response motifs observed in vivo are in fact the optimal neural drivers for particular drift dynamics. In studying this premise, we will first analyze a novel decoding scheme that generalizes the DDM to high dimensional, combinatorial environments. We will evaluate this model by formally optimizing its afferent inputs. In other words, we will postulate objective functions that reward fast, unambiguous detection and mathematically derive the exact form that the sensory neural activity should take in order to

achieve optimal performance. It turns out that the optimized motifs have an intuitive and interpretable form that is consistent with those observed in the early olfactory circuits of locust. We highlight this biological salience in the latter part of the chapter.

4.1 Background

4.1.1 Threshold-hitting Models for Choice Tasks

The 2A-FCT is one of the most pervasive, well-studied methods in behavioral experiment design. It is an idealized binary model of decision-making wherein a subject is presented with two alternatives and based on the integration of sufficient evidence, a decision is made in favor of one of the alternatives [70].

There are at least two different theoretical frameworks in which evidence can accumulate in a 2A-FCT. In a 1-dimensional (1D) construct, the assumption is that the *difference* between the neural responses corresponding to the two competing stimuli drives the integrator. Subsequently, this evidence difference is integrated over time until a certain threshold is reached, at which time a presumably 'correct' decision or detection is reached. This idea can be generalized into a scenario in which the differing lines of evidence are integrated independently, i.e., within an n-dimensional framework. In this latter scenario, the index set $\mathcal{I}_n = \{1, 2, \ldots, n\}$ represents the n different alternatives. In this chapter we will focus on this scenario as a schema for multidimensional processing of sensory evidence.

Classical DDM and Detection Paradigms

In order to build a complete mathematical specification, we denote $\boldsymbol{\nu}(t) \equiv [\nu_1(t), \nu_2(t), ..., \nu_n(t)]^T$ as the latent state that determines the outcome of the detection task. Note that in the

context of 2A-FCT, the latent state $\boldsymbol{\nu}(t) \in \mathbb{R}^2$. In the classical DDM framework [71, 72] the evolution of the latent state ν is governed by the dynamics :

$$\mathrm{d}\nu = k\mathrm{d}t + c\,\mathrm{d}W,\ \nu(0) = 0. \tag{4.1}$$

where k is the constant drift component, $c\,\mathrm{d}W$ is the diffusive component, usually modeled as white noise with mean 0, variance $c^2\mathrm{d}t$.

Using this state vector enables formalization of how the detection is made within the model. For a '**Forced Response**' or '**Interrogation**' paradigm, the outcome of the task depends on whether a response to the stimulus occurs within a prespecified time window, say τ. Assuming the process starts at $t = 0$, whichever dimension of $\nu(t)$ is higher at $t = \tau$ is chosen, i.e.,

$$\text{choice} = \max_{i \in \mathcal{I}_n} \nu_i(\tau) \tag{4.2}$$

In a '**Free Response**' paradigm a subject makes a decision on their own time. Here, we introduce a threshold Γ, which represents a quantitative notion of sufficient evidence for detection. In a 2D construct, the decision is based on whichever latent state reaches it's threshold first i.e. a detection is made at $t = \tau$ if,

$$\nu_i(\tau) \geq \Gamma_i \ \text{ with } \nu_i(t) < \Gamma_i,\ \forall t \in [0, \tau),\ i \in \mathcal{I}_2. \tag{4.3}$$

Here, τ is the *reaction time* (RT) [70, 71, 73] of the task. Note that by definition, the RT is fixed for the Interrogation paradigm. In this work, we will not differentiate between the decision time (DT), which is time associated with the decision process only and RT, which is a sum of DT and time associated with sensory, motor processes [70] that precedes the actual response from the subject.

Unambiguous Detection

A multi-alternative free response framework can produce choice ambiguity. An *unambiguous* detection implies the latent state ν is dominant along only one dimension when the threshold along that dimension is reached. Thus, perfect (totally unambiguous) detection of one of the alternatives, say $i = 1$ at $t = \tau$, corresponds to:

$$\boldsymbol{\nu}(\tau) = [\Gamma_1 \; 0]^T. \tag{4.4}$$

This can be interpreted as a low entropy configuration of the latent state. To formalize this notion, we modify (4.4) to introduce the level of ambiguity ϵ, which occurs when the latent state in (4.4) becomes

$$\boldsymbol{\nu}(\tau) \in \mathrm{B}_\epsilon(\mathbf{z}_1),\; \mathbf{z}_1 = [\Gamma_1 \;\; 0]^T,\; 0 < \epsilon < \min(\Gamma_1, \Gamma_2). \tag{4.5}$$

where $\mathrm{B}_\epsilon(.)$ denotes an open ball of radius ϵ (in the $\|.\|_2$ norm) around any point in the latent space. For a robust detection of stimulus we want ϵ to be as small as possible. We illustrate this in Figure 4.1, where we show an ideal state trajectory in the latent space $\boldsymbol{\nu} \in \mathbb{R}^2$, for decision index 1. In the schematic, as the state trajectory moves away from the positive ν_1 axis, the detection becomes ambiguous with respect to the desired choice ($i = 1$) and eventually leads to error. The level of ambiguity is closely related to the Error Rate (ER) [70, 74], which is defined as the proportion of incorrect responses by a subject under different trials for the same task. Smaller ambiguity (ϵ) results in lower ER.

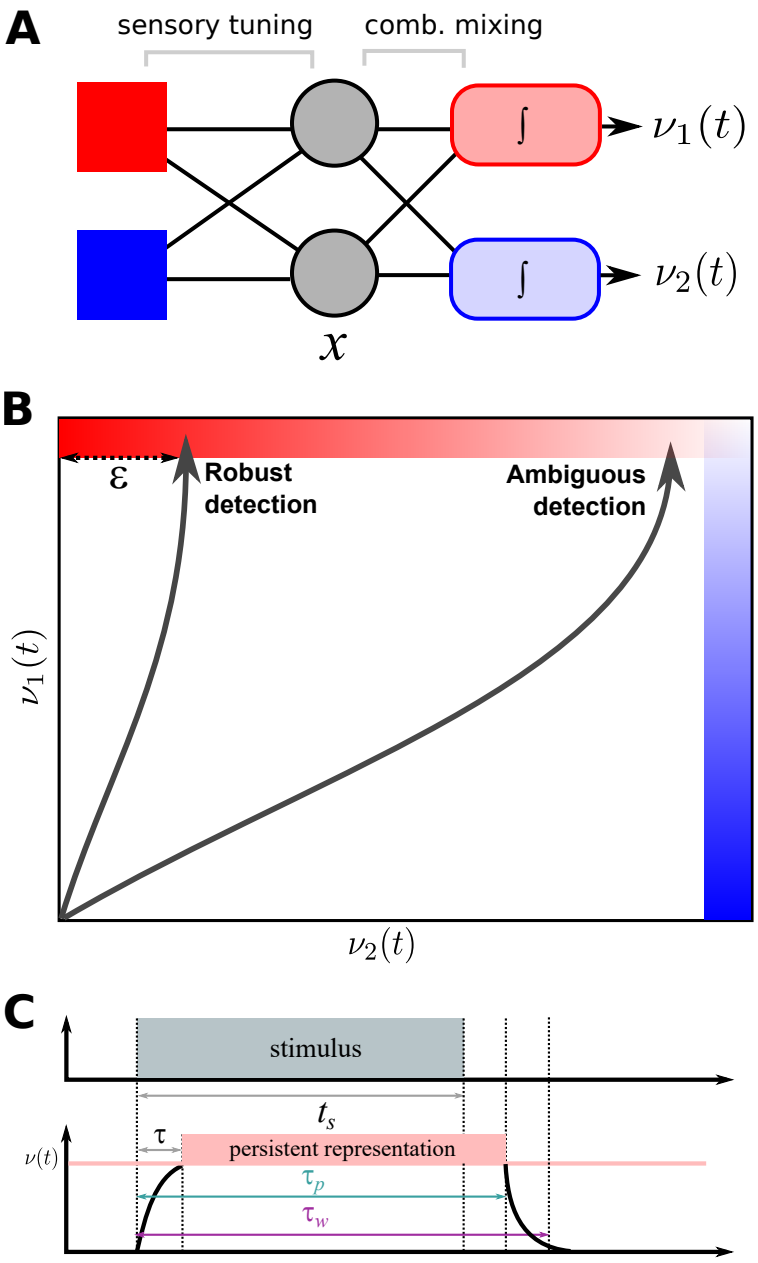

Figure 4.1: (A) We consider a multidimensional, integrative detection framework with combinatorial mixing of afferent inputs (stimuli). (B) In this decoding scheme, detections are made when latent states cross thresholds. Detection can be robust or ambiguous, depending on competing states. We will formulate an objective function designed to allow thresholds to be hit and held with minimal ambiguity. The level of ambiguity ϵ of a detection indicates how close competing latent states are to their respective thresholds. (C) Our objective function generalizes detection to also account for persistence and withdrawal of sensory representations.

4.1.2 Response motifs in early olfactory networks.

Our theoretical study is motivated in part by observations of the activity in early olfactory networks, i.e., sensory neuronal networks that interface with environment and, eventually, enable the perception of smell. In [40], detailed characterizations were made regarding the stimulus-evoked responses of projection neurons in the locust antennal lobe that receive direct sensory input from the olfactory receptor neurons. Note that here, a 'stimulus' refers to sensory input (i.e., an odor). It is observed that evoked responses contain two major, mutually exclusive motifs: phasic increase and overshoot of spiking activity during stimulus presentation followed by tonic activity that persists during stimulus maintenance ('ON' type); or inhibition (reduction of activity from baseline) during the stimulus presentation followed by pronounced phasic activation after stimulus termination ('OFF' type). The ON, OFF clusters can be further sub-classified according to the magnitude of their phasic parts, as shown in Figure 4.2.

We are interested in these motifs because they can be interpreted as 'evidence' that is decoded by higher brain circuits towards ultimately enabling stimulus detection and processing. How exactly does this decoding happen? Following from the above, our supposition is that the decoding is integrative, wherein this sensory activity is integrated in a high-dimensional latent state space towards complex detection boundaries. For such a scheme to work, the sensory neural activity motifs must allow the latent state to reach relatively distinct regions of the latent space so as to avoid sensory ambiguity and, further, to achieve such trajectories quickly. In this sense, we posit that early sensory networks are effective, perhaps even optimal, drivers of this higher integrative decoding process.

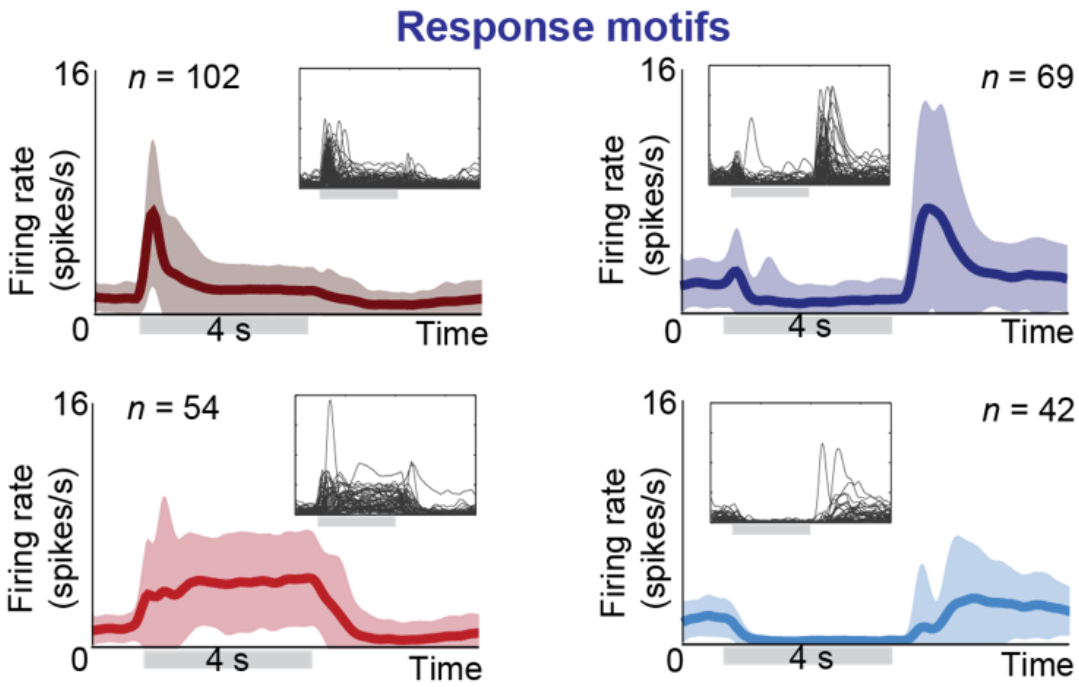

Figure 4.2: Response Motifs observed in Locust Olfactory Network

4.2 Problem Formulation

4.2.1 Persistent Response Paradigm

The paradigms discussed above model a single detection within a structured choice task framework. In contrast, we are interested in understanding behavioral responses to multidimensional, combinatorially-encoded stimuli that occur sequentially without overt periodicity. In this context, one can surmise a functional need for detections to not simply occur but *also persist and withdraw*. Thus, we introduce a third paradigm motivated by [75], [76], where we hypothesize that neural evidence supports the maintenance of a particular detection until $t = \tau_p > \tau$. This means for a stimulus with onset at $t = 0$, duration t_s and RT τ, we have $\tau_p > \max(\tau, t_s)$. Beyond $t = \tau_p$, latent states reset to a neutral regime so that they can respond to new stimulus without any bias (see schematic in Fig. 4.1). The latter is accounted for by introducing a withdrawal period $t \in (\tau_p, \tau_w)$, during which the neural response resets the latent states to within a ϵ' neighborhood of neutral. Note that our formulation is general enough to allow for representations that persist beyond stimulus termination. However, in most basic sensory detection settings, one expects $\tau_p \geq t_s$.

Thus, using our notation in a 2D latent space, to elicit a response in favor of the first choice, i.e., $(i = 1)$, we have,

$$\begin{aligned} &\boldsymbol{\nu}(t) \in \mathrm{B}_{\epsilon}(\mathbf{z}_1),\ \forall\, t \in [\tau, \tau_p],\ \tau_p > t_s,\ \boldsymbol{\nu}(0) = \mathbf{0}. \\ &\boldsymbol{\nu}(t) \in \mathrm{B}_{\epsilon'}(\mathbf{0}),\ \forall\, t \in (\tau_p, \tau_w). \end{aligned} \tag{4.6}$$

where ϵ and ϵ' denotes the level of ambiguity for the two phases, namely, detection and withdrawal of the stimulus, respectively.

Extensions to the DDM and Decision Landscapes

In our study, we will examine different drift dynamics motivated by the 'energy picture of decision making' [77]. For ease of presentation, we formulate these models for $\boldsymbol{\nu}(t) \in \mathbb{R}^2$ and reconcile these representations with the classical DDM and several of its extensions.

Null Model: We first describe the null model where the latent variables do not have internal drift and thus behave as perfect integrators. This takes the form,

$$\dot{\boldsymbol{\nu}} = \mathbf{b}\mathbf{x} + \mathbf{c}\mathrm{d}\mathbf{W}. \tag{4.7}$$

Note that for $\mathbf{b}$ a 2×2 identity matrix $\mathbb{I}_2$, (4.7) reduces to the Race model [78], wherein the evidence favoring each alternative is integrated independently.

Equilibrium Model: Here all the latent variables lie within a stable basin of attraction and all decision thresholds are located away from the equilibrium. This is equivalent to leaky integration of afferent activity. The two representations are given by,

$$\dot{\boldsymbol{\nu}} = \begin{bmatrix} -a_1 & 0 \\ 0 & -a_2 \end{bmatrix} \boldsymbol{\nu} + \mathbf{b}\mathbf{x} + \mathbf{c}\mathrm{d}\mathbf{W}, \quad (2\mathrm{D}), \tag{4.8}$$

where $a_{1,2} > 0$. Note that, here the equilibrium model with $\mathbf{b} = 0$, is a version of a stable Ornstein-Uhlenbeck process [79] without affine input. A more general version of a stable 2D Equilibrium model can be written as

$$\dot{\boldsymbol{\nu}} = \mathbf{A}\boldsymbol{\nu} + \mathbf{b}\mathbf{x} + \mathbf{c}\mathrm{d}\mathbf{W} \tag{4.9}$$

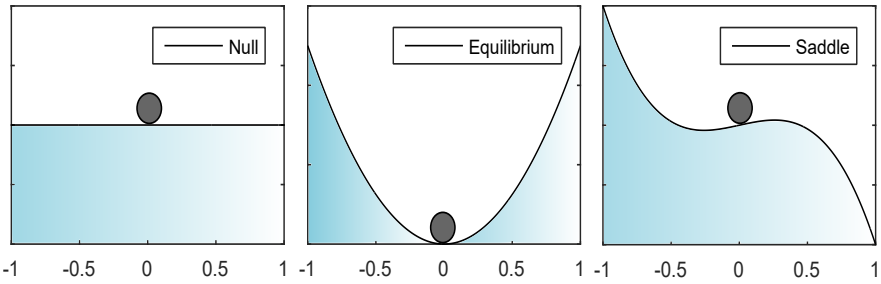

Figure 4.3: Different dynamic landscapes for decision making

where $\mathbf{A} \in \mathbb{R}^{2\times 2}$ such that $\sigma(\mathbf{A}) \in \mathbb{R}_-$, $\sigma(\mathbf{A})$ denotes the eigenspectrum of $\mathbf{A}$. For a diagonal $\mathbf{A}$, (4.9) reduces to the 2D model in (4.8). The Mutual Inhibition model of [80] is a special case of (4.9) with non-diagonal $\mathbf{A}$ (and, specifically, with reciprocal inhibitory coupling between the latent variables).

Saddle Model: If one of the decisions is made more frequently, bias is introduced in the DDM framework by modifying the initial state $\boldsymbol{\nu}(0)$. This is dependent on the prior probabilities of the two choices [81, 82]. Here, we propose a model that encodes bias within the latent state dynamics i.e.

$$\dot{\boldsymbol{\nu}} = \begin{bmatrix} -a_1 & 0 \\ 0 & a_2 \end{bmatrix} \boldsymbol{\nu} + \mathbf{bx} + \mathbf{c}\mathrm{d}\mathbf{W} \tag{4.10}$$

For the 2D representation in (4.10), the dynamics are biased against the latent state ν_1 and favors ν_2. More generally, such a model can be represented as in (4.9) but wherein $\sigma(\mathbf{A})$ now contains eigenvalues of opposite signs. The favored stimulus orientation is along the eigenvector corresponding to positive eigenvalue.

In Figure 4.3, we plot the dynamical landscape for the models described above.

4.2.2 Optimization Framework

Our main results involve the optimization of evidence trajectories with respect to the persistent response framework in (4.6).

Optimal Response for Speed, Accuracy, Energy Trade-off

We will specifically formulate a regularized optimization problem in order to elucidate the evidence motifs that best mediate a trade-off between fast (minimum time to reach threshold) and unambiguous (maximum separation between the latent variables) DDM-based detection.

Optimization Scheme: For simplicity but without loss of generality, we assume $M(>2)$ neurons (which can be interpreted as sensory units) are influencing a 2D latent state $\nu_{1,2}$. Since we are primarily interested in characterizing the evidence motifs, we will neglect the diffusive component of the DDM, focusing only on the deterministic dynamics associated with evidence accumulation. In (4.7)-(4.10), these two assumptions translate into $\mathbf{b} \in \mathbb{R}^{2\times M}$ and $\mathbf{c} = \mathbf{0}$.

Objective Functions: As mentioned above, we are concerned with multiple phases of detection: occurrence, maintenance and withdrawal. We assume, again without loss of generality that the objective is to induce and maintain a detection in the ν_1 dimension, then withdraw that detection. In this sense, the evidence trajectories can be viewed as solutions to the following problems.

(P1p)

$$\min_{\mathbf{y}} \quad \mathbb{J}(\mathbf{y}) = \int_0^{\tau_p} \frac{1}{2}[(\boldsymbol{\nu}(t)-\mathbf{z}_1)^T\mathbf{Q}_1(t)(\boldsymbol{\nu}(t)-\mathbf{z}_1) + \mathbf{x}(t)^T\mathbf{S}_1(t)\mathbf{x}(t) + \mathbf{y}(t)^T\mathbf{R}_1(t)\mathbf{y}(t)]\mathrm{d}t$$

$$(P1w) \qquad \min_{\mathbf{y}} \ \mathbb{J}(\mathbf{y}) = \int_{\tau_p}^{\tau_w} \frac{1}{2}[\boldsymbol{\nu}(t)^T \mathbf{Q}_2(t)\boldsymbol{\nu}(t) + \mathbf{x}(t)^T \mathbf{S}_2(t)\mathbf{x}(t) + \mathbf{y}(t)^T \mathbf{R}_2(t)\mathbf{y}(t)]\mathrm{d}t$$

where

$$\begin{aligned} &\dot{\boldsymbol{\nu}}(t) = f(\boldsymbol{\nu}, \mathbf{x}),\ \dot{\mathbf{x}} = \mathbf{y}, \\ &\boldsymbol{\nu}(0) = \mathbf{0},\ \mathbf{x}(0) = \mathbf{x}_0, \\ &\mathbf{Q}_j(t) \in \mathbb{R}^{2\times 2};\ \mathbf{S}_j(t), \mathbf{R}_j(t) \in \mathbb{R}^{M\times M} \\ &\mathbf{Q}_j(t), \mathbf{S}_j(t) \geq 0;\ \mathbf{R}_j(t) > 0,\ j = 1, 2. \end{aligned} \tag{4.11}$$

With $\mathbf{z}_1$ is defined in (4.5), (*P1p*), (*P1w*) become finite time regulator problems [83]. $\mathbf{Q}_i(t)$ dictates the ambiguity level ϵ, ϵ' in (4.6).

4.3 Results

4.3.1 Persistent responses are best achieved through biphasic neural responses

In this section we develop the solutions of the problems in (*P1p*), (*P1w*) and discuss the characteristics of these motifs in coding the sensory stimulus for efficient sensory detection. The key technical step is the reduction of the response optimization problems to that of the finite-time quadratic regulator from control theory. While most of the technical derivation is left to the Appendix, we note the main transformation from (*P1p*) is add the target $\mathbf{z}_1$ (which is constant) to the augmented state vector $\mathbf{v} = [\boldsymbol{\nu}^T\ \mathbf{x}^T]^T$ and ascribe to it the null dynamics $\dot{\mathbf{z}} = \mathbf{0}$ with initial condition $\mathbf{z}(0) = \mathbf{z}_1$. So we have,

$$\begin{aligned} &\dot{\mathbf{v}}_z = [f^T(\boldsymbol{\nu}, \mathbf{x})\ \ \mathbf{y}^T\ \ \mathbf{0}^T]^T = [g^T(\mathbf{v}, \mathbf{y})\ \ \mathbf{0}^T] \equiv \tilde{g}(\mathbf{v}, \mathbf{y}), \\ &\mathbf{v}_z = [\boldsymbol{\nu}^T\ \ \mathbf{x}^T\ \ \mathbf{z}^T]^T = [\mathbf{v}^T\ \mathbf{z}^T]^T \end{aligned} \tag{4.12}$$

and $(P1p)$ reduces to

$$(P1p^*) \qquad \begin{aligned} \min_{\mathbf{y}} \quad & \mathbb{J}(\mathbf{y}) = \int_0^{\tau_p} \frac{1}{2}[\mathbf{v}_z^T \bar{\mathbf{Q}}_1 \mathbf{v}_z + \mathbf{y}^T \mathbf{R}_1 \mathbf{y}]\mathrm{d}t \\ \text{s.t.} \quad & \dot{\mathbf{v}}_z = \tilde{g}(\mathbf{v}, \mathbf{y}), \mathbf{v}_z(0) = [\mathbf{0} \;\; \mathbf{x}_0 \;\; \mathbf{z}_1] \end{aligned}$$

where

$$\bar{\mathbf{Q}}_1 = \begin{bmatrix} \mathbf{Q}_1(t) & \mathbf{0}^{2\times M} & -\mathbf{Q}_1(t) \\ \mathbf{0}^{M\times 2} & \mathbf{S}_1(t) & \mathbf{0}^{M\times 2} \\ -\mathbf{Q}_1(t) & \mathbf{0}^{2\times M} & \mathbf{Q}_1(t) \end{bmatrix}. \tag{4.13}$$

Here, $(P1p^*)$ is in the normal form of the standard regulator problem. Since the drift dynamics are linear in the latent state $\boldsymbol{\nu}$, $(P1p^*)$ is the so-called Finite Time Linear Quadratic Regulator (LQR) problem. Similarly, $(P1w)$ can be reduced to

$$(P1w^*) \qquad \begin{aligned} \min_{\mathbf{y}} \quad & \mathbb{J}(\mathbf{y}) = \int_0^{\tau_w - \tau_p} \frac{1}{2}[\mathbf{v}^T \bar{\mathbf{Q}}_2 \mathbf{v} + \mathbf{y}^T \mathbf{R}_2 \mathbf{y}]\mathrm{d}t \\ \text{s.t.} \quad & \dot{\mathbf{v}} = g(\mathbf{v}, \mathbf{y}), \mathbf{v}(0) = [\boldsymbol{\nu}(\tau_p) \;\; \mathbf{x}(\tau_p)] \end{aligned}$$

where

$$\bar{\mathbf{Q}}_2 = \begin{bmatrix} \mathbf{Q}_2(t) & \mathbf{0}^{2\times M} \\ \mathbf{0}^{M\times 2} & \mathbf{S}_2(t) \end{bmatrix}. \tag{4.14}$$

Note that $\bar{\mathbf{Q}}_{1,2}(t)$ in (4.13), (4.14) is positive semi-definite (see Appendix C.1) and a (unique) solution to $(P1p^*)$, $(P1w^*)$ exists.

To study the nature of the solutions to these problems we consider a prototypical combinatorial decoding setup, depicted in Figure 4.4A. Here, the colors blue and red each impinge on $M = 41$ sensory neurons via Gaussian tuning curves. These curves are overlapped by $O = 11$ neurons. The tuning curves and selectivity of the latent states (for red and blue) are absorbed into the matrix $\mathbf{b}$ matrix in (4.7)-(4.10).

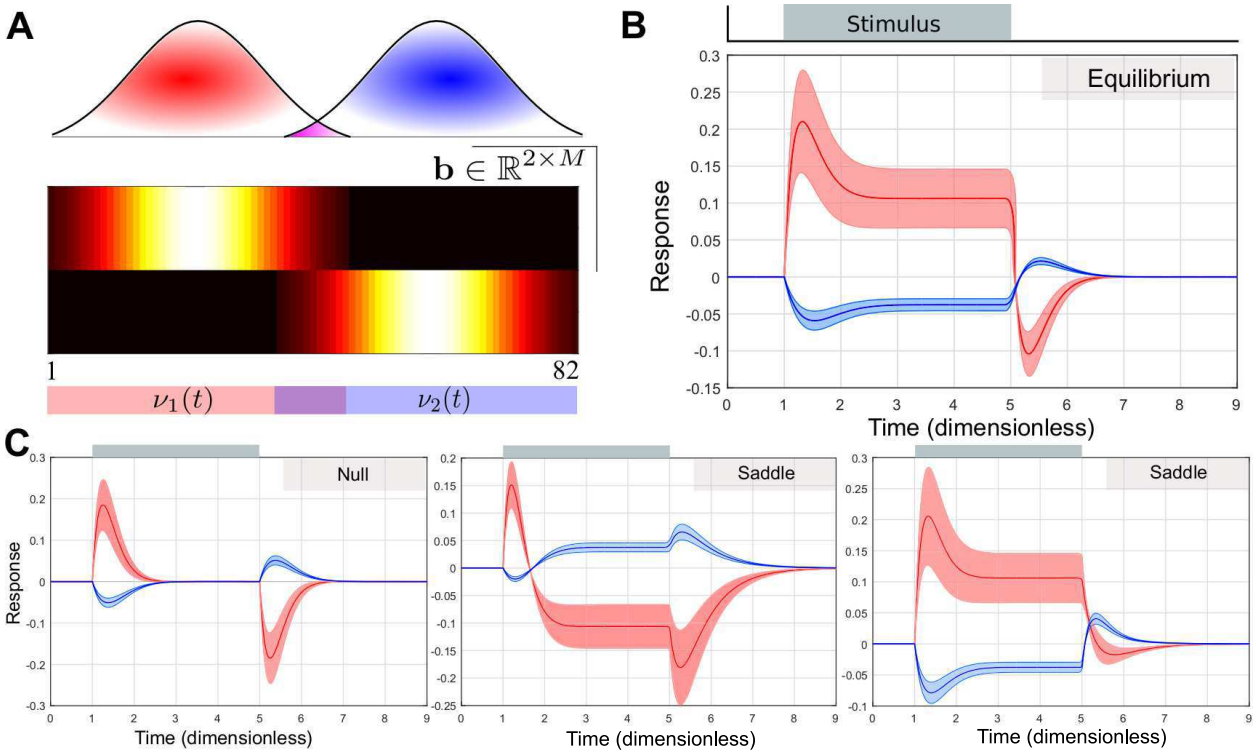

Figure 4.4: Optimal evidence for Persistent response Paradigm for the 2D Models during persistent and withdrawal phase.

We select penalty matrices that equally weight the detection time and ambiguity. The ensuing optimized response motifs for the persistent paradigm are shown in Figure 4.4B,C. Here, we plot the response motifs for the persistent and withdrawal phase (i.e., the solutions of $(P1p)$, $(P1w)$), assuming $t_s = \tau_p$. Due to asymmetry along the two directions corresponding to the two alternatives in the Saddle Model, we plot the optimal response for both $i = 1, 2$. A biphasic stimulus onset and offset response is observed in all cases. Further, the offset response is geometrically opposed to the onset response. Qualitatively, the equilibrium DDM model (i.e., 4.4B) produces overall motifs that are most consistent with experimental observations.

4.3.2 Phasic Responses are Needed for Fast, Persistent Detections

As seen in the previous section, the optimal neural trajectory for persistent detection exhibits an overshoot (phasic transient) followed by steady state (tonic) maintenance. From an energetic standpoint, the presence of phasic overshoot is costly; but the benefit of such dynamics is that it enables faster and more accurate detection. Indeed, Figure 4.5 shows the optimal response motifs as the regularization matrix $\mathbf{S}_1$ is scaled to more heavily penalize motif energy. Fig. 4.5A depicts a general reduction in ambiguity and detection time as more energy is tolerated, which is accompanied by a progressively more pronounced overshoot (Fig. 4.5B). It is interesting to note that this overshoot varies on the order of 300% depending on the energy regularizer, while the tonic (steady state) response only varies to within 50%.

Further, the phasic overshoot only arises due to the persistence of the detection. Indeed, if we repeat our optimization procedure for the more classical DDM detection paradigms discussed above in 4.1.1 (namely, free and forced detection), we find that the optimal response is always of the form:

$$x(t) = \sum_k e^{\beta_k t}, \tag{4.15}$$

where $\beta_k t$ are real coefficients (see Appendix C.2-C.4). Since in these cases the motifs end when a detection is made (i.e., there is no persistence), (4.15) implies that the optimized motifs for free or forced detection can never overshoot.

4.3.3 Responses are produced through a canonical model of recurrent inhibition

Finally, we note that the optimal response motifs we see in Figure 4.5 are readily realized through a prototypical, competitive neuronal network architecture. Indeed, as we see in these motifs, a feature of the optimal response is not only an increase from baseline of the primary response, but a decrease/inhibition from baseline of the competing response. It is highly intuitive that lateral inhibition within the sensory layer can mediate such dual responses.

Here we investigate a modified version of the competitive network architecture proposed by [76]. This structure consists of a hidden layer of inhibitory neurons which receives excitation from a primary layer of sensory neurons (that interfaces with the periphery). It is the sensory layer whose activity is read out by the integration mechanism that forms the detection. We show a layout of this network in Figure 4.6.

Calculation of Firing Rate

Assuming $\mathbf{u}$ as the input to an M neuron sensory layer, we can calculate the firing rate as in [1]. The synaptic current $\mathbf{I}_s \in \mathbb{R}^M$ follows a first order dynamics excited by a net activation from $\mathbf{u}$ and the inhibitory projection from the hidden layer,

$$\boldsymbol{\tau}_s \frac{\mathrm{d}\mathbf{I}_s}{\mathrm{d}t} = -\mathbf{I}_s + \mathbf{w}_s^e\, \mathbf{u}(t) - \mathbf{w}_i^e \mathbf{x}_h \tag{4.16}$$

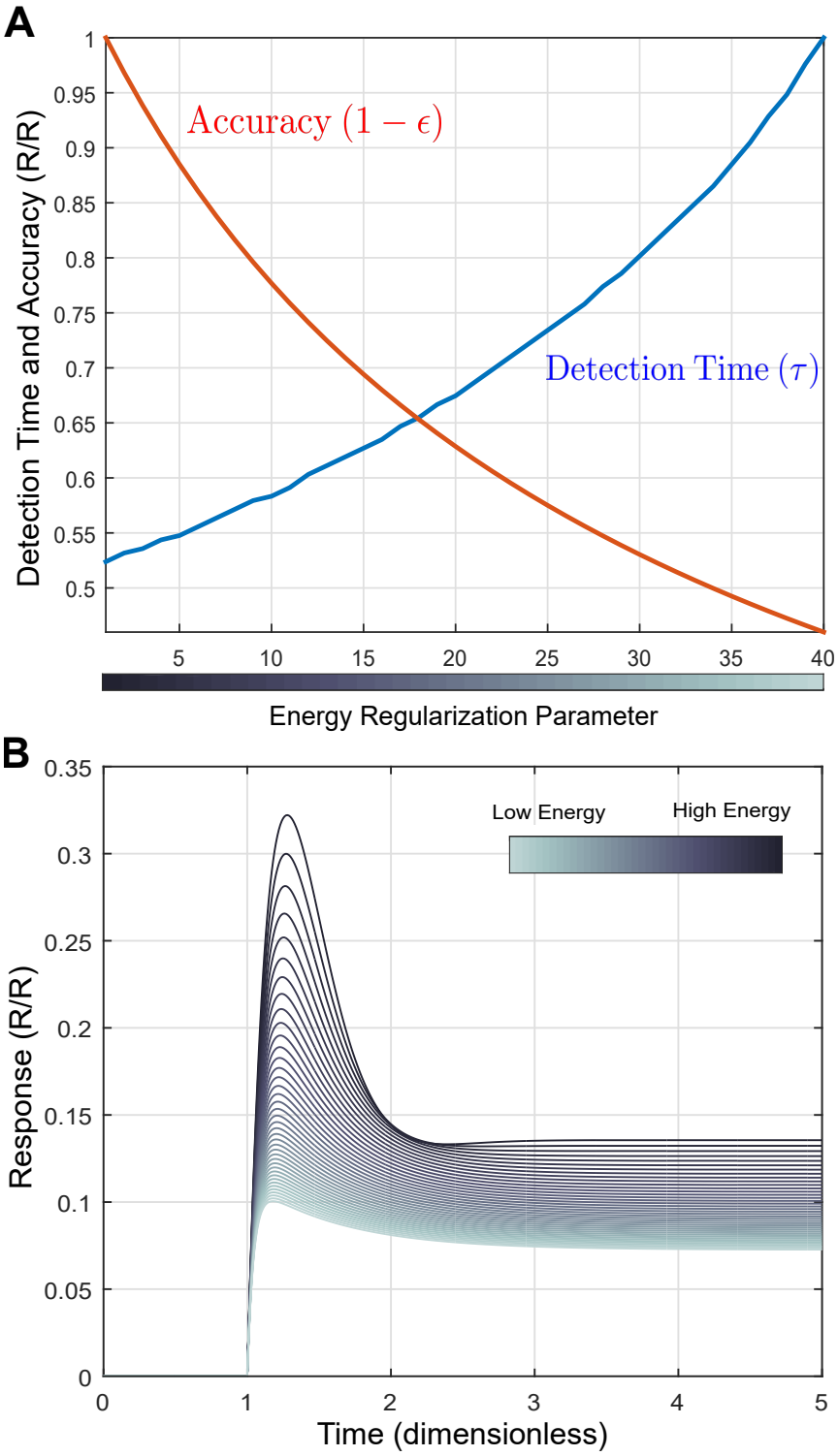

Figure 4.5: Role of energy in shaping the response motifs for speed-accuracy trade-off

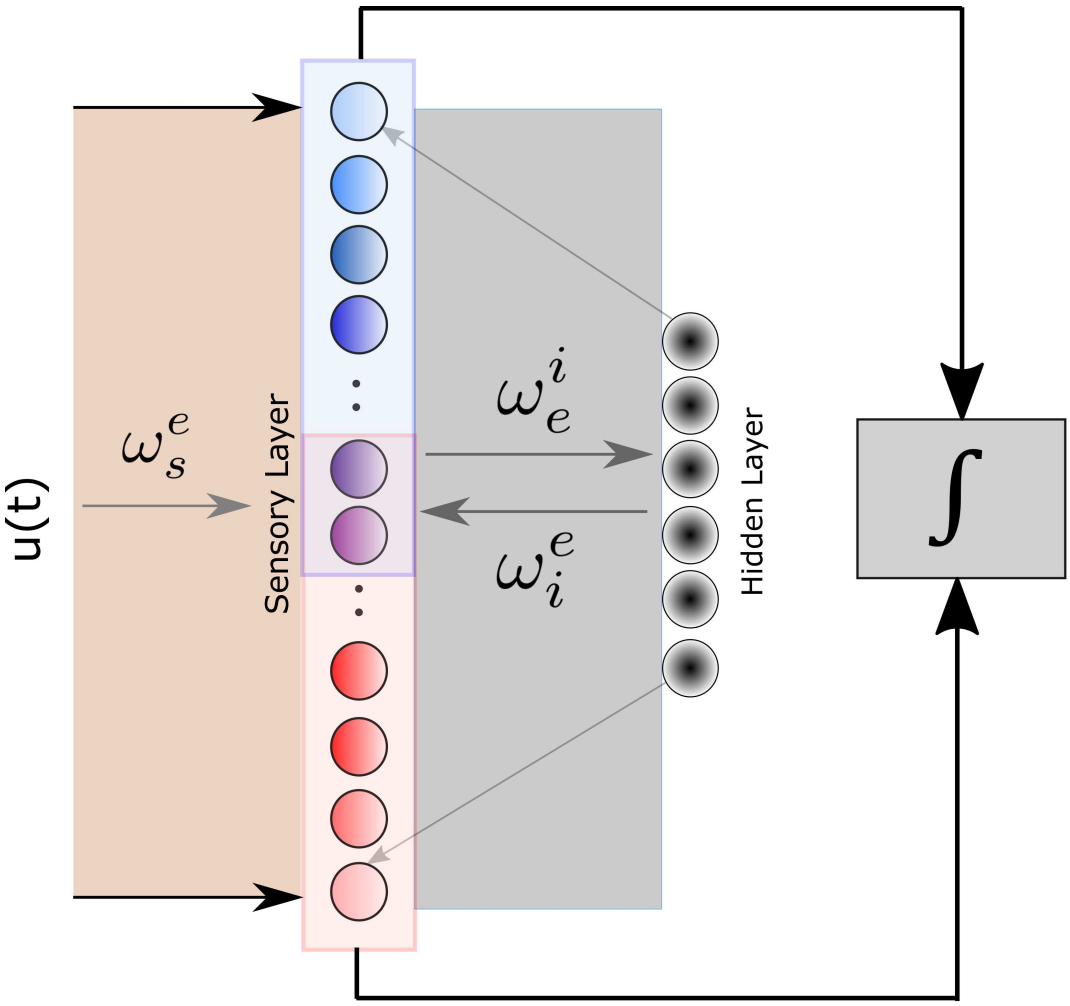

Figure 4.6: Proposed network architecture for unambiguous binary decision making. We assume that the feature space representation of the stimulus $\mathbf{u}(t)$ excites the sensory neurons in the first layer via $\mathbf{w}_s^e$, which then affects (possibly smaller number) inhibitory neurons in the hidden layer through $\mathbf{w}_e^i$. This hidden layer projects onto the sensory layer through ω_i^e, enabling the dominant stimulus to stand out in the detection process.

where $\boldsymbol{\tau}_s \in \mathbb{R}^{M\times M}$, the synaptic time constant is a diagonal matrix, $\mathbf{w}_s^e \in \mathbb{R}^{M\times M}$, $\mathbf{w}_e^i \in \mathbb{R}^{M\times L}$ denote the influence of $\mathbf{u}(t) \in \mathbb{R}^M$ and hidden layer firing rate $\mathbf{x}_h \in \mathbb{R}^L$ respectively.

From the synaptic current $\mathbf{I}_s$, we calculate the firing rate vector $\mathbf{x}_s$

$$\begin{aligned} \tau_r \frac{\mathrm{d}\mathbf{x}_s}{\mathrm{d}t} &= -\mathbf{x}_s + F(\mathbf{I}_s(t)), \\ F(\mathbf{I}_s) &= (1+\exp(-\frac{\mathbf{I}_s - \mathbf{I}_0}{\tau_f}))^{-1} \end{aligned} \tag{4.17}$$

where $F(I_j)$ is the sigmoidal activation function. Following our architecture, the hidden inhibitory layer with L neurons ($L < M$) receive this input $\mathbf{x}_s$ through a weighting matrix $\mathbf{w}_e^i \in \mathbb{R}^{L\times M}$. The synaptic current $\mathbf{I}_h \in \mathbb{R}^L$ of the hidden inhibitory neurons follow similar linear dynamics as in (4.16),

$$\boldsymbol{\tau}_h \frac{\mathrm{d}\mathbf{I}_h}{\mathrm{d}t} = -\mathbf{I}_h + \mathbf{w}_e^i\, \mathbf{x}_s \tag{4.18}$$

with $\boldsymbol{\tau}_h \in \mathbb{R}^{L\times L}$ the diagonal matrix of time constant. From the synaptic inputs $\mathbf{I}_h$, we can compute the firing rate $\mathbf{x}_h$ of the inhibitory layer as in (4.17). These neurons now in turn inhibit the sensory layer through a weighting pattern $\mathbf{w}_i^e$, shown in (4.16).

Now we show that this network is indeed capable of producing the optimal motifs observed in the simulations for problem (*P1p*)-(*P1w*). As example, we consider a detection task of discerning the color of an image patch which is dominated by blue in $5:1$ ratio with respect to red. Let us also assign 'blue' to decision index $i = 1$ and red to $i = 2$. We also assume a constant baseline activity present in the network. Now suppose the image belongs to the receptive field of $M = 6$ sensory neurons with an overlap of $O = 2$ and $L = 2$ inhibitory neurons. In this simplistic realization, this input can be expressed as $\mathbf{u}(t) \in \mathbb{R}^M$ where the blue, red sensitive and the overlapping neurons get step inputs on top of the baseline input acting on the network. We compute the firing rates generated by these layers using (4.16)-(4.18) for both the blue and red half in Figure 4.7. If we assume that only the sensory

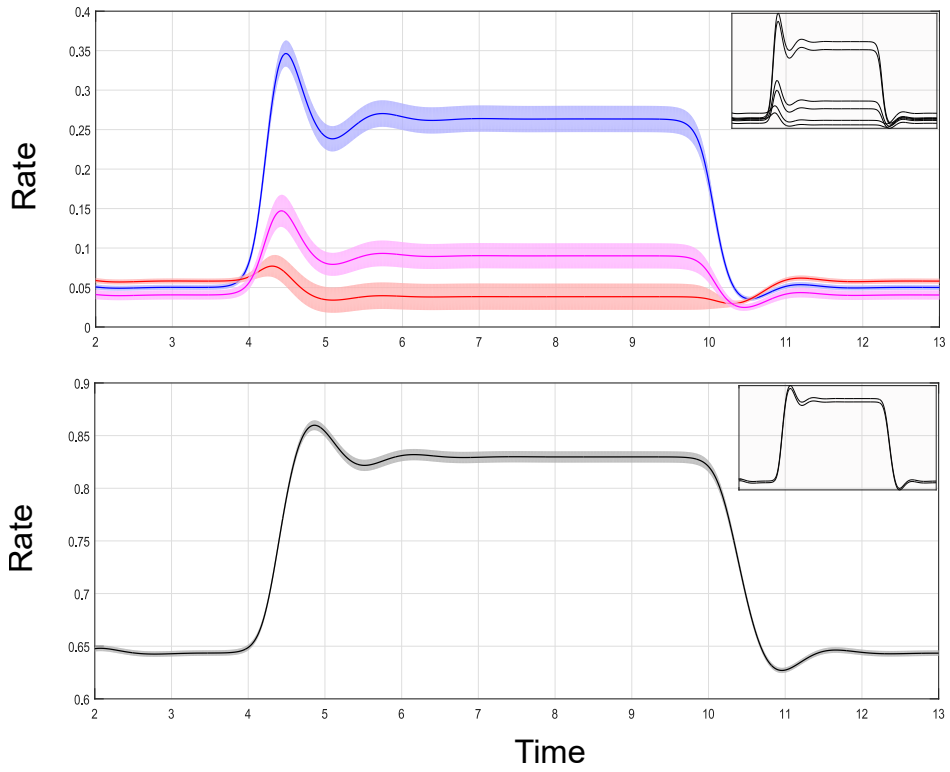

Figure 4.7: The firing rate for four different types of neurons in the two layers are shown. A step input representative of the sensory stimulus is applied to the network, proposed in Figure 4.6. Assuming that only the excitatory neurons participate in the final integrative process, as proposed in the architecture, we observe that the firing rates match the kernels for the optimal neural response.

neurons are involved in the decision making then we see that this network architecture is capable of achieving the kernels shown in the optimal decision making.

4.4 Discussion

In this chapter, we have performed a theoretical study of integrative decoding of sensory stimuli through the use of optimal control theory in conjunction with a generalized drift-diffusion detection schema. We specifically posited a decoding objective involving fast, unambiguous detection and maintenance of stimulus representations. Within this optimization framework, we showed that the putative best neural responses involve phasic overshoot to rapidly hit

a detection threshold, followed by tonic representation maintenance. These computational findings provide a potential explanation for previously observed activity motifs in early olfactory networks.

4.4.1 Optimal formation and maintenance of representations

Our theoretical framework departs from the classical drift-diffusion decoding schema by positing not simply threshold crossing, but rather persistence of the latent state within a small region corresponding to unambiguous detection (i.e., ideally along a base vector in the latent state space). The goal of maintaining representations is what ultimately causes the optimal motifs to dichotomize into an initial overshoot and eventual tonic phases, the former governing fast transients, with the latter governing robust maintenance.

4.4.2 Speed-energy vs. Speed-accuracy trade-offs

Our model also provides an interesting interpretation regarding the notion of speed-accuracy trade-off or, lack thereof. In fact, as shown in Figure 4.5, for the multivariate DDM framework, it is possible to achieve fast and unambiguous threshold hitting/maintenance simultaneously. Where the trade-off occurs is not between speed and accuracy, but rather between speed and energy of the underlying neural responses. Penalizing energy leads to motifs that while able to maintain representations, do so more slowly and less accurately. These motifs also lack the characteristic phasic overshoot observed in data. Indeed, it is this overshoot that is the primary manifestation of energy tolerance (leading to faster, more accurate responses), explaining why such phasic activation often appears in early sensory networks.

4.4.3 Multivariate threshold-detection and reset responses

Our model provides a theoretical framework within which to understand the offset responses observed in [40]. Indeed, the multivariate DDM requires a nonzero neural activation, from which a given latent state can integrate bidirectionally. Thus, the offset responses can be interpreted as mediating a (fast) reset of the latent states to neutral, from which the network is able to respond to future stimuli. That the offset responses are geometrically opposed to the onset responses is a putative reflection of the need to integrate 'backwards' along the onset trajectory.

4.4.4 Sensitivity to noise

Our theoretical studies are all performed in a deterministic setting, without an overt noise model. For instance, we might suppose a small amount of additive Gaussian noise impinging on the latent state integration process. In this case, it is important to note that the optimal motifs for the persistent detection paradigm remain unchanged [84]. Other forms of noise will, however, have nontrivial effects on the optimization problem studied herein.

Chapter 5

Optimal Evidence for Fast-Unambiguous Detection Problems

In this chapter, we characterize optimal evidence for fast and unambiguous sensory detection in threshold-based models. We apply the optimal control framework developed in Chapters 2 and 4, illustrate the geometric subtleties in the solutions, and point out the relation to classical problems in Calculus of Variation. We also reveal that inhibition in the optimal response is key to ambiguity reduction.

5.1 Problem Formulation

Using the detection framework discussed in the previous chapter (4.3), here we seek the optimal neural representation for a fast but unambiguous decoding of sensory input. We formulate two optimal control problems for a 2-dimensional threshold-based DDMs, resembling the 2A-FCT task model. The objective functional in these problems is designed to achieve a trade-off between speed (the time for the target state to hit the threshold) and accuracy (ensuring

that the non-target state remains well below it's threshold). We incorporate the accuracy aspect through a terminal cost $\varphi(\cdot)$ that penalizes higher values of the non-target state. We take φ as an increasing and convex function of the non-target state and consider both smooth and non-smooth models. This function associates a measure of unambiguity/accuracy with the problem and, for example, by choosing a piecewise defined function which has different slopes on opposite sides of a critical value x_c, we can bias the solution towards restricting the non-target state to lie below this critical value x_c. Interestingly, as we shall see below, such a non-smooth formulation sometimes has advantages in that it leads to an optimal control problem that has a simpler optimal synthesis than the one which is formulated with a smoothed version of such a penalty term φ.

We now formulate the problems we shall be analyzing. The state-space is $\mathbb{R}^2$, $\mathbf{x} = [x_1\ x_2]^T$, and without loss of generality we select the variable x_1 to be the target variable and x_2 to be the non-target variable. We write the system dynamics in the form

$$\dot{\mathbf{x}} = \mathbf{A}\mathbf{x} + \mathbf{b}\mathbf{u}, \quad \mathbf{x} \in \mathbb{R}^2, \tag{5.1}$$

with

$$\mathbf{A} = \begin{bmatrix} -a_1 & 0 \\ 0 & -a_2 \end{bmatrix}, \text{ and } \mathbf{b} = \begin{bmatrix} b_1 \\ b_2 \end{bmatrix} \tag{5.2}$$

with a_i and b_i, $i = 1, 2$, positive coefficients. We also assume that $a_1 \neq a_2$. The case when $a_1 = a_2$ leads to degenerate situations (which are easy to analyze) since the linear system is not completely controllable, but we omit these in the presentation. Also, the assumption that $\mathbf{A}$ is a diagonal matrix simplifies the notation, but, more generally, $\mathbf{A}$ could be any asymptotically stable matrix with real eigenvalues. Admissible controls are Lebesgue measurable functions u which take values in a compact interval $[\mathrm{U}_1, \mathrm{U}_2]$, the control set. Since the dynamics is linear, given any admissible control defined over an interval $[0, \tau]$ and any initial condition

$\mathbf{x}(0)$ there exists a unique solution to the dynamics (5.1) which is called the corresponding trajectory. We call the pair $(\mathbf{x}, u)$ a controlled trajectory. We then consider the following optimal control problem as our reference problem:

Problem 7. ***(P7)*** *With the terminal time τ free, minimize the objective*

$$\mathbb{J}(u) = \tau + \eta\, \varphi(x_2(\tau)) \tag{5.3}$$

over all admissible controls u subject to the dynamics (5.1), initial conditions in $\mathcal{G}$

$$\mathbf{x}(0) = \mathbf{x}_0 \in \mathcal{G} = [0,\ x_{th}] \times [0,\ x_{th}], \tag{5.4}$$

and terminal condition $x_1(\tau) = x_{th}$.

Here x_{th} denotes the detection threshold (similar to Γ in (4.3) Chapter 4) for both states and η is a regularization parameter. We make the following assumptions:

Assumption 2. • *The bounds in the control set are of high enough magnitude to effect rise and decay in the state variables, i.e., for all $\mathbf{x} \in \mathcal{G}$ we have that*

$$\mathbf{A}\mathbf{x} + \mathbf{b}\mathrm{U}_1 < 0 \text{ and } \mathbf{A}\mathbf{x} + \mathbf{b}\mathrm{U}_2 > 0. \tag{5.5}$$

Here we write $\mathbf{v} < 0$ when all elements of the vector $\mathbf{v}$ are negative. Let us also denote the vector fields corresponding to the constant controls U_1 and U_2 by X and Y, respectively.

• *The terminal cost is an increasing and convex, but not necessarily smooth function of the non-target state x_2. Generally, we assume that φ is of the form*

$$\varphi(x) = \begin{cases} \varphi_1(x) & \text{if } x < x_c, \\ \varphi_2(x) & \text{if } x \geq x_c. \end{cases} \tag{5.6}$$

where $\varphi_i(\cdot)$ are differentiable functions with $\varphi_1(x_c) = \varphi_2(x_c)$. Note that, if the composite function φ is not differentiable at $x = x_c$, then we have that

$$\lim_{x \to x_c^-} \frac{\mathrm{d}\varphi}{\mathrm{d}x} = \varphi_1'(x_c) < \varphi_2'(x_c) = \lim_{x \to x_c^+} \frac{\mathrm{d}\varphi}{\mathrm{d}x}. \tag{5.7}$$

An important aspect in this problem formulation is that the state space is all of $\mathbb{R}^2$. Consequently, in the optimal control problem it is allowed that trajectories may increase beyond their threshold values and then return to a more cost-effective lower value for the terminal cost $\varphi(x_2(\tau))$. This problem formulation therefore does not reflect the selectivity we are after, but it can be considered a *relaxed* formulation of the problem whose solution will allow us to clarify various aspects connected with the realistic problem formulation we are actually interested in. So does the problem formulation below when the *states are constrained to lie in the compact set $\mathcal{G}$.*

Problem 8. ***(P8)*** *With the terminal time τ free, minimize the objective*

$$\mathbb{J}(u) = \tau + \eta\, \varphi(x_2(\tau)) \tag{5.8}$$

over all admissible controls u subject to the dynamics (5.1), initial condition $\mathbf{x}(0) = \mathbf{x}_0 \in \mathcal{G}$, terminal condition $x_1(\tau) = x_{th}$ and state-space constraint $\mathbf{x} \in \mathcal{G}$, for all $t \in [0, \tau]$.

This problem simply enforces the constraint, but it also does not yet correspond to a formulation that would represent selectivity because it is still allowed for the trajectories to move along the threshold $x_{1,2} \equiv x_{th}$ which is an admissible boundary segment of the state-space. However, this is not useful since latent decision state x_1 would be activated instantly when it reaches the threshold value $x_1 = x_{th}$. This, however, causes that for some initial conditions optimal solutions do not exist and this will become plainly evident from the optimal solutions for the problems *P7* and *P8* which explain the pivotal role played by the state-space constraint for these problems.

5.2 Syntheses of Optimal Solutions

In this section we develop a synthesis of optimal controls u^* and their corresponding trajectories $\mathbf{x}^*$ for problems *P7* and *P8*. Optimal controls are bang-bang with at most one switching and, if there is a switching, the switching sequence depends on the relative magnitudes of the leak terms for the two states.

Proposition 8. *Optimal controls for problem P7 are bang-bang with at most one switching. If there is no switching, then optimal controls are constant at the maximum value* U_2*. Otherwise, if* $a_1 \neq a_2$*, then optimal controls have a unique switch from* U_2 *to* U_1 *if* $a_1 < a_2$ *and from* U_1 *to* U_2 *if* $a_1 > a_2$*. Thus optimal trajectories are of the forms* YX *and* XY*, respectively.*

***Proof**:* Necessary conditions for optimality of problem *P7* are given by the Pontryagin maximum principle [85] (e.g., see [50, 86, 87] for some more recent textbooks on the topic) with appropriate modifications to account for non-smooth formulations (e.g., [88, 89]).

The control Hamiltonian function is defined similarly as in (2.22)

$$\mathcal{H}(\lambda, \mathbf{x}, u) = \lambda_0 + \boldsymbol{\lambda}(\mathbf{A}\mathbf{x} + \mathbf{b}u), \tag{5.9}$$

with $\lambda_0 \in \{0, 1\}$ and $\boldsymbol{\lambda} \in (\mathbb{R}^2)^*$, the space of 2-dimensional row vectors. The multiplier $\boldsymbol{\lambda}$ satisfies the adjoint equation given by

$$\dot{\boldsymbol{\lambda}} = -\boldsymbol{\lambda}\mathbf{A}, \quad \text{i.e., } \dot{\lambda}_i = a_i\lambda_i,\ i = 1, 2, \tag{5.10}$$

and it follows from the maximum principle that

1. $\boldsymbol{\lambda}(t) \neq 0$ for all times t,
2. the optimal control u^* minimizes $\mathcal{H}$ over the control set $[\mathrm{U}_1, \mathrm{U}_2]$ along the multiplier $\boldsymbol{\lambda}$ and the optimal trajectory $\mathbf{x}^*$,
3. the function $\mathcal{H}$ vanishes identically along the multiplier $\boldsymbol{\lambda}$ and the optimal controlled trajectory $(\mathbf{x}^*, u^*)$ and
4. a transversality condition on the multiplier (which will be specified below) holds at the terminal time.

If we define the switching function as

$$\Phi(t) = \boldsymbol{\lambda}(t)\mathbf{b}, \tag{5.11}$$

then the minimization condition implies that

$$u^*(t) = \begin{cases} \mathrm{U}_2 & \text{if } \Phi(t) < 0, \\ \mathrm{U}_1 & \text{if } \Phi(t) > 0. \end{cases} \tag{5.12}$$

It is clear from the problem formulation and relation (5.5) that the control must be constant at its maximum value $u^*(t) \equiv \mathrm{U}_2$ if there is no switching. In general, the derivative of the

switching function Φ is given by

$$\dot{\Phi}(t) = \dot{\boldsymbol{\lambda}}(t)\mathbf{b} = -\boldsymbol{\lambda}(t)\mathbf{A}\mathbf{b} = a_1 b_1 \lambda_1(t) + a_2 b_2 \lambda_2(t). \tag{5.13}$$

If the system has a switching at time t_s, then it holds that $\Phi(t_s) = 0$, i.e.,

$$b_1 \lambda_1(t_s) = -b_2 \lambda_2(t_s). \tag{5.14}$$

Hence

$$\dot{\Phi}(t_s) = b_2(a_2 - a_1)\lambda_2(t_s). \tag{5.15}$$

Since $\boldsymbol{\lambda}(t) \neq 0$, it follows that $\lambda_2(t_s)$ does not vanish and λ_1 and λ_2 have constant and opposite signs over the full interval.

We *claim* that it follows form the transversality conditions at the endpoint that $\lambda_2(\tau) > 0$. For, if the function φ is differentiable at the endpoint, then the standard transversality conditions of the maximum principle (e.g., see [50]) imply that

$$\boldsymbol{\lambda}(\tau) = \lambda_0 \varphi_{\mathbf{x}}(x_2(\tau)) + \nu D_{\mathbf{x}} \psi(\mathbf{x}(\tau)). \tag{5.16}$$

Here $\psi(\mathbf{x}) = x_1 - x_{th} \equiv 0$ describes the terminal constraint and the set $\mathcal{N} = \{\mathbf{x} \in \mathbb{R}^2 | x_1 = x_{th}\}$ denotes the terminal manifold. Thus $\lambda_1(\tau)$ is free while

$$\lambda_2(\tau) = \lambda_0 \frac{\partial \varphi}{\partial x_2}(x_2(\tau)). \tag{5.17}$$

Since there is a switching, λ_2 cannot vanish and thus, in particular $\lambda_0 = 1$ and since φ is increasing, we also have that $\frac{\partial \varphi}{\partial x_2}(x_2(\tau)) > 0$. The same argument carries over to the case when $x_2(\tau) = x_c$ and the function φ is not differentiable, with the only change that instead

of the derivative $\frac{\partial \varphi}{\partial x_2}(x_2(\tau))$ now the whole range of values in the interval $[\varphi_1'(x_c), \varphi_2'(x_c)]$ are allowed as terminal values for the multiplier. But as before, since φ is non-decreasing, all these values are positive. This proves our claim.

It thus follows from (5.15) that the derivative of the switching function has the same sign at every switching and thus there can at most be one switching. If $a_1 > a_2$, then $\dot{\Phi}(t_s) < 0$ and thus the switching is from U_1 to U_2 while it is from U_2 to U_1 if $a_1 < a_2$. This proves the proposition. □

Knowing the switching structure of optimal controls, it is possible to determine the global structure of all solutions, i.e., construct an optimal synthesis. For 2-dimensional systems such syntheses follow well-established patterns that have been classified in [90] and are largely determined by the following two geometric objects in $\mathbb{R}^2$: the switching curve $\mathcal{S}$ where the controls switch and a cut-locus $\mathcal{C}$ from which multiple optimal controls exist.

Definition 8. *The switching curve $\mathcal{S}$ is the set of points in state space $\mathbb{R}^2$ that lie on trajectories when the control switches between* U_1 *and* U_2*, i.e.,*

$$\mathbf{x}^*(t_s) \in \mathcal{S} \Longleftrightarrow \Phi(t_s) = \lambda^*(t_s)\mathbf{b} = 0, \tag{5.18}$$

If the corresponding trajectories cross the switching curve transversally (at a non-zero angle), we call $\mathcal{S}$ a *transversal crossing.* In this case, the switching curve does not correspond to a trajectory of the system. In time-optimal control problems there also commonly exist switching curves which are trajectories of the system.

Definition 9. *If all the controls switch to one and the same trajectory of the system, we call such a trajectory a* separatrix $\mathcal{S}_p$.

Thus a separatrix is an extremal and in our model it separates the region where optimal controls are constant from initial conditions where optimal controls have a switching. We denote such controls by u_{sw}.

Definition 10. *The cut-locus $\mathcal{C}$ is the set of points from which it is possible to reach the terminal manifold optimally with both a constant control $u \equiv \mathrm{U}_{1,2}$ and a control u_{sw} that has a switching, i.e.,*

$$\mathcal{C} = \{\mathbf{x} \in \mathbb{R}^2 \mid \mathbb{J}(\mathrm{U}_i) = \mathbb{J}(u_{sw}) \ \ \textit{for}\ \mathbf{x}(0) = \mathbf{x},\ i \in \{1,2\}\}. \tag{5.19}$$

The cut-locus also separates regions in the state-space where optimal controls are constant from those where optimal controls have a switching. In general, for our problem, this separating set consists of concatenations of cut-loci and switching curves.

We note that a non-smooth terminal cost does not change the switching profile, but it leads to a modified, and in fact simpler form of the synthesis when compared with smooth models. If the penalty is high enough, we shall see that the non-smoothness of φ on the terminal manifold at x_c, as described in (5.6), (5.7), has the effect of attracting trajectories towards this point.

We now develop the optimal syntheses for the cases $a_1 < a_2$ and $a_1 > a_2$.

Simulation Parameters : In our examples, we consider the following form for the cost function $\varphi(x)$ as in (5.6),

$$\varphi(x) = \begin{cases} \varphi_1(x) = e + fx^r & \text{if } x < x_c \\ \varphi_2(x) = p(\frac{x}{x_c})^r & \text{if } x \geq x_c. \end{cases} \tag{5.20}$$

where $e, p, r > 0$ and $f = (p - e)x_c^{-r}$, ensuring $\varphi_1(x_c) = \varphi_2(x_c)$. For the various syntheses shown for $P7$, we have changed e, f, p, r to reveal the different constructions seen in Figure 5.2-5.5. Note that these functions are strictly increasing and convex. This is an assumption on the penalty term we implicitly make throughout this chapter. For our computations, we have used the following model parameters

$$\begin{aligned} &a_1 = 0.05,\ a_2 = 0.1,\ b_1 = 2,\ b_2 = 3, \\ &x_{th} = 30,\ \mathrm{U}_1 = 0,\ \mathrm{U}_2 = 5,\ \eta = 1, \end{aligned} \tag{5.21}$$

with a_1 and a_2 reversed for the case $a_1 > a_2$. Also, without loss of generality, from now on we take $\mathrm{U}_1 = 0$ and set $\mathrm{U}_2 = \mathrm{U}$.

5.2.1 Optimal synthesis for $a_1 < a_2$

For $a_1 < a_2$ optimal controls are either constant or they have exactly one switching from U_2 to U_1. Since the x_1-coordinate is decreasing over the final segment along U_1, it follows that the switching curve $\mathcal{S}$ lies above the terminal set $\mathcal{N}$ and outside the set $\mathcal{G}$. Furthermore, everywhere in the set $\mathcal{G}$ the optimal control is given by U_2. Let Υ_h denote the trajectory in $\mathcal{G}$ corresponding to the control U_2 which terminates in the corner point $[x_{th}\ x_{th}]^T$. It is clear that for initial conditions that lie below Υ_h optimal controls must have a switch and corresponding trajectories are of the type YX. This is also the optimal structure for points $x_f = [x_{th}\ \bar{x}_2]^T$ on the terminal set $\mathcal{N}$ if the incremental cost of making the switch is less than the gain made in the decrease of the penalty function realized through the switching. In this case, the control with a switch does better than the constant control U_2.

Since we know that optimal trajectories are of the YX type, it is easy to compute the optimal controls for points in $\mathcal{N}$: given $x_f = [x_{th}\ \bar{x}_2]^T \in \mathcal{N}$, for $\varepsilon \geq 0$ consider the control

$$u_\varepsilon(t) = \begin{cases} \mathrm{U}_2 = \mathrm{U} & \text{for } 0 \leq t \leq \varepsilon, \\ \mathrm{U}_1 = 0 & \text{for } \varepsilon < t < \zeta(\varepsilon), \end{cases} \tag{5.22}$$

where $\zeta(\varepsilon)$ is the unique time when the corresponding X-trajectory reaches the terminal set from above. This function is easily computed and we have that

$$\zeta = \varepsilon + \frac{1}{a_1} \ln \left(e^{-a_1 \varepsilon} + \left(1 - e^{-a_1 \varepsilon}\right) \frac{b_1 \mathrm{U}}{a_1 x_{th}} \right). \tag{5.23}$$

In particular, this function does not depend on the initial point $\bar{x}_2$. We note that ζ is strictly increasing with slope $\zeta'(\varepsilon) > 1$ and strictly concave, $\zeta''(\varepsilon) < 0$. The end-point of this trajectory is given by

$$x_2(\zeta(\varepsilon)\,;\,\bar{x}_2) = e^{-a_2 \zeta(\varepsilon)} \left(\bar{x}_2 + \frac{b_2}{a_2} \mathrm{U}\,(e^{a_2 \varepsilon} - 1) \right) \tag{5.24}$$

and is linear in $\bar{x}_2$. If we denote this point by $\xi(\varepsilon\,;\,\bar{x}_2)$, then the difference in the cost function is given by

$$\Delta(\varepsilon\,;\,\bar{x}_2) = \zeta(\varepsilon) + \varphi(\xi(\varepsilon)\,;\,\bar{x}_2) - \varphi(\bar{x}_2). \tag{5.25}$$

For $\varepsilon = 0$ the trajectory reduces to the initial point $\bar{x}_2$ with $\Delta(0\,;\,\bar{x}_2) = 0$ while it is clear that for ε large enough, $\Delta(\varepsilon\,;\,\bar{x}_2)$ will be positive. Thus there always exists a minimum value over $[0, \infty)$ which is easily computed numerically and this minimum determines the optimal control. If the function $\Delta(\varepsilon\,;\,\bar{x}_2)$ remains positive for all times, then the minimum is attained for $\varepsilon = 0$, i.e., at this point the optimal controlled trajectory reaches the terminal manifold with the control U from below. In Figure 5.1 we illustrate this function for two

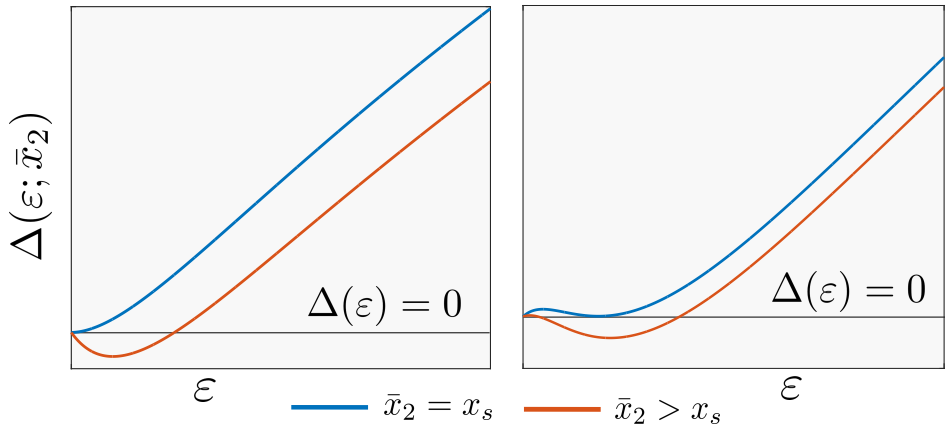

Figure 5.1: Illustration of $\Delta(\varepsilon\,;\,\bar{x}_2)$ corresponding to a switching curve with transversal crossing (left) or a cut-locus (right) in the neighborhood of x_s, which is the intersection between $\mathcal{S}_p$ and $\mathcal{N}$, for $(P7)$ with $a_1 < a_2$.

different points on $\mathcal{N}$ for two different smooth $\varphi(.)$ (left and right panel). We shall see that the optimal synthesis is determined by a switching curve with a transversal crossing at $\mathcal{N}$ (left) or cut-locus (right) that may arise, as revealed by the nature of this function. In both cases the blue curve denotes the onset of switching and corresponds to $\bar{x}_2 = x_s$. However, the function $\Delta(\varepsilon\,;\,\bar{x}_2)$ can become negative (c.f., the red curves in Fig. 5.1) and in this case it is better to continue with the control and then switch to $\mathrm{U}_1 = 0$ to return to the terminal manifold. Overall, we have the following general result:

Proposition 9. *Let $a_1 < a_2$ and suppose the terminal cost $\varphi(x)$ in $P7$ is a smooth, strictly monotonically increasing and convex function. Then switching curves are transversal crossings and there exists a unique point $x_s > 0$ such that the following holds:*

1. *Points $P = [x_{th}\ \bar{x}_2]^T$ with $\bar{x}_2 < x_s$ are endpoints of optimal controlled trajectories both from below and from above: trajectories corresponding to the constant control U_2 terminate at P from below and trajectories corresponding to the control U_1 (with or without a prior switching) terminate at P from above.*

2. *The point* $P_s = [x_{th}\ x_s]^T$ *is the endpoint of only the trajectory corresponding to the constant control* U_2 *from below.*

3. *Points* $P = [x_{th}\ \bar{x}_2]^T$ *with* $x_2 > x_s$ *are not endpoints of optimal controlled trajectories. In this case all trajectories corresponding to* U_2 *cross* $\mathcal{N}$ *at* P *and return to* $\mathcal{N}$ *at a lower value after the switching.*

Proof*:* We prove Proposition 9 by contradiction. Recall that

$$\Delta(\varepsilon, \bar{x}_2) = \zeta(\varepsilon) + \varphi(\xi(\varepsilon); \bar{x}_2) - \varphi(\bar{x}_2) \tag{5.26}$$

and consider the following function

$$\tilde{\Delta}(\bar{x}_2) = \min_{\varepsilon} \Delta(\varepsilon, \bar{x}_2) \tag{5.27}$$

Let us assume the contrary, i.e., there is no unique x_s and the synthesis contains $x_s' > x_s$ such that extremals ending at the terminal manifold from below with $0 \leq \bar{x}_2 \leq x_s$ have no switching, for $x_s < \bar{x}_2 < x_s'$ have one switching and for $x_s' \leq \bar{x}_2 \leq x_{th}$ once again there is no switching. Then according to our assumption we have the following for $\tilde{\Delta}(\bar{x}_2)$

$$\tilde{\Delta}(\bar{x}_2) = \begin{cases} 0 & \text{for } \bar{x}_2 \in [0, x_s] \\ k(\bar{x}_2) < 0 & \text{for } \bar{x}_2 \in (x_s, x_s') \\ 0 & \text{for } \bar{x}_2 \in [x_s', x_{th}] \end{cases} \tag{5.28}$$

with $k(\bar{x}_2)$ some function of $\bar{x}_2$. The other sequence, i.e. first switching to no switching in $\mathcal{G}$ and the corresponding $\tilde{\Delta}(\bar{x}_2)$, taking sign $-, +$ respectively is not feasible and we'll show this later. Now let us consider a point $\bar{x}_2' \in (x_s, x_s')$ and the corresponding switching time is $\bar{\varepsilon}$.

Thus we have

$$\bar{\varepsilon} = \arg\min_{\varepsilon} \Delta_1(\varepsilon, \bar{x}_2') \tag{5.29}$$

Since $\Delta(0, \bar{x}_2') = 0$, $\lim_{\varepsilon\to\infty} \Delta(\varepsilon) \to \infty$, for the switching time $\bar{\varepsilon}$ we have

$$\frac{\partial \Delta}{\partial \varepsilon}(\bar{\varepsilon}, \bar{x}_2') = 0,\ \Delta(\bar{\varepsilon}, \bar{x}_2') = k' < 0 \tag{5.30}$$

Since $\zeta(\bar{\varepsilon}) > 0$, from (5.26) we get

$$\varphi(\xi(\bar{\varepsilon}, \bar{x}_2')) - \varphi(\bar{x}_2') < 0 \tag{5.31}$$

and with φ increasing, this means

$$\xi(\bar{\varepsilon}, \bar{x}_2') < \bar{x}_2' \tag{5.32}$$

Rewriting (5.24) as

$$x_2(\zeta(\varepsilon)\ ;\ \bar{x}_2) = \xi(\varepsilon, \bar{x}_2) = m(\varepsilon)\ \bar{x}_2 + c(\varepsilon), \tag{5.33}$$

where

$$m(\varepsilon) = \mathrm{e}^{-a_2\zeta(\varepsilon)} < 1,\ \ 0 < m < 1,\ c(\varepsilon) = \mathrm{e}^{-a_2\zeta(\varepsilon)} \frac{b_2}{a_2} \mathrm{U}(\mathrm{e}^{a_2\varepsilon} - 1) \tag{5.34}$$

i.e., for a given ε, ξ is linear in $\bar{x}_2$. From (5.32), and fixing $\varepsilon = \bar{\varepsilon}$ in (5.33), for any $\bar{x}_2 \geq \bar{x}_2'$ with $\bar{x}_2 = \bar{x}_2' + h$, $h \geq 0$, we have that

$$\xi(\bar{x}_2, \bar{\varepsilon}) = m(\bar{\varepsilon})\bar{x}_2' + c(\bar{\varepsilon}) = m(\bar{x}_2' + h) + c = (m\bar{x}_2' + c) + mh = \xi(\varepsilon, \bar{x}_2') + mh < \bar{x}_2' + h = \bar{x}_2, \tag{5.35}$$

i.e.,

$$\xi(\bar{x}_2, \bar{\varepsilon}) < \bar{x}_2,\ \forall\, \bar{x}_2 \geq \bar{x}_2'. \tag{5.36}$$

Next we take partial of $\Delta(.)$ with respect to $\bar{x}_2$

$$\frac{\partial \Delta(\varepsilon, \bar{x}_2)}{\partial \bar{x}_2} = m(\varepsilon)\varphi'(\xi(\varepsilon; \bar{x}_2)) - \varphi'(\varepsilon, \bar{x}_2) \tag{5.37}$$

For $\bar{x}_2 \geq \bar{x}_2'$ with (5.36) and plugging $\varepsilon = \bar{\varepsilon}$ in (5.37), we have

$$\frac{\partial \Delta(\bar{x}_2, \bar{\varepsilon})}{\partial \bar{x}_2} < 0, \tag{5.38}$$

since φ is strictly convex. From (5.30) we know

$$\Delta(\bar{\varepsilon}, \bar{x}_2') = k' \tag{5.39}$$

Let us consider $\bar{x}_2'' \in [x_s', x_{th}]$ and since $\bar{x}_2'' > \bar{x}_2'$, from (5.38) (5.39),

$$\Delta(\bar{\varepsilon}, \bar{x}_2'') = k'' < k' < 0 \tag{5.40}$$

Thus there exists $\varepsilon = \bar{\varepsilon}$ such that $\Delta(\bar{\varepsilon}, \bar{x}_2'') < 0$, but from (5.28) we have

$$\tilde{\Delta}(\bar{x}_2'') = \min_{\varepsilon} \Delta(\varepsilon, \bar{x}_2'') = 0, \tag{5.41}$$

which is a contradiction. For the other sequence of signs we can use the same argument to show that $\tilde{\Delta}$ cannot change sign from negative to positive. Thus we can claim that there is a unique x_s on $\mathcal{N}$ which separates the switching profile within $\mathcal{G}$. □

In Figure 5.2 we present the synthesis of $P7$ and it's features by changing the smooth penalty function φ. The middle panel shows the synthesis of optimal controlled trajectories away from the terminal point $P_s = [x_{th}\ x_s]^T$. The portion near P_s is left blank as there exist two cases for how the synthesis looks like near P_s depending on whether a switching curve $\mathcal{S}$ or a

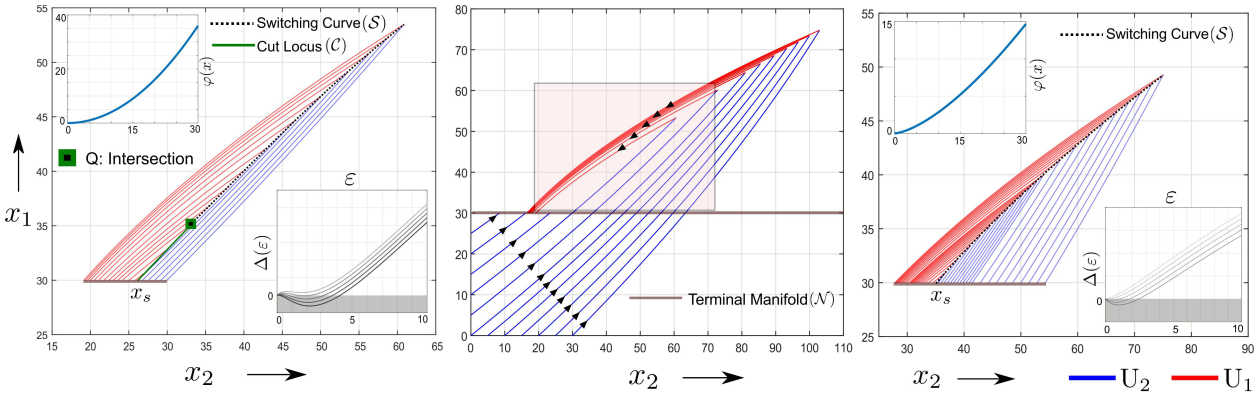

Figure 5.2: Syntheses for $P7$ under smooth φ's with $a_1 < a_2$. The general structure is shown in the middle where the highlighted rectangle indicates the region in which the synthesis may differ. (Left) A cut-locus is generated at x_s which ultimately intersects the switching curve at Q. (Right) The switching curve has a transversal crossing at x_s. In the insets we show $\Delta(\varepsilon; \bar{x}_2)$ by varying $\bar{x}_2$ in the neighborhood of x_s for these two cases.

cut-locus $\mathcal{C}$ emerges from this point. These two cases are shown as blow-ups in the right and left panels respectively of Fig. 5.2.

The right panel shows the synthesis for the case when the limiting point P_s is the intersection of the switching curve with the terminal manifold, $P_s = \mathcal{S} \cap \mathcal{N}$. If Υ_s denotes the backward trajectory (in $\mathcal{G}$) corresponding to the control U_2, then to the left of Υ_s optimal controls are constant given by U_2 and the corresponding trajectories end as they reach $\mathcal{N}$ from below, while optimal controls have a switch for initial conditions that lie to the right of Υ_s. In this case, optimal trajectories are of the type YX and then return to a point to the left of x_s. This situation corresponds to the case when the function Δ is strictly positive for points $\bar{x}_2 < x_s$ and has minima for positive values of ε for $\bar{x}_2 > x_s$ which converge to $\varepsilon = 0$ as $\bar{x}_2 \to x_s$ from the right.

The panel on the left in Figure 5.2 shows the synthesis when the function Δ for the base point x_s still has the minimum value zero, but this minimum is also attained for a positive value $\varepsilon_0 > 0$, $\Delta(\varepsilon_0) = 0$. In this case, it is equally optimal to terminate the trajectory for the control U_2 as it reaches the terminal manifold from below or to continue with this control and

switch at time ε_0 and then return to the terminal manifold from above. Thus the point P_s lies on the cut-locus for the trajectories which use the constant control U_2 and those which follow the switching strategy u_{sw}. Indeed, in this case a cut-locus $\mathcal{C}$ emerges from P_s which divides the set above $x_1 = x_{th}$ into two regions where, respectively, $u = \mathrm{U}_1$ and $u = \mathrm{U}_2$ are optimal. This cut-locus $\mathcal{C}$ then merges with the switching curve $\mathcal{S}$ in a point Q and the frame $(\mathcal{C}, \mathcal{S})$ determines the optimal synthesis.

The optimal synthesis can take a qualitatively different form if the penalty function φ becomes non-smooth in which case the switching curve can become a separatrix. Suppose φ is not differentiable at $x = x_c$ and denote by $\mathcal{Y}_c$ the Y-trajectory which terminates at the critical point x_c from below and by $\mathcal{X}_c$ the X-trajectory which terminates at the critical point x_c from above. If the difference between the derivatives of φ_2 at x_c from the right and φ_1 at x_c from the left, denoted by κ,

$$\kappa = \frac{\partial \varphi_2}{\partial x}(x_c^+) - \frac{\partial \varphi_1}{\partial x}(x_c^-) \tag{5.42}$$

is small enough then non-smoothness of φ has no bearing on the synthesis (Figure 5.3 left), whereas, if κ is larger than a critical value, specifically κ_c (See Appendix D.1),

$$\kappa \geq \kappa_c \tag{5.43}$$

then all optimal controls for initial points to the right of $\mathcal{Y}_c$ have a switch and they reach the terminal set $\mathcal{N}$ at x_c along the trajectory $\mathcal{X}_c$. This feature is illustrated in the diagram on the right in Figure 5.3. It is generated by the non-smoothness of the penalty $\varphi(x)$ which causes all the trajectories to be attracted to the terminal point x_c on $\mathcal{N}$ which takes over the role of the point x_s in Proposition 9. We have the following behavior which is proven with a similar argument as above.

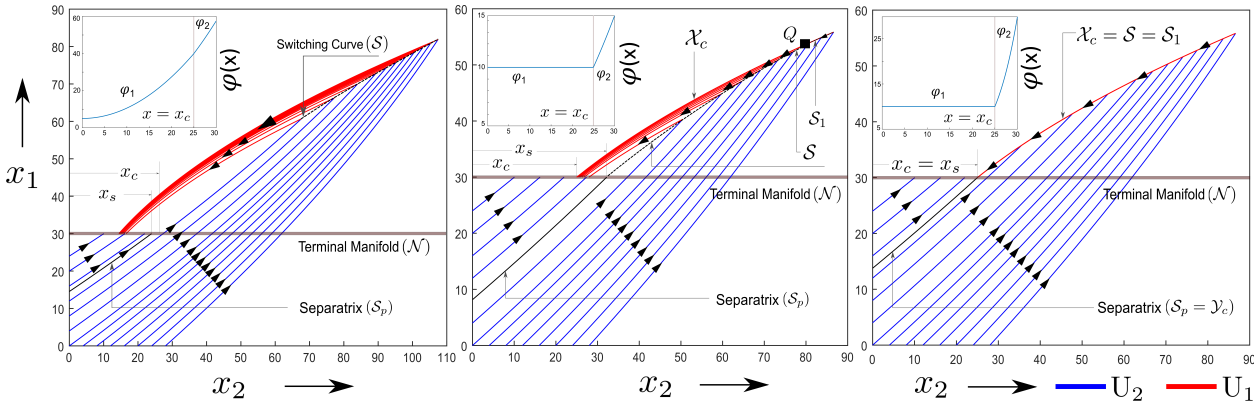

Figure 5.3: Illustration of the optimal syntheses for problem $P7$ under non-smooth φ's with $a_1 < a_2$. The different penalties are shown in the inset. (Left) The non-smooth φ has no effect on the synthesis. (Right) φ with $\kappa > \kappa_c$ such that x_c attracts all switched trajectories in $\mathcal{G}$. (Middle) Mix of the two features with the switching curve being a combination of the transversal crossing and a subset $\mathcal{S}_1$ of $\mathcal{X}_c$.

Proposition 10. *Let $a_1 < a_2$ and suppose the terminal cost $\varphi(x)$ in $P7$ is strictly monotonically increasing and convex, but non-smooth at x_c with $\kappa > \kappa_c$. Then the switching curve is a separatrix given by the trajectory $\mathcal{X}_c$ and the following hold:*

1. *Points $P = [x_{th}\ \bar{x}_2]^T$ with $\bar{x}_2 < x_c$ are only endpoints of optimal controlled trajectories corresponding to the constant control U_2 which terminate at P from below.*

2. *The point $P_c = [x_{th}\ x_c]^T$ is the endpoint for both the trajectories $\mathcal{X}_c$ from above and $\mathcal{Y}_c$ from below.*

3. *Points $P = [x_{th}\ \bar{x}_2]^T$ with $\bar{x}_2 > x_c$ are not endpoints of optimal controlled trajectories. In this case all trajectories corresponding to U_2 cross $\mathcal{N}$ at P and then switch to the control U_1 as the trajectory intersects $\mathcal{X}_c$ and then return to $\mathcal{N}$ in the point x_c along $\mathcal{X}_c$.*

In such a situation, the switching curve thus is the trajectory $\mathcal{X}_c$ of the system and the trajectory $\mathcal{Y}_c$ becomes the separatrix in $\mathcal{G}$ between initial conditions for which optimal

controls are constant and for which they have a switching. Note the simpler structure for this synthesis.

More generally, for smaller values of κ (See Appendix D.1), with

$$\kappa_c' \leq \kappa < \kappa_c \tag{5.44}$$

these two features mix as shown in the middle diagram of Figure 5.3. It is always the trajectory $\mathcal{X}_c$ that forms the limiting behavior of trajectories entering $\mathcal{N}$ from above, but not the full curve consists of switching points. There exists a unique point Q on this trajectory marked by a black square in the figure such that points on $\mathcal{X}_c$ above Q are switching points while points below Q are not. In the figure, we denote the portion of $\mathcal{X}_c$ above Q by $\mathcal{S}_1$. At the point Q the switching curve separates from $\mathcal{X}_c$ into a separate curve which is a transversal crossing. This part of the switching locus may still merge with a cut-locus and the combined curve intersects the terminal set $\mathcal{N}$ in a point $x_s > x_c$ leading to similar local behavior near x_s as in the smooth case. Altogether, the switching curve consists of the union of this transversal crossing and the portion $\mathcal{S}_1$ of $\mathcal{X}_c$ joined at Q. For this case, the points x_s and x_c which coincided in Proposition 10, separate and we have the following behavior:

Proposition 11. *Let $a_1 < a_2$ and suppose the terminal cost $\varphi(x)$ in P7 is strictly monotonically increasing and convex, but non-smooth at x_c. For κ satisfying* (5.44)*, there exists a point $x_s > x_c$ such that the following holds:*

1. *Points $P = [x_{th}\ \bar{x}_2]^T$ with $\bar{x}_2 < x_c$ are only endpoints of optimal controlled trajectories corresponding to the constant control* U_2 *which terminate at P from below.*

2. *The point $P_c = [x_{th}\ x_c]^T$ is the endpoint for both the trajectories $\mathcal{X}_c$ from above and $\mathcal{Y}_c$ from below.*

3. *Points* $P = [x_{th}\ \bar{x}_2]^T$ *with* $x_c < \bar{x}_2 < x_s$ *are endpoints of optimal controlled trajectories both from below and from above: trajectories corresponding to the constant control* U_2 *terminate at* P *from below and trajectories corresponding to the control* U_1 *(with or without a prior switching) terminate at* P *from above.*

4. *The point* $P_s = [x_{th}\ x_s]^T$ *is the endpoint of only the trajectory corresponding to the constant control* U_2 *from below.*

5. *Points* $P = [x_{th}\ \bar{x}_2]^T$ *with* $\bar{x}_2 > x_s$ *are not endpoints of optimal controlled trajectories. In this case all trajectories corresponding to* U_2 *cross* $\mathcal{N}$ *at* P *and then return to the terminal manifold after switching to the control* U_1 *(either along a transversal crossing or as the trajectory intersects* $\mathcal{X}_c$*).*

In order to highlight the differences between a smooth and non-smooth penalty function, in Figure 5.4 we modify the example considered in the middle portion of Figure 5.3 by smoothing the terminal cost around x_c with a polynomial function $\varphi_3(x)$ such that

$$\begin{aligned} \varphi_3(x-\delta) &= \varphi_1(x-\delta),\ \varphi_3'(x-\delta) = \varphi_1'(x-\delta) \\ \varphi_3(x+\delta) &= \varphi_2(x+\delta),\ \varphi_3'(x+\delta) = \varphi_2'(x+\delta) \end{aligned} \tag{5.45}$$

with a small and positive δ. With this change, the trajectory $\mathcal{X}_c$ no longer plays a special role in the synthesis. The returning trajectories to the terminal manifold progressively move closer to each other on the left but do not converge to a single segment as before.

Summarizing, already for this simple model of decision problem a variety of optimal solutions arises. Of these, the synthesis shown in the right panel of Figure 5.3 has the simplest structure, but it only arises if the jump κ satisfies (5.43).

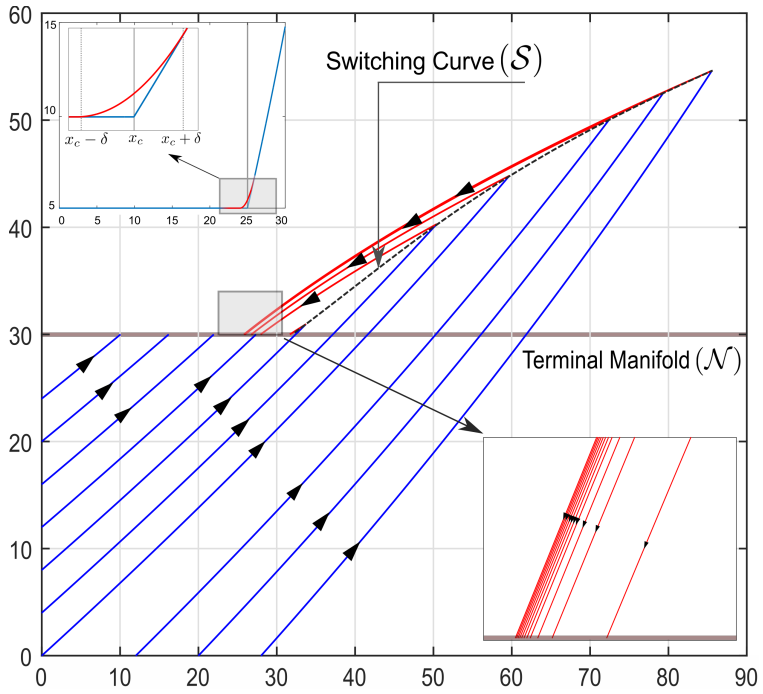

Figure 5.4: Synthesis for the smoothed version of φ in Figure 5.3 (right) which illustrates that the convergence feature of the X trajectories to a unique point x_c is specific to non-smooth φ.

5.2.2 Optimal synthesis for $a_1 > a_2$.

In this case, possible switchings are from U_1 to U_2. Hence the switching curve $\mathcal{S}$ lies in the set $\mathcal{G}$, i.e., within the limits imposed by the thresholds. Optimal trajectories, after a possible initial decrease in both variables, reach the terminal value $x_2(\tau) = x_{th}$ from within $\mathcal{G}$. In fact, the region $\mathcal{G}$ is positively invariant for the control system and we only need to consider this region.

The analysis is very much symmetric to the previous one with the simplification that the entire optimal synthesis is within $\mathcal{G}$. We therefore just indicate these structures. Figure 5.5 depicts the typical types of optimal syntheses for different $\varphi(x)$ under the specific parameter condition. The figure on the left shows a synthesis where the switching curve is a transversal crossing, the figure on the right gives the other extreme where all trajectories for the control

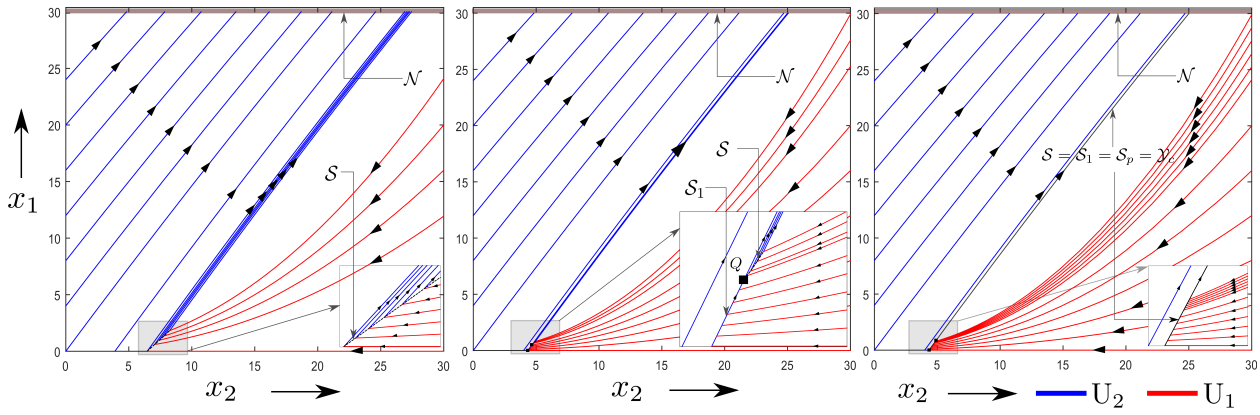

Figure 5.5: Illustration of the optimal syntheses for problem $P7$ under non-smooth φ with $a_1 > a_2$. The optimal controls are either U_2 or a switched control from U_1 to U_2. (Left) The non-smoothness has no effect on the synthesis. (Right) The non-smoothness is high enough such that X trajectories switch on intersection with $\mathcal{Y}_c$. (Middle) Mix of these two syntheses, similar to Figure 5.3 (middle), where a subset $\mathcal{S}_1$ of the switching curve $\mathcal{S}$ coincides with $\mathcal{Y}_c$.

U_1 switch as they intersect the trajectory $\mathcal{Y}_c$ and then all these trajectories end on the terminal manifold in the point x_c. As above, the first case (left) corresponds to a φ with a small enough κ while the latter one (right) arises if the one-sided derivatives at x_c from left and right has a sufficiently large gap (See Appendix D.1). The intermediate case (middle) corresponds to a situation when these two cases intermingle. The black square again denotes the point Q where the character of the switching curve changes from a transversal crossing (above Q) to a separatrix, namely the portion of the trajectory $\mathcal{Y}_c$ below Q. Similar to the case $a_1 < a_2$, the trajectory $\mathcal{Y}_c$ plays the critical role of channeling optimal solutions to the critical point x_c on the terminal manifold. We note that, in contrast to the case $a_1 < a_2$, for $a_1 > a_2$ no cut-locus exists in the synthesis.

5.2.3 Synthesis of the optimal control problem *P8* with state constraint.

We now analyze problem *P8* which is simply problem *P7* with $\mathbf{x} \in \mathcal{G}$ enforced as a state-space constraint. In the case $a_1 > a_2$, all extremals in the optimal synthesis for problem *P7* are entirely contained within $\mathcal{G}$. Thus all these controlled trajectories are admissible for problem *P8* as well and, since they are even optimal over the larger class of admissible controlled trajectories for problem *P7*, this is also the optimal solution for problem *P8*. Essentially, while the class of admissible controlled trajectories has been made smaller, the optimal solution from problem *P7* was retained. This no longer is the case for $a_1 < a_2$ when trajectories with a switching decrease in the final phase to reach the terminal manifold, i.e., violate the state-space constraints matter of problem *P8*. We henceforth assume that $a_1 < a_2$.

We briefly discuss the reduced dynamics when a state -space constraint is active. The lower limits $x_1 = 0$ and $x_2 = 0$ will never become active and the upper limits $x_1 = x_{th}$ and $x_2 = x_{th}$ are order 1 state-space constraints, i.e., the corresponding boundary controls u_∂ can be computed by simply setting the first derivatives of these variables to zero. We have that

$$u_{\partial,i} = \frac{a_i}{b_i} x_{th}, \qquad i = 1, 2. \tag{5.46}$$

Along the boundary segments, it matters whether the system moves the other variable towards 0 or towards x_{th}. This depends on the ratio, discussed in (2.19), Appendix A.1.1

$$\vartheta_1 = \frac{b_1 a_2}{b_2 a_1}. \tag{5.47}$$

For example, suppose the constraint $x_2 = x_{th}$ is active. Then, along the boundary control we have that

$$\dot{x}_1 = -a_1 x_1 + b_1 \frac{a_2}{b_2} x_{th} = -a_1 x_1 \left(1 - \vartheta_1 \frac{x_{th}}{x_1}\right). \tag{5.48}$$

If $\vartheta_1 < 1$, this derivative is negative near $x_1 = x_{th}$ and thus trajectories cannot reach the target manifold along this boundary segment while this is possible if $\vartheta_1 > 1$. Similarly, if $x_1 = x_{th}$ is active, then

$$\dot{x}_2 = -a_2 x_2 + b_2 \frac{a_1}{b_1} x_{th} = -a_2 x_2 \left(1 - \frac{1}{\vartheta_1} \frac{x_{th}}{x_2}\right). \tag{5.49}$$

For $\vartheta_1 < 1$, this derivative is positive near $x_2 = x_{th}$ and thus trajectories can move to the right. But the penalty function is non-decreasing and thus this will not be advantageous. Hence trajectories simply terminate when they reach the terminal manifold. On the other hand, if $\vartheta_1 > 1$, then this derivative is negative and states with a lower penalty may be reachable using the boundary control. If this can be done by lowering the overall cost, then trajectories will end with such a boundary segment. We start with the simpler scenario.

Proposition 12. *For $\vartheta_1 \leq 1$, the optimal control for P8 is bang-bang with at most one switching: trajectories either reach the terminal manifold directly under U_2 or go through a switching from U_1 to U_2, similar to the case $a_1 > a_2$ for problem P7.*

Proof: In this case, the value of the objective cannot be improved by moving along the state constraint $x_2 \equiv x_{th}$ if $x_1 = x_{th}$ or it is not possible to reach the terminal manifold $\mathcal{N}$ along $x_1 \equiv x_{th}$ if $x_2 = x_{th}$. Inside the region $\mathcal{G}$ the conditions of the standard maximum principle apply and thus, for any initial condition $\mathbf{x}(0) = [x_1(0)\ x_2(0)]^T$, the synthesis is governed by

the following optimization problem:

$$\begin{aligned} \underset{x}{\text{minimize}} \quad & \varphi(\varrho(x)) + \beta(x) + \mu(x) \\ \text{subject to} \quad & 0 \leq x \leq x_2(0). \end{aligned} \tag{5.50}$$

Here x denotes the value for the x_2 coordinate after an initial segment with $u \equiv \mathrm{U}_1$, $\beta(x)$ is the time during the initial decay period under U_1,

$$\beta(x) = \frac{1}{a_2} \log\left(\frac{x_2(0)}{x}\right), \; x_1(\beta(x)) = x_1(0)\left(\frac{x}{x_2(0)}\right)^{\frac{a_1}{a_2}}, \tag{5.51}$$

$\mu(x)$ denotes the time for the target state x_1 to reach the threshold from it's decayed value at $t = \beta(x)$, given by $x_1(\beta(x))$,

$$\mu(x) = \frac{1}{a_1} \log\left(\frac{{}^{b_1}\!/_{a_1}\mathrm{U} - x_1(\beta(x))}{{}^{b_1}\!/_{a_1}\mathrm{U} - x_{th}}\right), \tag{5.52}$$

and $\varrho(x)$ denotes the terminal value of the x_2 coordinate on $\mathcal{N}$,

$$\varrho(x) = \left(\frac{{}^{b_1}\!/_{a_1}\mathrm{U} - x_{th}}{{}^{b_1}\!/_{a_1}\mathrm{U} - x_1(\beta(x))}\right)^{\frac{a_2}{a_1}} x + \frac{b_2}{a_2}\mathrm{U}\left(1 - \left(\frac{{}^{b_1}\!/_{a_1}\mathrm{U} - x_{th}}{{}^{b_1}\!/_{a_1}\mathrm{U} - x_1(\beta(x))}\right)^{\frac{a_2}{a_1}}\right). \tag{5.53}$$

In this formulation, if the solution of (5.50) turns out to be $x = x_2(0)$, the optimal control is simply bang to the terminal manifold. In this case, the segment with U_1 is absent. □

Proposition 13. *For $\vartheta_1 > 1$, the optimal control for problem P8 is a concatenation of bang and boundary controls: (a) If the extremal for the constant control U_2 hits the constraint boundary $x_2 = x_{th}$ first, then the control switches to the boundary control $u_{\partial,2} = \frac{a_2}{b_2} x_{th}$, until the corner point for $x_1 = x_{th}$ is reached, and then concludes with the other boundary control $u_{\partial,1} = \frac{a_1}{b_1} x_{th}$. This control terminates when the best terminal point (in the sense of minimizing the objective) on the constraint $\mathcal{N}$ is reached. (b) If the extremal for the constant control*

U_2 *first hits the constraint boundary* $x_1 = x_{th}$*, the optimal controls may terminate at that point or still use the boundary control to move along* $\mathcal{N}$ *until the best terminal point has been reached. Summarizing, optimal controls are piecewise constant, start with* U_2*, and possibly are followed by two boundary arcs.*

Proof*:* Controls in the optimal synthesis for the unconstrained problem are either U_2 or a concatenation of U_2 with U_1 in that order. If there is a switching, the final segments of the trajectories lie outside $\mathcal{G}$ and violate the state constraint for *P8*, and the control U_1 is only used outside of $\mathcal{G}$. With the state constraint imposed, this control no longer is feasible. The constant control $u^* = \mathrm{U}_2$ defines a smooth family of controlled trajectories on $\mathcal{G}$ until the extremals hit the constraints. In the case $\vartheta_1 > 1$, the state can move along the boundary segments to reach the target value and to improve the cost. Whether the last segment exists and if it does, where it ends on $\mathcal{N}$, specifically the x_2 co-ordinate, is determined by the solution of the following optimization problem:

$$\begin{aligned} \underset{x}{\text{minimize}} \quad & \varphi(x) + \alpha(x) \\ \text{subject to} \quad & 0 \leq x \leq x', \end{aligned} \tag{5.54}$$

where x' is the x_2 co-ordinate of the point where the extremals hit $\mathcal{N}$ under U_2 or $x' = x_{th}$ if this trajectory first hits the constraint $x_2 = x_{th}$ and

$$\alpha(x) = \frac{1}{a_2} \log\left(\frac{\frac{b_2}{a_2} u_{\partial,1} - x'}{\frac{b_2}{a_2} u_{\partial,1} - x} \right), \tag{5.55}$$

is the time taken to reach x on $\mathcal{N}$ from x' under $u_{\partial,1} = \frac{a_1}{b_1} x_{th}$.

The optimization program in (5.54) defines a compromise between reducing the penalty at the end point x and the cost of moving on $\mathcal{N}$ to reach x. Note that for the same set of parameters, the end point of the extremals here and for problem *P7* need not be the same.

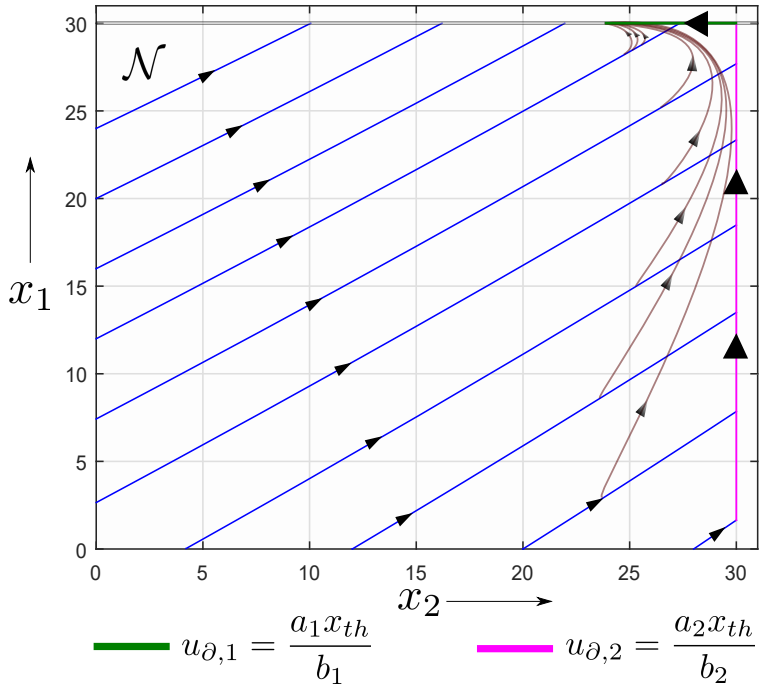

Figure 5.6: Optimal synthesis of controlled trajectories for problem *P8* with a family of sub-optimal approximating trajectories which do not encounter the constraints.

Like for all the other problems considered above, the optimality of this field of controlled trajectories follows from regular synthesis type constructions [50] along similar modifications as they are made in detail in [51]. □

In Figure 5.6 we show the synthesis for *P8* with $\vartheta_1 > 1$ and the critical point of the terminal cost being $x_c = 20$. The solution of (5.54) here, is given by $x = 23.9$ and any extremal intersecting $\mathcal{N}$ to the right of this value, has a segment with u_∂ that keeps x_1 invariant at x_{th} (shown in green). The boundary arc along $x_2 = x_{th}$ is plotted in magenta.

5.2.4 Implications for the threshold hitting problem

At this point, it is important to revisit the motivation of the threshold hitting problems considered in this chapter. We added the penalty φ along the terminal manifold in (5.3), (5.8) to ensure that the optimal control u^*, along with driving the target variable (x_1) to

the threshold, keeps the other state (x_2) away from it's own threshold. Since the thresholds here, are associated with the occurrence of an event, accuracy or unambiguity is an equally important aspect of this problem. In Proposition 13, we see that the extremals which involve switching, move along $x_{1,2} = x_{th}$ to reach an inexpensive point on $\mathcal{N}$. But for the real underlying problem these trajectories are inadmissible, because as soon as one of the thresholds is hit, the corresponding event associated to that state, takes place, rendering the boundary arcs irrelevant. Thus, even though the extremals with the boundary arcs are indeed the optimal solution to *P8*, they do not reflect the underlying premises of the problem. In fact, we have the following result:

Proposition 14. *For the threshold hitting problem with $\vartheta_1 > 1$, there is no optimal solution.*

Proof: If $\vartheta_1 > 1$, then the optimal synthesis for problem *P8* involves boundary arcs along $x_1 = x_{th}$ and possibly $x_2 = x_{th}$. But as we have discussed above, once the extremal hits one of the thresholds, in the context of the problem, the latter part of the extremal is inconsequential. Thus the extremals with boundary arcs are inadmissible for the threshold hitting problems. On the other hand, it is straightforward to find controls such that the trajectories closely follow the optimal trajectories of problem *P8* and reach the target point on the terminal manifold without actually touching one of the thresholds. These trajectories get arbitrarily close to the optimal solutions of problem *P8*, but the limiting curve is no longer an admissible controlled trajectory. □

This resembles the qualitative nature of the optimal synthesis for the classical problem of minimum surfaces of revolution in the calculus of variations [91] and we briefly recall that structure in Figure 5.7. Here the goal is to find a non-negative curve connecting two points $[0\ y_0]^T$ and $[t_1\ y_1]^T$, $t_1,\ y_0,\ y_1 > 0$ which, when rotated around the t-axis, generates a surface with minimum surface area. If one restricts curves to be positive smooth functions, then all

extremals are given by the family of catenaries:

$$y(t) = \sigma \cosh\left(\frac{t-\theta}{\sigma}\right), \theta \in \mathbb{R},\ \sigma > 0, \tag{5.56}$$

with $y_0 = \sigma \cosh(-\frac{\theta}{\sigma})$, imposed by the initial condition. Introducing $p = -\frac{\theta}{\sigma}$, (5.56) can be expressed as the one parameter family

$$y(t\ ;\ p) = \frac{y_0}{\cosh p} \cosh\left(p + \frac{t}{y_0}\cosh p\right). \tag{5.57}$$

In Figure 5.7 (left), we plot the catenaries for $t_1 = 2$, as we vary the parameter p. The resultant curves are the extremals between any two points for this problem. In Figure 5.7 (middle), we show the surface generated by a rotation around t axis for one such catenary between $[0\ 1]^T$ and $[2\ 2.65]^T$, i.e., $y_0 = 1$ and $y_1 = 2.65$. It turns out, however, that for some terminal values there are smooth curves that perform better than the catenaries, but these are not extremals. The reason is that there is a non-smooth curve, the so-called Goldschmidt extremal, which performs better than the catenary. This is the curve which simply joins the two points along t axis by a couple of vertical segments of length y_0 and y_1 respectively. The surface generated in this case are two circles at the endpoints, as shown in Figure 5.7 (right). If only positive smooth curves are considered, this extremal is inadmissible. But we can approximate it arbitrarily closely with positive smooth curves and since the Goldschmidt extremal does better, so do this non-extremal smooth curves [50, 91].

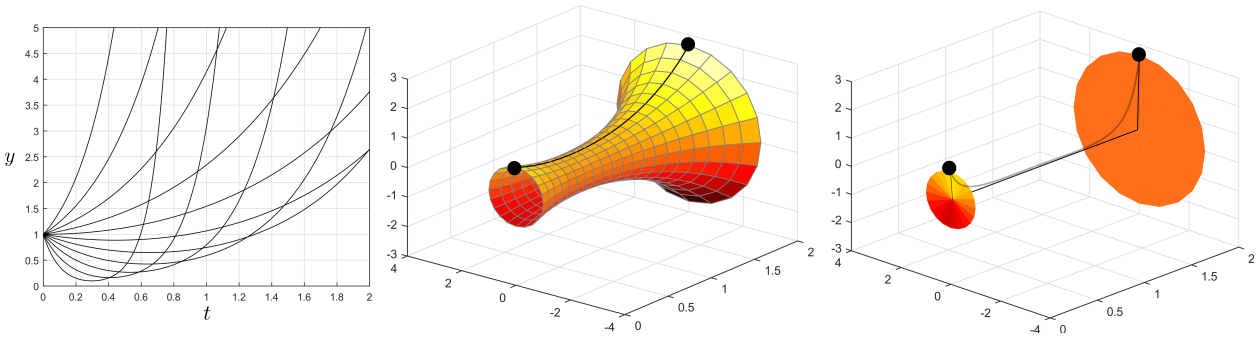

Figure 5.7: Solutions for the problem of minimum surface of revolution. (Left) The family of catenaries. (Middle) Surface generated by an extremal of the catenary family. (Right) Goldschmidt extremal and the resultant surface. An approximating smooth curve is also shown.

5.3 Discussion

In our analysis of the problems *P7*, *P8*, we have two key observations. First, for the robust threshold hitting problems, inhibition - which is represented by a presence of a segment with U_1 in the optimal control - is key to the construction of any optimal solution. We showed that in the only case in the parameter region where inhibition does not play a role in the synthesis, $a_1 < a_2$ and $\vartheta_1 > 1$, there is no optimal solution. In all the other cases, stated in Section 5.2.2 and Proposition 12, inhibition is part of the optimal strategy for unambiguous induction of an event.

The second observation is fairly intuitive, in which we argue that higher threshold facilitates a more robust response for these problems. To see this, let us consider the simple scenario of the system reaching the terminal manifold from origin, $\mathbf{x}(0) = [0\ 0]^T$, under bang control U. In this scenario, the terminal value of the free state variable x_2 is given by

$$x_2(\tau) = \frac{b_2}{a_2}\mathrm{U}\left(1 - \left(\frac{{}^{b_1}\!/_{a_1}\mathrm{U} - x_{th}}{{}^{b_1}\!/_{a_1}\mathrm{U}}\right)^{\frac{a_2}{a_1}}\right), \tag{5.58}$$

if we use the distance between $x_2(\tau)$ and the threshold as a measure of robustness χ. Now, keeping everything else the same, we can represent χ as a function of x_{th}. Differentiating with respect to x_{th}, we have

$$\frac{\mathrm{d}\chi}{\mathrm{d}x_{th}} = 1 + \frac{b_2}{b_1}\left(\frac{{}^{b_1}\!/_{a_1}\mathrm{U} - x_{th}}{{}^{b_1}\!/_{a_1}\mathrm{U}}\right)^{\frac{a_2}{a_1}-1} > 0 \tag{5.59}$$

where $\chi = x_{th} - \frac{b_2}{a_2}\mathrm{U}\left(1 - \left(\frac{{}^{b_1}\!/_{a_1}\mathrm{U} - x_{th}}{{}^{b_1}\!/_{a_1}\mathrm{U}}\right)^{\frac{a_2}{a_1}}\right)$. Thus we can conclude that for a higher threshold, in the context of decision making, there is more room to maneuver a robust response.

Chapter 6

Conclusion

In this chapter, we summarize the contributions of this thesis, and discuss the relevance of our results.

6.1 Summary and Remarks

In our work, we first examine the problem of controlling timed activity of networks of neurons from a dynamical systems point of view, (namely LIF neurons), with a focus on basic theoretical formulation and the development of rigorous solution methodologies. Due to state constraints imposed by both the selectivity criterion and spike generation mechanism, we show that Boundary-arc type phenomena emerge in this scenario. Formal analysis and synthesis is carried out to establish how the proposed solutions are geometrically disassociated in terms of their initial conditions. The developed solutions, which leverage the Maximum Principle and dynamic programming, are shown to be efficacious in controlling the LIF models.

Clearly, our results here are of a theoretical nature. While the control-theoretic features revealed are themselves interesting from a mathematical standpoint, they serve the broader purpose of establishing fundamental limits on the selective control of neurons with common inputs. The qualitative nature of the derived solutions (e.g., OFF-BANG, boundary arc strategies) are already more complex than the fixed-amplitude, square pulse designs currently used in practice. Given the massive growth in stimulation technology development, understanding these limits, even for a relatively simple model class, may provide insight into how experimentalists should tune their stimulation parameters for experimental objectives. For instance, our analytical conditions (e.g., $\vartheta_1 \gtrless \frac{V_T}{V_G}$) amount to a criteria on the amount of heterogeneity needed within a neuronal population in order to enable control. Without sufficient heterogeneity, it is simply impossible for a common input to 'split' the spiking of neurons in a selective manner. Exploiting this heterogeneity is at the heart of the derived control solution (e.g., OFF-BANG solutions that leverage increased leak dynamics). Building on these baseline characterizations, we establish relaxation approaches such as regularized optimal control problems to induce targeted spikes and penalize collateral activity in neuronal populations.

We expand the problem domain in Chapter 3 to introduce non-linearity and noise within the spiking process through a stochastic framework, namely PPGLM. In this setting, the spike patterns are now events binned over the time span resulting in a binary matrix of neural activity. We use probability as a function of the extrinsic control to identify the 'controllable subspace', i.e., the subset of all possible patterns that can be realized with a specified probability – the viable pattern set. Such an analysis provides an important means to compare the extent to which different PPGLMs can be controlled. We demonstrate the accuracy of the proposed analysis via numerical simulation. Finally, we show how the analysis

can naturally pair with a design paradigm to compute optimal controls for inducing a desired pattern on the PPGLM, and further, for underlying dynamical models of neurons.

Next, we demonstrate how similar optimal control formulations can be used to analyze intrinsic neural control- i.e., how neurons control themselves in processing higher level perceptual tasks. Our results demonstrate that the temporal responses of the early olfactory system are consistent with optimal control of a DDM for a quadratic, threshold-based cost. We show that established detection paradigms are unable to replicate these motifs under similar optimization schemes, underlining a presence of persistent mechanism in which sensory information could be processed. We also indicate that canonical, competitive architecture between sensory and inhibitory pool of neurons can generate these neural responses. Thus, these results indicate how neural responses in early sensory networks may achieve optimal formation and maintenance of representations of a persistent stimulus. More generally, our results provide an optimization-based framework for studying traversal of the latent state space in DDMs, driven by neural responses, with nontrivial drift landscapes.

Finally, we analyze a general class of detection problems mediated by threshold-hitting on integrative dynamics. We provide detailed control-theoretic analysis that shows paradoxical solutions that arise in the case of time-accuracy trade-off objective function. Indeed, in some cases, optimal evidence for such objectives may not exist. We prove that inhibition is a key component of the 'optimal evidence' in these scenarios.

6.2 Outlook

This dissertation has provided a blend of mathematical analysis, computational studies and theoretical formulation. We have in particular provided a rather detailed study of optimal control of threshold hitting as motivated by the problem of neurocontrol. Given the analytical

complexity of the exact analysis problem, we showed the merit of various relaxations, both in terms of objective function, but also in terms of mathematical formulation, i.e., by considering probabilistic models.

Of course, the ultimate goal will be to eventually enact these control solutions on actual neurocontrol platforms. In this regard, a major barrier is the identification of model parameters from experimental data. Indeed, neural system identification was only minimally treated in this dissertation, and there is ample room for future work in this domain. Similarly, control approaches that do not rely on an explicit model or that learn an abstract one 'on the fly' (so-called, model-free control approaches), may have merit given the analytical difficulties associated with exact analysis.

Finally, this research highlights the potential of control-theoretic methods to serve as tools for hypothesis generation and scientific inquiry, beyond simply engineering applications. While originating from a motivation for the latter, we uncovered interesting links to theoretical neuroscience and conceptual frameworks within which to posit, admittedly in a constrained but nonetheless intriguing way, the functional meaning of brain activity. Understanding how and why the brain 'controls' itself in this manner is a very interesting problem to consider in future work.

Appendix A

Optimal Control of LIF neurons

A.1 Derivation of Impulsive Synaptic Coupling Model

To derive (2.5), we start with a classical continuous-time model of synaptic dynamics [49] wherein, assuming $V_{rest} = 0$ in (2.3), the membrane potential of each neuron evolves according to:

$$\mathcal{C}\frac{\mathrm{d}v(t)}{\mathrm{d}t} = -\frac{v(t)}{R} + \beta u(t) + I_{syn}(t), \tag{A.1}$$

with

$$\begin{aligned} I_{syn}(t) &= g_{syn}(t)(v(t) - E_{syn}), \\ g_{syn}(t) &= \bar{g}_s \mathrm{e}^{-\frac{(t-t_s)}{\kappa_s}} \mathrm{H}(t - t_s). \end{aligned} \tag{A.2}$$

where t_s is the arrival time of a presynaptic action potential from the other neuron, g_{syn} is the synaptic conductance, H is a Heaviside step function, κ_s is the time constant for the conductance, $\bar{g}_s$ is the maximum conductance for the synapse, and E_{syn} denotes the reversal potential. For selective spiking, we want the postsynaptic neuron to be protected from this incoming synapse with respect to the membrane potential.

In the typical case of an excitatory synapse, we have $E_{syn} \approx 0$ and the contribution from the spike in the presynaptic neuron becomes

$$\Delta v(t) = \frac{1}{\mathcal{C}} \int_{t_s}^{t} \bar{g}_s \mathrm{e}^{-\frac{(t-t_s)}{\kappa_s}} v(t) \mathrm{d}t \tag{A.3}$$

Now, assuming a separation in time scale between the synaptic time constant κ_s and the membrane time constant κ i.e. $\kappa_s \ll \kappa$, we can approximate the integral in (A.3) by keeping the voltage of the postsynaptic neuron constant at $v(t_s)$ over the integration window. Using this, we have

$$\Delta v(t) \leq \frac{1}{\mathcal{C}} \int_{t_s}^{\infty} I_{syn}(t) \mathrm{d}t = \frac{\bar{g}_s \kappa_s}{\mathcal{C}} v(t_s) \leq \frac{\bar{g}_s \kappa_s}{\mathcal{C}} V_T \tag{A.4}$$

So the effect of a synaptic event on the postsynaptic neuron can be crudely summarized as an almost instantaneous rise in voltage bounded by (A.4). Thus, the model (2.5) approximates this effect with an impulsive synaptic action, where

$$\Delta v(t) \equiv \rho_{syn}(t) \leq \frac{\bar{g}_s \kappa_s}{\mathcal{C}} V_T \equiv \bar{\rho}_{syn} \tag{A.5}$$

A.1.1 Geometrical Aspects of Selective Spiking Solution

Here, we first discuss the role of ϑ_1 (2.19) in determining the two different selective spiking solutions presented in sections 2.2.1, 2.2.2. We also geometrically show that pairwise feasibility is not achievable when both neurons are Case 2, as described in section 2.2.3.

We first derive the equation for the line of quasistatic equilibrium defined in (2.53). This is the set of points in the phase plane for which $\dot{\mathbf{v}}(u) = \mathbf{0}$ for any constant control $u \in \mathcal{U}$. Using

this condition we have,

$$\dot{v}_1 = -a_1 v_1 + b_1 u = \dot{v}_2 = -a_2 v_2 + b_2 u = 0 \tag{A.6}$$

Since u is a constant, we can eliminate u to get the equation for the quasistatic equilibrium

$$\frac{v_1}{v_2} = \vartheta_1 \tag{A.7}$$

where $\vartheta_1 = \frac{b_1 a_2}{b_2 a_1}$. Now the two different solution presented in Proposition 1 and 2 are dependent on the existence of the boundary segment, i.e., for a boundary control u_{arc} for which Neuron 2 is voltage invariant ($\dot{v}_2(u_{arc}) = 0$), regardless of whether the voltage of Neuron 1 increases. To satisfy this, we must have

$$\dot{v}_1(u_{arc})|_{v_1 = V_T} > 0 \tag{A.8}$$

We can answer this question from the analysis on the quasistatic equilibrium line as u_{arc} is constant. If the line intersects $v_1 = V_T$ before $v_2 = V_G$, we have from (A.7) (see Figure A.1(a))

$$\vartheta_1 > \frac{V_T}{V_G} \tag{A.9}$$

Using this, we can calculate the direction of vector field at $v_1 = V_T$ in (A.8)

$$\begin{aligned} \dot{v}_1(u_{arc})|_{v_1 = V_T} &= -a_1 V_T + b_1 u_{arc} = -a_1 V_T + b_1 \frac{a_2 V_G}{b_2} \\ &= a_1 V_G \left(\frac{b_1 a_2}{b_2 a_1} - \frac{V_T}{V_G} \right) = a_1 V_G \left(\vartheta_1 - \frac{V_T}{V_G} \right) > 0 \end{aligned} \tag{A.10}$$

We show this in Figure A.1(a), where the quasistatic equilibrium intersects $v_2 = V_G$ beyond $v_1 = V_T$. This ensures the vector field is positive under the boundary control such that the target neuron reaches threshold while keeping the other neuron at V_G. Now if we assume

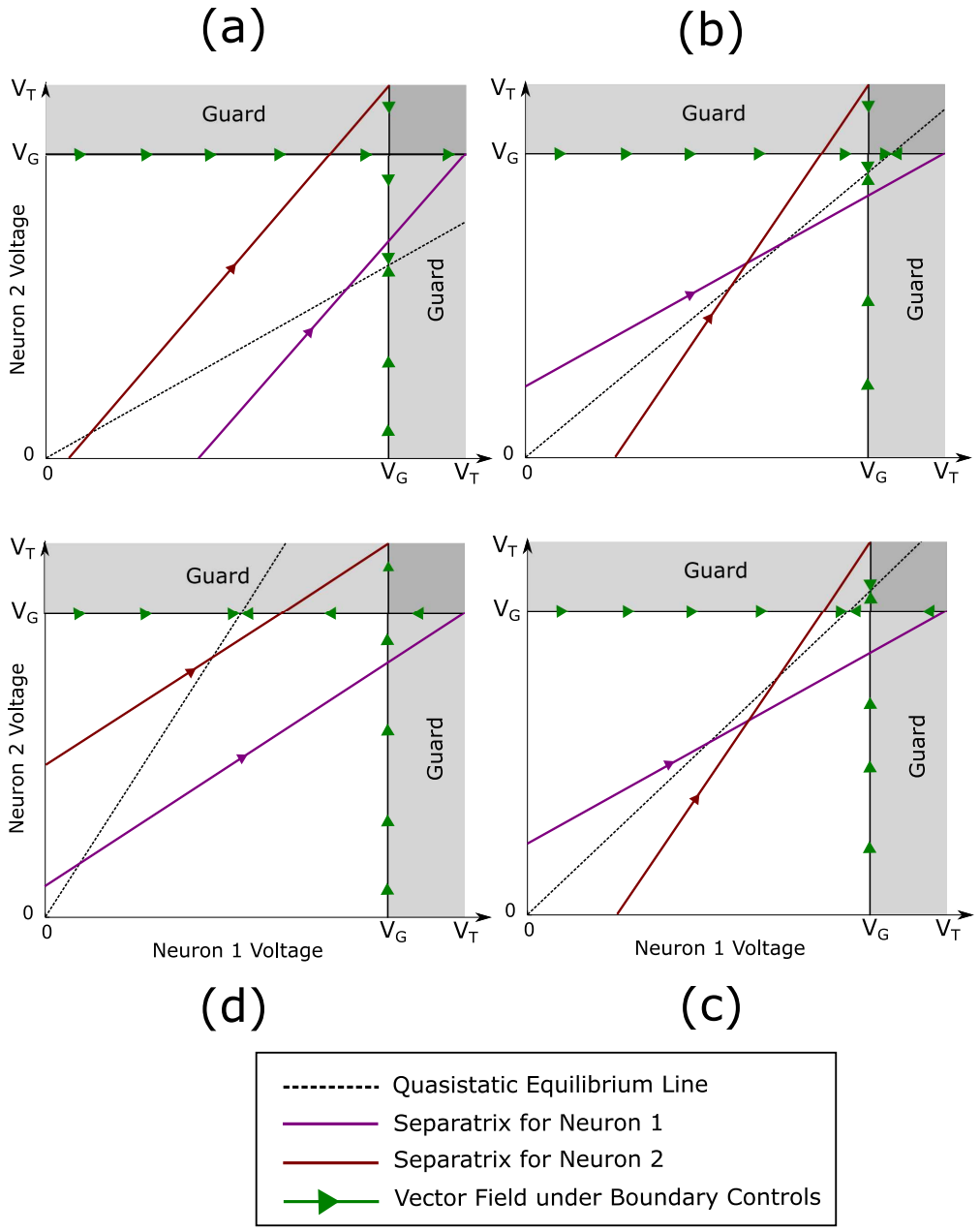

Figure A.1: Representation of the solution space with respect to the quasistatic equilibrium line. (a) When Neuron 1 satisfies Case 1 i.e. $\vartheta_1 > {}^{V_T}/_{V_G}$, which implies $\vartheta_2 < {}^{V_T}/_{V_G}$, i.e. Neuron 2 satisfies Case 2. (b), (c) The parameters of the neurons are such that $1 \leq \vartheta_1 \leq {}^{V_T}/_{V_G}$ and ${}^{V_G}/_{V_T} \leq \vartheta_1 \leq 1$ respectively which implies both neurons are Case 2. Note that for these two scenarios, the selective spiking is not possible for both the neurons. (d) The parameters satisfy $\vartheta_2 > {}^{V_T}/_{V_G}$, i.e. Neuron 2 is Case 1 which implies Neuron 1 is Case 2, $\vartheta_1 < {}^{V_T}/_{V_G}$. For (a) and (d), selective spiking is possible for both neurons.

$\vartheta_1 \leq \frac{V_T}{V_G}$ (see Figure A.1 (b,c,d)), we can similarly show as in (A.10) that

$$\dot{v}_1(u_{arc})|_{v_1=V_T} < 0 \tag{A.11}$$

for this case, and we need to adopt the solution presented in Proposition 2 to fire Neuron 1 selectively. So we see that the nature of selective spiking solution, i.e., (BANG/ BANG-BOUNDARY) or (BANG/OFF-BANG), is contingent upon the ratio ϑ_1.

Figure A.1 presents an intuitive representation of the geometric aspects of the solution space discussed in section 2.2.1-2.2.3 with respect to ϑ_1, ϑ_2. Here, we analyze the pairwise feasibility for all possible parameter combinations. If $\vartheta_1 > \frac{V_T}{V_G}$ ($\implies \vartheta_2 < \frac{V_T}{V_G}$) and Lemma 1 for Neuron 2 holds, then the neurons are pairwise feasible, i.e., from any point in the phase plane we can fire either neuron selectively. Similarly, if we have $\vartheta_1 < \frac{V_G}{V_T}$ ($\implies \vartheta_2 > \frac{V_T}{V_G}$), i.e., Neuron 2 is Case 1, Neuron 1 is Case 2, and Lemma 1 holds for Neuron 1, we can once again achieve pairwise feasibility. These two scenarios are depicted in Figure A.1 (a,d), respectively. When $\frac{V_G}{V_T} \leq \vartheta_{1,2} \leq \frac{V_T}{V_G}$ (i.e. both neurons are Case 2), for pairwise feasibility we must have Lemma 1 satisfy for each neuron individually. This creates a situation shown in Figure A.1 (b,c) where the separatrices for Neuron 1 and Neuron 2 intersect, which implies that at the point of intersection we have two different vector fields under the same control ($u = \mathrm{U}$) which is a contradiction. Hence, if both neurons are Case 2, we cannot have pairwise feasibility.

A.2 Computation of Λ controllable sets

We show the calculation for Neuron 1 here. There are two possible situations, namely, $\Lambda \leq T_s$ and $\Lambda > T_s$, which result in two different switching structures where T_s denotes time to reach

$[V_T\ V_G]^T$ along the separatrix Γ from the initial condition

$$\mathbf{v}(0) = \{(v_1, v_2) : \mathbf{v} \in \Gamma, v_2 = 0\}. \tag{A.12}$$

If $\Lambda \leq T_s$, we can find the neuron voltages (v_1, v_2) from which Neuron 1 reaches V_T in time Λ

$$v_1 = \mathrm{e}^{a_1\Lambda}(V_T - \frac{b_1}{a_1}\mathrm{U}(1 - \mathrm{e}^{-a_1\Lambda})) \tag{A.13}$$

Note that v_2 does not come in (A.13) since $\forall\ \mathbf{v} \in \Gamma_+$, Neuron 1 reaches threshold without Neuron 2 hitting the guard.

For $\Lambda > T_s$, we assume that it takes $\bar{t}$ for Neuron 2 to hit the guard V_G, under bang control,

$$\begin{aligned} V_G &= \mathrm{e}^{-a_2\bar{t}}v_2 + \frac{b_2}{a_2}\mathrm{U}(1 - \mathrm{e}^{-a_2\bar{t}}) \\ \bar{t} &= \frac{1}{a_2}\log\left(\frac{v_2 - \frac{b_2}{a_2}\mathrm{U}}{V_G - \frac{b_2}{a_2}\mathrm{U}}\right). \end{aligned} \tag{A.14}$$

The voltage of Neuron 1 at this time is calculated using (2.38). This means for (v_1, v_2) to be on the Λ-controllable set, Neuron 1 must reach the threshold V_T in $(\Lambda - \bar{t})$ along the boundary arc, i.e.

$$V_T = \mathrm{e}^{-a_1(\Lambda-\bar{t})}v_1(\bar{t}) + \frac{b_1}{a_1}\mathrm{U}(1 - \mathrm{e}^{-a_1(\Lambda-\bar{t})}). \tag{A.15}$$

Simplifying (A.15), we get

$$v_1 = \mathrm{e}^{a_1\Lambda}\left(V_T - \frac{b_1}{a_1}u_{arc} - \mathrm{e}^{-a_1\Lambda}g(v_2)\left(\frac{b_1}{a_1}\mathrm{U}\left(1 - \frac{1}{g(v_2)}\right) - \frac{b_1}{a_1}u_{arc}\right)\right) \tag{A.16}$$

where $g(v_2) = \left(\frac{v_2 - \frac{b_2}{a_2}\mathrm{U}}{V_G - \frac{b_2}{a_2}\mathrm{U}} \right)^{\frac{a_1}{a_2}}$. From this, we can find the Λ controllable set for the selective spiking of Neuron 1.

Similarly, for Neuron 2 we can find the set $\zeta_2(\Lambda)$.

A.3 Calculation of Off-time for Fixed-time Selective Spiking

In this section, we will show how the off-time in (2.75) can be calculated to induce a spike in a specified time. Without loss of generality, we once again assume the target pattern $\Sigma_P = [(1, t_1)]$, $\mathbf{v}(0) = [v_1\ 0]^T$, and $t_1 < T_s$. For the other cases, the computation is similar and follows from the optimal control structure discussed in Section 2.2.1, 2.2.2. Let us denote the voltage at the end of the off segment $\mathbf{v}(\hat{t}) = [\hat{v}_1\ 0]^T$. Now, using (2.47) in (2.75) we have,

$$\begin{aligned} &\frac{1}{a_1}\log\left(\frac{v_1}{\hat{v}_1}\right) - \frac{1}{a_1}\log(E(\hat{v}_1)) = t_1 \\ &\hat{v}_1 = \frac{\frac{b_1}{a_1}\mathrm{U}}{1 - (V_T - \frac{b_1}{a_1}\mathrm{U})\exp(a_1(t_1 - \frac{1}{a_1}\log(v_1)))} \end{aligned} \tag{A.17}$$

Substituting $\hat{v}_1$ in $\hat{t} = \frac{1}{a_1}\log\left(\frac{v_1}{\hat{v}_1}\right)$, we get the desired off-time. Note that for $t_1 \gg T_s$, we will need to use the boundary segment in (A.17).

Appendix B

Controllability Analysis of PPGLM

B.1 Proof of Lemma 2

The proof is a direct consequence of the fact that the PPGLM likelihood described in our model has a global maximum with respect to its inputs [92]. To prove this, it is enough to show that the likelihoods in (3.7), (3.11) are concave functions of $\mathbf{U}$. First for the log-link model, if we substitute (3.4) into (3.7) we have

$$L(\mathbf{N} \mid \mathbf{X}) = \sum_{c=1}^{C} \sum_{i=1}^{I} \Big(\delta N_{c,i} \, (\theta_c^T \mathbf{x}_i + \log \Delta) - \Delta \exp(\theta_c^T \mathbf{x}_i) \Big). \tag{B.1}$$

Stacking the difference process $\delta\mathbf{N}$ and the control input $\mathbf{U}$ into column vectors $\mathbf{n} \in \mathbb{R}^{CI}$, $\mathbf{u} \in \mathbb{R}^{SI}$ respectively and with modified parameter matrix $\bar{\Theta} \in \mathbb{R}^{CI \times (P+1)SI}$ corresponding to the extrinsic control part of the covariate matrix, we can write (B.1) as

$$L(\mathbf{N} \mid \mathbf{u}) = \mathbf{n}^T \bar{\Theta} \, \mathbf{D}' \mathbf{u} - \Delta \mathbf{1}^T \mathbf{K} \exp(\bar{\Theta} \, \mathbf{D}' \mathbf{u}) + \Psi(\delta \mathbf{N}) \log \Delta + r, \tag{B.2}$$

where $\mathbf{K} \in \mathbb{R}^{CI \times CI}$ is a diagonal matrix where the contributions of the process history and background activity for each process and time index are placed along the diagonals, $r = \mathbf{1}^T \log(\mathbf{K})\mathbf{n}$ is a constant (logarithm is applied to each element on the diagonal of $\mathbf{K}$) and $\mathbf{D}' \in \mathbb{R}^{(P+1)SI \times SI}$ is a design matrix that extracts the delayed inputs from $\mathbf{U}$ into a vector $\in \mathbb{R}^{(P+1)SI}$. Note that the likelihood is a combination of a linear term along with a negative exponential, which clearly makes the Hessian negative definite i.e. L is ***strictly*** concave with respect to the extrinsic inputs.

For the SEMPP with the logistic link model, we can similarly write (3.11)

$$L(\mathbf{N}^* \mid \mathbf{u}) = \mathbf{n}^{*T} \bar{\Theta}\, \mathbf{D}'\mathbf{u} - \mathbf{1}^T \log(\mathbf{1} + \mathbf{K}^s \exp(\bar{\Theta}\, \mathbf{D}'\mathbf{u})) + r', \tag{B.3}$$

where $\mathbf{n}^* \in \mathbb{R}^{MI}$, $\mathbf{K}^s \in \mathbb{R}^{I \times MI}$ is a block diagonal matrix where each block is a row of contributions of the process history and background activity for each marked process and time index and $r' = \mathbf{1}^T \log(\text{diag}(\mathbf{K}^s))\mathbf{n}$, $\text{diag}(\mathbf{K}^s)$ is a diagonal matrix where the blocks of $\mathbf{K}^s$ constitutes the diagonal. Since we want to show the concavity of the likelihood with respect to $\mathbf{u}$, we can ignore the linear term in (B.3) and concentrate on the second term. Let us denote this as l_2,

$$l_2(\mathbf{u}) = -\sum_{i=1}^{I} \log(1 + \mathbf{k}_i^T \exp(\bar{\Theta}\, \mathbf{D}'\mathbf{u})) \tag{B.4}$$

and $\mathbf{k}_i$ is the i-th row of the matrix $\mathbf{K}^s$. Note that all elements of $\mathbf{K}^s$ i.e. $k_{i,j} \geq 0, \forall i = 1, \ldots, I$, $j = 1, \ldots, MI$. Taking the gradient we have

$$\nabla l_2 = -\sum_{i=1}^{I} \frac{1}{1 + \mathbf{k}_i^T \exp(\bar{\mathbf{U}})} \Xi^T \text{diag}(\mathbf{k}_i) \exp(\bar{\mathbf{U}}), \tag{B.5}$$

where $\Xi = \bar{\Theta}\,\mathbf{D}'$ and $\bar{\mathbf{U}} = \Xi\mathbf{u}$. Now let us denote $\text{diag}(\mathbf{k}_i) = \mathbf{K}_i^s$ and calculate the Hessian for each i,

$$\nabla^2 l_2^i = -\frac{1}{z_i^2}(z_i \Xi^T \mathbf{K}_i^s \,\text{diag}(\exp(\bar{\mathbf{U}}))\Xi - \Xi^T \mathbf{K}_i^s \exp(\bar{\mathbf{U}})\exp(\bar{\mathbf{U}})^T \mathbf{K}_i^s \Xi), \tag{B.6}$$

where $z_i = 1 + \mathbf{k}_i^T \exp(\bar{\mathbf{U}})$. For strict concavity we need to show that $\forall\, \mathbf{y} \in \mathbb{R}^{MI}$,

$$\mathbf{y}^T \nabla^2 l_2\, \mathbf{y} < 0. \tag{B.7}$$

From (B.6) and (B.7),

$$\mathbf{y}^T \nabla^2 l_2^i\, \mathbf{y} = -\frac{1}{z_i^2}(\Xi\mathbf{y})^T \bigg(z_i \mathbf{K}_i^s \,\text{diag}(\exp(\bar{\mathbf{U}})) - \mathbf{K}_i^s \exp(\bar{\mathbf{U}})\exp(\bar{\mathbf{U}})^T \mathbf{K}_i^s \bigg) \Xi\mathbf{y}. \tag{B.8}$$

Denoting $\Xi\mathbf{y} = \mathbf{w}$, $\bar{\mathbf{U}}^e = \text{diag}(\exp(\bar{\mathbf{U}})$ and substituting z_i

$$\begin{aligned} \mathbf{y}^T \nabla^2 l_2^i\, \mathbf{y} &= -\frac{1}{z_i^2}\bigg(\mathbf{w}^T \mathbf{K}_i^s \bar{\mathbf{U}}^e \mathbf{w} + \mathbf{w}^T (\sum_{j=1}^{MI} k_{i,j} \bar{u}_{j,j}^e) \mathbf{K}_i^s \bar{\mathbf{U}}^e - \mathbf{K}_i^s \exp(\bar{\mathbf{U}})\exp(\bar{\mathbf{U}})^T \mathbf{K}_i^s) \mathbf{w} \bigg) \\ &= t_1^i + t_2^i. \end{aligned} \tag{B.9}$$

Now let us analyze the second term separately,

$$\begin{aligned} t_2^i &= -\frac{1}{z_i^2}\bigg(\sum_j k_{i,j} \bar{u}_{j,j}^e \sum_j k_{i,j} \bar{u}_{j,j}^e w_j^2 - (\sum_j k_{i,j} \bar{u}_{j,j}^e w_j)^2 \bigg) \\ &= -\frac{1}{z_i^2}\bigg(\sum_j v_{i,j} \sum_j v_{i,j} w_j^2 - (\sum_j v_{i,j} w_j)^2 \bigg), \qquad \text{where } v_{i,j} = k_{i,j} \bar{u}_{j,j}^e \\ &\leq 0 \qquad \text{(From Cauchy-Schwarz inequality).} \end{aligned} \tag{B.10}$$

Now for the complete Hessian with (B.9), we have

$$\mathbf{y}^T\nabla^2 l_2\,\mathbf{y} = \sum_i \mathbf{y}^T\nabla^2 l_2^i\,\mathbf{y} = \sum_i (t_1^i + t_2^i) \leq \sum_i t_1^i = -\mathbf{w}^T \sum_i \frac{1}{z_i^2}\mathbf{K}_i^s\bar{\mathbf{U}}^e\mathbf{w} = -\mathbf{w}^T\bar{\mathbf{K}}\mathbf{w} < 0, \tag{B.11}$$

where $\bar{\mathbf{K}} = \sum_i \frac{1}{z_i^2}\mathbf{K}_i^s\bar{\mathbf{U}}^e \in \mathbb{R}^{MI\times MI}$ is a diagonal matrix and the negative definiteness comes from the fact that all the entries in matrix $\bar{\mathbf{K}}$ are positive, since the terms come from exponential of the co-variates. So the likelihood in (B.3) is ***strictly*** concave as well. Note that for any pattern $\mathbf{N}$ with at least one spike i.e., $\Psi(\delta\mathbf{N}) > 0$, we can show

$$\nabla L(\mathbf{N}^*|\mathbf{u}) \not\to \mathbf{0},\ \text{if } \exists\ j \in \{1\dots SI\} \text{ such that } u_j \to \pm\infty. \tag{B.12}$$

Along with ***strict*** concavity, (B.12) means that the first-order condition for maximum is satisfied for a finite $\mathbf{U}^*$ i.e., the maximum $L^* = L(\mathbf{N}|\mathbf{U}^*)$ will be global and unique. Now for any ϵ with $-\epsilon > L^*$, there is no control that satisfies (3.15) and thus ϵ- controllability is not achieved for unconstrained input.

B.2 Proof of Lemma 3

Consider an arbitrary realization $\mathbf{N}$ containing $\Psi(\delta\mathbf{N})$ events overall and a box constraint on each extrinsic input i.e. $u_{s,i} \in \mathcal{U} = [u_{min}\ u_{max}]\ \forall\ s, i$. The likelihood in this case follows from (B.2)

$$L(\mathbf{N}\mid\mathbf{u}) = \mathbf{n}^T\bar{\Theta}\,\mathbf{D}'\mathbf{u} - \Delta\mathbf{1}^T\mathbf{K}\exp(\bar{\Theta}\,\mathbf{D}'\mathbf{u}) + \Psi(\delta\mathbf{N})\log\Delta + r. \tag{B.13}$$

The first-order condition for maximum of $L(\mathbf{N}\mid\mathbf{u})$ is a transcendental equation, thus, the solution $\mathbf{U}^*$ cannot be derived in general and does not necessarily reside in the constrained space $\mathcal{U}$. Ideally we will need $L(\mathbf{U}^*)$ to analyze any dependence of maximum likelihood on spike count. But for $\mathbf{U} \in \mathcal{U}$ and bounded parameters Θ, the likelihood in (B.13) is dominated

by the term $\Psi(\delta\mathbf{N})\log\Delta$, i.e.,

$$\lim_{\Delta\to 0} L(\mathbf{N} \mid \mathbf{u}) \propto \frac{1}{\Psi(\delta\mathbf{N})} \text{ (since } \log\Delta < 0), \tag{B.14}$$

and a higher event count dictates the degradation of likelihood.

B.3 Proof of Lemma 4

Here the variable of interest is the portion of the parameter vector Θ represented by $\beta_q^{m,c}$ for $q = 1 \dots Q$, $m = 1 \dots M$, $c = 1 \dots C$ in (3.9). For the log link model in (3.7), $M = C$. Let us denote these set of values by $\boldsymbol{\alpha} \in \mathbb{R}^{C^2Q}$ and rewrite the likelihood in (3.7) as a function of $\boldsymbol{\alpha}$ following (B.2) in Appendix B.1,

$$L(\mathbf{N} \mid \boldsymbol{\alpha}) = \mathbf{n}^T\mathbf{Z}\boldsymbol{\alpha} - \Delta\mathbf{1}^T\mathbf{K}_p \exp(\mathbf{Z}\boldsymbol{\alpha}) + \Psi(\delta\mathbf{N})\log\Delta + r_{\boldsymbol{\alpha}}, \tag{B.15}$$

where $r_{\boldsymbol{\alpha}}$ is the contribution from other co-variates namely inputs and background activity independent of $\boldsymbol{\alpha}$, $\mathbf{Z} \in \mathbb{B}^{CI\times C^2Q}$ is a matrix composed of the relevant process history terms for each variable, time index and $\mathbf{K}_p \in \mathbb{R}^{CI\times CI}$ is a diagonal matrix similar to (B.2).

For the SEMPP model we can rewrite (3.11) for $\boldsymbol{\alpha} \in \mathbb{R}^{MCQ}$ following (B.3),

$$L(\mathbf{N}^* \mid \boldsymbol{\alpha}) = \mathbf{n}^{*T}\mathbf{Z}\boldsymbol{\alpha} - \mathbf{1}^T\log(\mathbf{1} + \mathbf{K}_p^s \exp(\mathbf{Z}\boldsymbol{\alpha})) + r'_{\boldsymbol{\alpha}}, \tag{B.16}$$

with $\mathbf{K}_p^s$ as the analog to $\mathbf{K}_p$ in (B.15). We note that both (B.15), (B.16) follow the same structure as their counterparts (B.2), (B.3) and thus we can conclude that the likelihoods are strictly concave with respect to the connectivity parameters $\boldsymbol{\alpha}$ as well. Now to show that a critical amount of connectivity, e.g., $\boldsymbol{\alpha}_c$ helps in the controllability of any arbitrary pattern,

we investigate the first-order condition at $\boldsymbol{\alpha} = \mathbf{0}$. Computing the gradient of the likelihood in (B.15) we have

$$\begin{aligned} \nabla L_{\boldsymbol{\alpha}}|_{\boldsymbol{\alpha}=\mathbf{0}} &= (\mathbf{n}^T\mathbf{Z})^T - \Delta\mathbf{Z}^T\mathbf{K}_p \exp(\mathbf{Z}\boldsymbol{\alpha})|_{\boldsymbol{\alpha}=\mathbf{0}} \\ &= \mathbf{Z}^T(\mathbf{n} - \Delta\mathbf{K}_p\mathbf{1}). \end{aligned} \tag{B.17}$$

Now, the first-order condition for maximum is satisfied if

$$\mathbf{n} - \Delta\mathbf{K}_p\mathbf{1} \in \ker(\mathbf{Z}^T), \tag{B.18}$$

which does not hold in general for any $\mathbf{N}$, $\mathbf{U}$ and the rest of the parameters β_0^c, $\gamma_p^{m,s}$ $\forall\, c, m, s$ and this proves that $\boldsymbol{\alpha}_c \neq \mathbf{0}$. We also claim that $\boldsymbol{\alpha}_c$ does not diverge, i.e.,

$$\nabla L_{\boldsymbol{\alpha}}|_{\boldsymbol{\alpha}=\boldsymbol{\alpha}_c} = (\mathbf{n}^T\mathbf{Z})^T - \Delta\mathbf{Z}^T\mathbf{K}_p \exp(\mathbf{Z}\boldsymbol{\alpha}_c) = \mathbf{0} \tag{B.19}$$

has a solution. To see this, consider the case $\beta_1^{1,2} \to \infty$. Now since $\mathbf{Z} \in \mathbb{B}$, $\beta_1^{1,2} \to \infty$ implies a spike in the second neuron for previous time bin maximizes the probability of spike in the first neuron for the current time bin. But for a spike pattern $\mathbf{N}'$ in which such a sequence does not occur, the log-likelihood becomes

$$L(\mathbf{N}' \mid \boldsymbol{\alpha}_c) \to -\infty. \tag{B.20}$$

If $\beta_1^{1,2} \to -\infty$, likewise any pattern with consecutive spike from second and first neuron will have zero probability same as (B.20). This can also be seen from the first-order condition. So we can conclude that in general for any arbitrary pattern

$$\boldsymbol{\alpha}_c \neq \mathbf{0},\ |\boldsymbol{\alpha}_c^j| \leq \boldsymbol{\alpha}_{max} < \infty,\ \ \forall\, j = 1 \ldots C^2Q. \tag{B.21}$$

Appendix C

Intrinsic Control for Sensory Detection Tasks

C.1 Existence of Solution for Reduced Regulator

Here we prove that the matrices $\bar{\mathbf{Q}}_{1,2}$ for the regulator in $(P1p^*)$, $(P1w^*)$ are positive semi-definite. We first identify the eigenvalues of $\bar{\mathbf{Q}}_1$ using

$$\det(\bar{\mathbf{Q}}_1 - \lambda\mathbb{I}) = 0 \Rightarrow \det\begin{bmatrix} \mathbf{Q}_1 - \lambda\mathbb{I} & \mathbf{0} & -\mathbf{Q}_1 \\ 0 & \mathbf{S}_1 - \lambda\mathbb{I} & \mathbf{0} \\ -\mathbf{Q}_1 & 0 & \mathbf{Q}_1 - \lambda\mathbb{I} \end{bmatrix} = 0 \tag{C.1}$$

where $\mathbb{I}$ is identity matrices of appropriate dimensions. From (C.1)

$$\det\begin{bmatrix}\mathbf{Q}_1-\lambda\mathbb{I} & \mathbf{0} & -\mathbf{Q}_1\\ 0 & \mathbf{S}_1-\lambda\mathbb{I} & \mathbf{0}\\ -\mathbf{Q}_1 & 0 & \mathbf{Q}_1-\lambda\mathbb{I}\end{bmatrix}=\det\begin{bmatrix}\mathbf{Q}_1-\lambda\mathbb{I} & -\mathbf{Q}_1 & \mathbf{0}\\ 0 & \mathbf{Q}_1-\lambda\mathbb{I} & \mathbf{0}\\ \mathbf{0} & \mathbf{0} & \mathbf{S}_1-\lambda\mathbb{I}\end{bmatrix} \tag{C.2}$$
$$=\det((\mathbf{Q}_1-\lambda\mathbb{I})^2-\mathbf{Q}_1^2)\det(\mathbf{S}_1-\lambda\mathbb{I})=\det(\lambda\mathbb{I})\det(2\mathbf{Q}_1-\lambda\mathbb{I})\det(\mathbf{S}_1-\lambda\mathbb{I})=0$$

Thus $\sigma(\bar{\mathbf{Q}}_1)=\{0,\ldots,0,\sigma(2\mathbf{Q}_1),\sigma(\mathbf{S}_1)\}$, where $\sigma(.)$ denotes the eigenspectrum of a matrix. We have $\mathbf{S}_1>0$ and since $\mathbf{Q}_1\geq 0$ to begin with, so is $2\mathbf{Q}_1$, which implies $\bar{\mathbf{Q}}_1$ is positive semi-definite. For $\bar{\mathbf{Q}}_2$ can show that, $\sigma(\bar{\mathbf{Q}}_2)=\{\sigma(\mathbf{Q}_2),\sigma(\mathbf{S}_2)\}$ and thus, $\bar{\mathbf{Q}}_2\geq 0$.

C.2 Optimal Response in Forced paradigm

We first seek these motifs for the forced response paradigm. Without loss of generality, for a candidate optimal neural response $\mathbf{x}(t)$ that triggers decision 1 unambiguously after a fixed time τ, we can formulate the following problem

$$\begin{aligned}&\min_{\mathbf{y}} \quad \mathbb{J}(\mathbf{y})=\frac{1}{2}\int_0^\tau(\gamma\mathbf{x}^T(t)\mathbf{x}(t)+\varrho\mathbf{y}^T(t)\mathbf{y}(t))\mathrm{d}t+\varphi(\boldsymbol{\nu}(\tau))\\ &\text{s.t.} \quad \dot{\boldsymbol{\nu}}(t)=f(\boldsymbol{\nu},\mathbf{x}),\ \dot{\mathbf{x}}=\mathbf{y},\ \boldsymbol{\nu}(0)=\mathbf{0},\ \mathbf{x}(0)=\mathbf{x}_0\\ &\qquad\ \varphi(\boldsymbol{\nu}(\tau))=\frac{1}{1+\exp(\xi\alpha(\nu_1(\tau)-\nu_2(\tau)))},\ \alpha=1,\ \xi>0.\end{aligned} \tag{P2-interrogation}$$

where $\varphi(\boldsymbol{\nu}(\tau))$ is a sigmoidal penalty function on the terminal decision state $\boldsymbol{\nu}(\tau)$, $f(\boldsymbol{\nu},\mathbf{x})$ denote drift dynamics (4.7)-(4.10) from Section 4.2.1 and $\mathbf{x}_0$ is the response in the beginning of detection cycle. For $\alpha=1$, the penalty is high for negative values of the difference $\nu_1(\tau)-\nu_2(\tau)$. This ensures that $\nu_1(\tau)>\nu_2(\tau)$, which is desired for decision 1 from (4.2). The quadratic term in $\mathbf{x}$ in the objective penalizes response energy over the detection period τ, which enhances the sensitivity of the decision making process. This also has the effect

of distributing the net response is over the sensory network [93]. $\mathbf{y}$ is the response velocity and ϱ, enforces a continuity constraint on $\mathbf{x}$. γ determines the trade-off between ambiguity reduction and sensitivity, with the regularization parameters following $\varrho \ll \gamma < 1$. The optimal motif for decision 2 can be obtained from (P2-interrogation) with $\alpha = -1$.

***Solution**:* For (P2-interrogation), the Lagrangian is,

$$L = \frac{1}{2}(\gamma \mathbf{x}^T \mathbf{x} + \varrho \mathbf{y}^T \mathbf{y}), \tag{C.3}$$

We construct an augmented state vector $\mathbf{v} \in \mathbb{R}^{M+2}$ by adding $\mathbf{x}$ to the latent state $\boldsymbol{\nu}$ such that,

$$\dot{\mathbf{v}} = [f^T(\boldsymbol{\nu}, \mathbf{x}) \;\; \mathbf{y}^T]^T \equiv g(\mathbf{v}, \mathbf{y}), \; \mathbf{v} = [\boldsymbol{\nu}^T \;\; \mathbf{x}^T]^T. \tag{C.4}$$

From the dynamic models in (4.7)-(4.10) the vector field g can be expressed as

$$g = \begin{bmatrix} \dot{\boldsymbol{\nu}} \\ \mathbf{x} \end{bmatrix} = \begin{bmatrix} \mathbf{A} & \mathbf{b} \\ \mathbf{0} & \mathbf{0} \end{bmatrix} \begin{bmatrix} \boldsymbol{\nu} \\ \mathbf{x} \end{bmatrix} + \begin{bmatrix} \mathbf{0} \\ \mathbb{I} \end{bmatrix} \mathbf{y}. \tag{C.5}$$

Now the Hamiltonian can be written as,

$$\mathcal{H} = L + \boldsymbol{\lambda}^T g(\mathbf{v}, \mathbf{y}). \tag{C.6}$$

where $\boldsymbol{\lambda} \in \mathbb{R}^{M+2}$ is the adjoint vector with dynamics,

$$\dot{\boldsymbol{\lambda}} = -\nabla_{\mathbf{v}} L - \left(\frac{\partial g(\mathbf{v}, \mathbf{y})}{\partial \mathbf{v}} \right)^T \boldsymbol{\lambda} \equiv -L_{\mathbf{v}} - g_{\mathbf{v}}^T \boldsymbol{\lambda}. \tag{C.7}$$

From the minimum condition

$$\mathbf{y}^*(t) = -\frac{1}{\varrho}\frac{\partial(\boldsymbol{\lambda}^T g(\mathbf{v},\mathbf{y}))}{\partial \mathbf{y}} \equiv -\frac{1}{\varrho} g_{\mathbf{y}}^T \boldsymbol{\lambda}, \tag{C.8}$$

and the transversality condition of the maximum principle we have,

$$\begin{aligned} &\lambda_j(\tau) = \nabla_{\boldsymbol{\nu}} \varphi(\boldsymbol{\nu}(\tau)) \equiv \varphi_{\boldsymbol{\nu}},\ j = 1, 2, \\ &\lambda_j(\tau) = 0,\ j = 3, \ldots, M+2, \end{aligned} \tag{C.9}$$

Substituting $\mathbf{y}^*$ from (C.8) in the augmented state dynamics (C.7), we now have a two point boundary value problem with boundary conditions defined in (C.9) and (P2-interrogation).

C.3 Optimal Response in Free Response paradigm

Next we formulate these problems for Free response paradigm. Once again without loss of generality, for unambiguous detection of choice 1, the optimal neural response not only drives the desired latent state to threshold but also suppress the competing state. Thus we consider the following regularized minimum time problem,

$$\text{(P2-free)} \qquad \begin{aligned} \min_{\mathbf{y}} \quad & \mathbb{J}(\mathbf{y}) = \int_0^\tau \left(1 + \frac{\gamma}{2}\mathbf{x}^T(t)\mathbf{x}(t) + \frac{\varrho}{2}\mathbf{y}^T(t)\mathbf{y}(t)\right)\mathrm{d}t + \frac{\alpha}{2}\nu_2^2(\tau) \\ \text{s.t.} \quad & \dot{\boldsymbol{\nu}}(t) = f(\boldsymbol{\nu}, \mathbf{x}),\ \dot{\mathbf{x}} = \mathbf{y}, \\ & \boldsymbol{\nu}(0) = \mathbf{0},\ \mathbf{x}(0) = \mathbf{x}_0,\ \nu_1(\tau) = \Gamma, \end{aligned}$$

where α penalizes the terminal value of the competing latent state, in this case $\nu_2(\tau)$. γ, α regulates the trade-off between RT, response energy (sensitivity) and ambiguity.

***Solution**:* In the Free response paradigm, RT τ is unknown and the optimal neural response is a trade-off between speed, sensitivity and ambiguity. Here we first rescale the time $s = {}^t/_\tau$,

so that we have a fixed endpoint problem $s \in [0, 1]$. The transformation modifies the dynamics by

$$\frac{\mathrm{d}\boldsymbol{\nu}}{\mathrm{d}s} = \tau \frac{\mathrm{d}\boldsymbol{\nu}}{\mathrm{d}t}, \ \frac{\mathrm{d}\mathbf{x}}{\mathrm{d}s} = \tau \frac{\mathrm{d}\mathbf{x}}{\mathrm{d}t} \tag{C.10}$$

Adding τ to the state vector with dynamics $\frac{\mathrm{d}\tau}{\mathrm{d}s} = \dot{\tau} = 0$, to the augmented state vector in (C.4), we have

$$\begin{aligned} \dot{\mathbf{v}}_\tau &= \tau[f^T(\boldsymbol{\nu}, \mathbf{x}) \ \ \mathbf{y}^T \ \mathbf{0}^T]^T = \tau[g^T(\mathbf{v}, \mathbf{y}) \ \ \mathbf{0}^T]^T \equiv \bar{g}(\mathbf{v}, \mathbf{y}), \\ \mathbf{v}_\tau &= [\boldsymbol{\nu}^T \ \ \mathbf{x}^T \ \ \tau]^T = [\mathbf{v}^T \ \ \tau]^T \end{aligned} \tag{C.11}$$

The Lagrangian and the Hamiltonian for this problem can be written as,

$$L = 1 + \frac{\gamma}{2}\mathbf{x}^T\mathbf{x} + \frac{\varrho}{2}\mathbf{y}^T\mathbf{y}; \ \mathcal{H} = L + \boldsymbol{\lambda}^T g(\mathbf{v}, \mathbf{y}) \tag{C.12}$$

where $\boldsymbol{\lambda} \in \mathbb{R}^{M+2}$. The adjoint dynamics and the optimal response velocity is given by

$$\dot{\boldsymbol{\lambda}} = -L_{\mathbf{v}} - g_{\mathbf{v}}^T\boldsymbol{\lambda}, \ \mathbf{y}^*(t) = -\frac{1}{\varrho} g_{\mathbf{y}}^T \boldsymbol{\lambda}, \tag{C.13}$$

similar to Section C.2. Since the terminal time τ is free and the Hamiltonian is time invariant, from the transversality condition of maximum principle we have

$$\begin{aligned} &\mathcal{H}(\tau) = \mathcal{H}(1) = 0, \\ &\lambda_2(\tau) = \alpha\nu_2(\tau), \ \lambda_j(\tau) = 0, \ j = 3, \ldots, M+2. \end{aligned} \tag{C.14}$$

The boundary condition on the latent state being it triggers decision 1 from (P2-free), $\nu_1(\tau) = \nu_1(1) = \Gamma$. Thus we have a Two Point Boundary Value problem as before with the differential equation formed from (C.11), (C.13) and boundary conditions in (C.14), (P2-free).

C.4 Response Motif Characteristics for Forced and Free Paradigm

Note that for both Interrogation and Free paradigm the nature of the optimal response is governed by the adjoint variables $\boldsymbol{\lambda}$. From (C.7) and (C.8) and similarly (C.13) we can combine the dynamics of $\boldsymbol{\lambda}$ and $\mathbf{x}$ into

$$\begin{bmatrix} \dot{\boldsymbol{\lambda}} \\ \mathbf{x} \end{bmatrix} = \left[\begin{array}{cc|c} -\mathbf{A}^T & \mathbf{0}^{2\times M} & \mathbf{0}^{2\times M} \\ -\mathbf{b}^T & \mathbf{0}^{M\times M} & -\gamma\mathbb{I}_M \\ \hline \mathbf{0}^{M\times 2} & -\frac{1}{\varrho}\mathbb{I}_M & \mathbf{0}^{M\times M} \end{array}\right] \begin{bmatrix} \boldsymbol{\lambda} \\ \mathbf{x} \end{bmatrix} \tag{C.15}$$

where $L_{\mathbf{v}} = \begin{bmatrix} \mathbf{0}^{2\times 1} \\ \gamma\mathbf{x} \end{bmatrix}$, $g_{\mathbf{v}} = \begin{bmatrix} \mathbf{A} & \mathbf{b} \\ \mathbf{0}^{M\times M} & \mathbf{0}^{M\times M} \end{bmatrix}$, $g_{\mathbf{y}} = \begin{bmatrix} \mathbf{0}^{2\times M} \\ \mathbb{I}_M \end{bmatrix}$.

From (C.15) we can easily see that the optimal response takes the following exponential form

$$\mathbf{x}(t) = [\mathbf{0}^{M\times M+2} \;\; \mathbb{I}_M]\, \mathrm{e}^{\bar{\mathbf{A}}t} \begin{bmatrix} \boldsymbol{\lambda}(0) \\ \mathbf{x}(0) \end{bmatrix} \tag{C.16}$$

where $\bar{\mathbf{A}} = \begin{bmatrix} -\mathbf{A}^T & \mathbf{0} & \mathbf{0} \\ -\mathbf{b}^T & \mathbf{0} & -\gamma\mathbb{I} \\ \mathbf{0} & -\frac{1}{\varrho}\mathbb{I} & \mathbf{0} \end{bmatrix} \in \mathbb{R}^{2M+2}$. The eigenvalues of $\bar{\mathbf{A}}$ can be calculated using[3]

$$\det(\bar{\mathbf{A}} - \lambda\mathbb{I}_{2M+2}) = \det \left[\begin{array}{c|cc} -\mathbf{A}^T - \lambda\mathbb{I}_2 & \mathbf{0} & \mathbf{0} \\ \hline -\mathbf{b}^T & -\lambda\mathbb{I}_M & -\gamma\mathbb{I}_M \\ \mathbf{0} & -\frac{1}{\varrho}\mathbb{I} & -\lambda\mathbb{I}_M \end{array}\right] = \det(-\mathbf{A}^T - \lambda\mathbb{I}_2)\det((\lambda^2 - \frac{\gamma}{\varrho})\mathbb{I}_M) = 0 \tag{C.17}$$

Thus the eigenspectrum of $\bar{\mathbf{A}}$ is given by

$$\sigma(\bar{\mathbf{A}}) = \Big\{\sigma(-\mathbf{A}^T), \underbrace{\pm\sqrt{\frac{\gamma}{\varrho}}, \ldots, \pm\sqrt{\frac{\gamma}{\varrho}}}_{M}\Big\} = \Big\{-\sigma(\mathbf{A}), \underbrace{\pm\sqrt{\frac{\gamma}{\varrho}}, \ldots, \pm\sqrt{\frac{\gamma}{\varrho}}}_{M}\Big\} \tag{C.18}$$

From (4.7)-(4.10), we have $\sigma(\mathbf{A}) \in \mathbb{R}$ and $\sigma(\bar{\mathbf{A}}) \in \mathbb{R}$. If $\pm\sqrt{\frac{\gamma}{\varrho}} \notin \sigma(\mathbf{A})$, it can be shown that $\bar{\mathbf{A}}$ is diagonalizable, which proves that for both Forced and Free response paradigms the optimal motifs are exponential, taking the form in (4.15) with $\beta_k \in \sigma(\bar{\mathbf{A}})$, $k = 1, \ldots, 2M+2$.

[3]Note the difference between $\boldsymbol{\lambda}$, which is the adjoint vector and λ, which denotes the eigenvalues of a matrix.

Appendix D

Synthesis for Optimal Evidence in Detection Problems

D.1 Critical Measure for non-smoothness of the Penalty

In this section we ascertain the critical values of κ, namely κ_c, κ_c' in (5.43),(5.44) relating to Proposition 10, 11 for $a_1 < a_2$. From our discussion of $\Delta(\varepsilon\,;\,\bar{x}_2)$ and Figure 5.1, we can see that for the point of non-smoothness x_c on $\mathcal{N}$ to attract the returning trajectories as seen in Figure 5.3 (right panel), we must have

$$\begin{aligned} &\Delta'(0\,;\,x_s)|_{\varphi_1} = \Delta'(0\,;\,x_c)|_{\varphi_1} > 0 \\ &\Delta'(0\,;\,x_s)|_{\varphi_2} = \Delta'(0\,;\,x_c)|_{\varphi_2} \leq 0 \\ &\xi'(0\,;x_c) < 0 \end{aligned} \tag{D.1}$$

i.e., $\Delta(.)$ at $\bar{x}_2 = x_c$ would result in no switching under $\varphi \equiv \varphi_1$, and a switching for $\varphi \equiv \varphi_2$. We also use the fact that in this case x_s and x_c coincide. Using (D.1) we have

$$\Delta'(0\,;\,x_c)|_{\varphi_1} - \Delta'(0\,;\,x_c)|_{\varphi_2} \geq \Delta'(0\,;\,x_c)|_{\varphi_1} \tag{D.2}$$

Differentiating (5.25) with respect to ε, and using (D.1), (D.2) we have that

$$\begin{aligned} &(\varphi_1'(x_c) - \varphi_2'(x_c))\xi'(0\,;x_c) \geq \zeta'(0) + \varphi_1'(x_c)\xi'(0\,;x_c) \\ &\varphi_2'(x_c) - \varphi_1'(x_c) = \kappa \geq \frac{\zeta'(0) + \varphi_1'(x_c)\xi'(0\,;x_c)}{|\xi'(0\,;x_c)|} = \kappa_c, \end{aligned} \tag{D.3}$$

where $|.|$ denotes absolute value. From (5.23), (5.24) we can calculate

$$\zeta'(0) = \frac{b_1 \mathrm{U}}{a_1 x_{th}},\ \xi'(0\,;x_c) = b_2\mathrm{U} - a_2 x_c \zeta'(0) \tag{D.4}$$

and thus

$$\begin{aligned} \kappa_c &= \frac{\frac{b_1\mathrm{U}}{a_1 x_{th}} + \varphi_1'(x_c)(b_2\mathrm{U} - a_2 x_c \frac{b_1\mathrm{U}}{a_1 x_{th}})}{a_2 x_c \frac{b_1\mathrm{U}}{a_1 x_{th}} - b_2\mathrm{U}}, \\ x_c &> \frac{a_1 b_2}{a_2 b_1} x_{th} = \frac{x_{th}}{\vartheta_1} \end{aligned} \tag{D.5}$$

will result in the feature where all switched trajectories converge to x_c (as shown in Figure 5.3 right).

Next we look at the scenario presented in Proposition 11 and Figure 5.3 (middle panel), where we see a mix of the two features, i.e., regular synthesis as in smooth penalty upto a certain point x_s' on $\mathcal{N}$ and convergence to x_c via $\mathcal{X}_c$ beyond that. Since in this case the separatrix intersects $\mathcal{N}$ to the right of x_c, we have

$$x_c < x_s < x_s' \leq x_{th} \tag{D.6}$$

Let us consider the derivative of $\Delta(\varepsilon\,;\,\bar{x}_2)$ at $\varepsilon = \bar{\varepsilon}$ and $\bar{x}_2 = x'_s$ such that $\xi(\bar{\varepsilon}\,;\,x'_s) = x_c$. From our earlier analysis we know that at this point

$$\Delta'(0\,;\,x'_s)|_{\varphi_2} = 0,\ \Delta'(0\,;\,x'_s)|_{\varphi_1} \geq 0 \tag{D.7}$$

From (D.7) we can similarly derive the specific κ as in (D.2)

$$\Delta'(\bar{\varepsilon}\,;\,x'_s)|_{\varphi_1} - \Delta'(\bar{\varepsilon}\,;\,x'_s)|_{\varphi_2} = \Delta'(\bar{\varepsilon}\,;\,x'_s)|_{\varphi_1} \tag{D.8}$$

Using the range of x'_s in (D.6) we can get the range of κ in which we see the mix of the two limiting behaviors. Note that for $x'_s = x_c$, we have $\varepsilon = 0$ and solving for κ in (D.8) we get $\kappa = \kappa_c$. To calculate κ'_c we need to use the other end point of (D.6), i.e., $x'_s = x_{th}$. Thus from (D.8) we have

$$\kappa'_c = \frac{\Delta'(\bar{\varepsilon}\,;\,x_{th})|_{\varphi_1}}{|\xi'(\bar{\varepsilon}\,;\,x_{th})|} = \frac{\zeta'(\bar{\varepsilon}) + \varphi'_1(x_c)\xi'(0\,;x_{th})}{|\xi'(\bar{\varepsilon}\,;\,x_{th})|} \tag{D.9}$$

where $\bar{\varepsilon}$ can be solved from,

$$\xi(\bar{\varepsilon}\,;\,x_{th}) = \left(\frac{\mathrm{e}^{-a_1\bar{\varepsilon}}x_{th} + \frac{b_1}{a_1}\mathrm{U}(1-\mathrm{e}^{-a_1\bar{\varepsilon}})}{x_{th}}\right)^{-a_2/a_1}\left(\mathrm{e}^{-a_2\bar{\varepsilon}}x_{th} + \frac{b_2}{a_2}\mathrm{U}(1-\mathrm{e}^{-a_2\bar{\varepsilon}})\right) = x_c. \tag{D.10}$$

The calculation of κ_c, κ'_c for $a_1 > a_2$ can be carried out similarly with the construction of $\Delta(\bar{\varepsilon}\,;\,\bar{x}_2)$ for $\bar{x}_2 \in \mathcal{N}$, but now for a switching sequence of U_1, U_2.

References

[1] Peter Dayan and Laurence F Abbott. *Theoretical neuroscience*. Vol. 10. Cambridge, MA: MIT Press, 2001.

[2] Charles M Gray and Wolf Singer. "Stimulus-specific neuronal oscillations in orientation columns of cat visual cortex". In: *Proceedings of the National Academy of Sciences* 86.5 (1989), pp. 1698–1702.

[3] Katrina MacLeod, Alex Bäcker, and Gilles Laurent. "Who reads temporal information contained across synchronized and oscillatory spike trains?" In: *Nature* 395.6703 (1998), pp. 693–698.

[4] Patricia M DiLorenzo and Jonathan D Victor. *Spike timing: mechanisms and function*. CRC Press, 2013.

[5] Jason T Ritt and ShiNung Ching. "Neurocontrol: Methods, models and technologies for manipulating dynamics in the brain". In: *American Control Conference (ACC), 2015*. IEEE. 2015, pp. 3765–3780.

[6] Garrett B Stanley. "Reading and writing the neural code". In: *Nature neuroscience* 16.3 (2013), pp. 259–263.

[7] Joel S Perlmutter and Jonathan W Mink. "Deep brain stimulation". In: *Annu. Rev. Neurosci.* 29 (2006), pp. 229–257.

[8] Boris Rosin, Maya Slovik, Rea Mitelman, Michal Rivlin-Etzion, Suzanne N Haber, Zvi Israel, Eilon Vaadia, and Hagai Bergman. "Closed-loop deep brain stimulation is superior in ameliorating parkinsonism". In: *Neuron* 72.2 (2011), pp. 370–384.

[9] Jochen Ditterich, Mark E Mazurek, and Michael N Shadlen. "Microstimulation of visual cortex affects the speed of perceptual decisions". In: *Nature neuroscience* 6.8 (2003), pp. 891–898.

[10] C Daniel Salzman, Kenneth H Britten, and William T Newsome. "Cortical microstimulation influences perceptual judgements of motion direction". In: *Nature* 346.6280 (1990), p. 174.

[11] Karl Deisseroth. "Optogenetics". In: *Nature methods* 8.1 (2011), pp. 26–29.

[12] Zachary F Mainen and Terrence J Sejnowski. "Reliability of spike timing in neocortical neurons". In: *Science* 268.5216 (1995), p. 1503.

[13] Logan Grosenick, James H Marshel, and Karl Deisseroth. "Closed-Loop and Activity-Guided Optogenetic Control". In: *Neuron* 86.1 (2015), pp. 106–139.

[14] ShiNung Ching and Jason T. Ritt. "Control strategies for underactuated neural ensembles driven by optogenetic stimulation." eng. In: *Front Neural Circuits* 7 (2013), p. 54. DOI: 10.3389/fncir.2013.00054.

[15] Jr-Shin Li, Isuru Dasanayake, and Justin Ruths. "Control and synchronization of neuron ensembles". In: *IEEE Transactions on automatic control* 58.8 (2013), pp. 1919–1930.

[16] Dan Wilson, Abbey B Holt, Theoden I Netoff, and Jeff Moehlis. "Optimal entrainment of heterogeneous noisy neurons". In: *Frontiers in neuroscience* 9 (2015).

[17] M. Rosenblum and A. Pikovsky. "Controlling synchronization in an ensemble of globally coupled oscillators." In: *Phys Rev Lett* 92:114102 (2004).

[18] Mikhail V Ivanchenko, Grigory V Osipov, Vladimir D Shalfeev, and Jürgen Kurths. "Phase synchronization in ensembles of bursting oscillators". In: *Physical review letters* 93.13 (2004), p. 134101.

[19] Ali Nabi, Mohammad Mirzadeh, Frederic Gibou, and Jeff Moehlis. "Minimum energy desynchronizing control for coupled neurons". In: *Journal of computational neuroscience* 34.2 (2013), pp. 259–271.

[20] Alexandre Iolov, Susanne Ditlevsen, and André Longtin. "Stochastic optimal control of single neuron spike trains". In: *Journal of Neural Engineering* 11.4 (2014), p. 046004.

[21] Donald L Snyder and Michael I Miller. *Random point processes in time and space*. Springer Science & Business Media, 2012.

[22] Peter McCullagh and John A Nelder. *Generalized linear models*. Vol. 37. CRC press, 1989.

[23] Yosihiko Ogata. "Space-time point-process models for earthquake occurrences". In: *Annals of the Institute of Statistical Mathematics* 50.2 (1998), pp. 379–402.

[24] Ignacio Rodriguez-Iturbe, DR Cox, and Valerie Isham. "Some models for rainfall based on stochastic point processes". In: *Proceedings of the Royal Society of London A: Mathematical, Physical and Engineering Sciences*. Vol. 410. 1839. The Royal Society. 1987, pp. 269–288.

[25] Victor S Frost and Benjamin Melamed. "Traffic modeling for telecommunications networks". In: *Communications Magazine, IEEE* 32.3 (1994), pp. 70–81.

[26] Liam Paninski, Jonathan Pillow, and Jeremy Lewi. "Statistical models for neural encoding, decoding, and optimal stimulus design". In: *Progress in brain research* 165 (2007), pp. 493–507.

[27] Jeff M Bronstein et al. "Deep brain stimulation for Parkinson disease: an expert consensus and review of key issues". In: *Archives of neurology* 68.2 (2011), pp. 165–165.

[28] Günther Deuschl et al. "A randomized trial of deep-brain stimulation for Parkinson's disease". In: *New England Journal of Medicine* 355.9 (2006), pp. 896–908.

[29] M. Rosenblum and A. Pikovsky. "Delayed feedback control of collective synchrony: an approach to suppression of pathological brain rhythms." In: *Phys Rev E* 70 (2004), p. 041904.

[30] Ali Nabi and Jeff Moehlis. "Time optimal control of spiking neurons." eng. In: *J Math Biol* 64.6 (May 2012), pp. 981–1004. DOI: 10.1007/s00285-011-0441-5.

[31] Ali Nabi and Jeff Moehlis. "Single input optimal control for globally coupled neuron networks". In: *J. Neural Eng.* 8 (2011), 065008 (12pp).

[32] Dan Wilson and Jeff Moehlis. "A Hamilton-Jacobi-Bellman approach for termination of seizure-like bursting". In: *Journal of computational neuroscience* 37.2 (2014), pp. 345–355.

[33] Anatoly Zlotnik and Jr-Shin Li. "Optimal entrainment of neural oscillator ensembles". In: *Journal of neural engineering* 9.4 (2012), p. 046015.

[34] Dominique M Durand and Eduardo N Warman. "Desynchronization of epileptiform activity by extracellular current pulses in rat hippocampal slices." In: *The Journal of physiology* 480.Pt 3 (1994), p. 527.

[35] Arthur T Winfree. *The geometry of biological time*. Vol. 12. Springer Science & Business Media, 2001.

[36] Peter A Tass, Li Qin, Christian Hauptmann, Sandra Dovero, Erwan Bezard, Thomas Boraud, and Wassilios G Meissner. "Coordinated reset has sustained aftereffects in Parkinsonian monkeys". In: *Annals of neurology* 72.5 (2012), pp. 816–820.

[37] I Adamchic, C Hauptmann, UB Barnikol, N Pawelcyk, OV Popovych, T Barnikol, et al. "Coordinated reset has lasting aftereffects in patients with Parkinson's disease". In: *Mov. Disord* 29 (2014), pp. 1679–1684.

[38] Christoph Boergers and Nancy Kopell. "Synchronization in networks of excitatory and inhibitory neurons with sparse, random connectivity". In: *Neural Computation* 15.3 (2003), pp. 509–538.

[39] Yashar Ahmadian, Adam M Packer, Rafael Yuste, and Liam Paninski. "Designing optimal stimuli to control neuronal spike timing". In: *Journal of neurophysiology* 106.2 (2011), pp. 1038–1053.

[40] Debajit Saha et al. "Engaging and disengaging recurrent inhibition coincides with sensing and unsensing of a sensory stimulus". In: *Nature Communications* 8 (2017).

[41] Ian Krajbich and Antonio Rangel. "Multialternative drift-diffusion model predicts the relationship between visual fixations and choice in value-based decisions". In: *Proceedings of the National Academy of Sciences* 108.33 (2011), pp. 13852–13857.

[42] Andrew M Colman. *A dictionary of psychology*. Oxford University Press, USA, 2015.

[43] Anirban Nandi, Jason T Ritt, and ShiNung Ching. "Non-negative inputs for underactuated control of spiking in coupled integrate-and-fire neurons". In: *Decision and Control (CDC), 2014 IEEE 53rd Annual Conference on*. IEEE. 2014, pp. 3041–3046.

[44] Anirban Nandi, Heinz Schättler, Jason T Ritt, and ShiNung Ching. "Fundamental Limits of Forced Asynchronous Spiking with Integrate and Fire Dynamics". In: *The Journal of Mathematical Neuroscience* 7.1 (2017), p. 11.

[45] Anirban Nandi, Heinz Schättler, and ShiNung Ching. "Selective spiking in neuronal populations". In: *American Control Conference (ACC), 2017*. IEEE. 2017, pp. 2811–2816.

[46] Anirban Nandi, MohammadMehdi Kafashan, and ShiNung Ching. "Control Analysis and Design for Statistical Models of Spiking Networks". In: *IEEE Transactions on Control of Network Systems* (2017).

[47] Anirban Nandi, MohammadMehdi Kafashan, and ShiNung Ching. "Controlling point process generalized linear models of neural spiking". In: *American Control Conference (ACC), 2016*. IEEE. 2016, pp. 5779–5784.

[48] Anthony N Burkitt. "A review of the integrate-and-fire neuron model: I. Homogeneous synaptic input". In: *Biological cybernetics* 95.1 (2006), pp. 1–19.

[49] Wulfram Gerstner and Werner M Kistler. *Spiking neuron models: Single neurons, populations, plasticity*. Cambridge university press, 2002.

[50] Heinz Schättler and Urszula Ledzewicz. *Geometric optimal control: theory, methods and examples*. Vol. 38. Springer Science & Business Media, 2012.

[51] Heinz Schättler. "Local fields of extremals for optimal control problems with state constraints of relative degree 1". In: *Journal of dynamical and control systems* 12.4 (2006), pp. 563–599.

[52] Jonathan D Victor and Keith P Purpura. "Nature and precision of temporal coding in visual cortex: a metric-space analysis". In: *Journal of neurophysiology* 76.2 (1996), pp. 1310–1326.

[53] Jonathan D. Victor and Keith P. Purpura. "Analysis of Parallel Spike Trains, Grün, Sonja and Rotter, Stefan". In: *Analysis of Parallel Spike Trains*. Boston, MA: Springer US, 2010. Chap. Spike Metrics, pp. 129–156. DOI: 10.1007/978-1-4419-5675-0_7.

[54] Rudolph Emil Kalman. "A new approach to linear filtering and prediction problems". In: *Journal of Fluids Engineering* 82.1 (1960), pp. 35–45.

[55] Michael Grant, Stephen Boyd, and Yinyu Ye. *CVX: Matlab software for disciplined convex programming*. 2008.

[56] Lawrence F Shampine, Jacek Kierzenka, and Mark W Reichelt. "Solving boundary value problems for ordinary differential equations in MATLAB with bvp4c". In: *Tutorial notes* 2000 (2000), pp. 1–27.

[57] Peter Dayan and LF Abbott. "Theoretical neuroscience: computational and mathematical modeling of neural systems". In: *Journal of Cognitive Neuroscience* 15.1 (2003), pp. 154–155.

[58] Wilson Truccolo, Uri T Eden, Matthew R Fellows, John P Donoghue, and Emery N Brown. "A point process framework for relating neural spiking activity to spiking history, neural ensemble, and extrinsic covariate effects". In: *Journal of neurophysiology* 93.2 (2005), pp. 1074–1089.

[59] Murat Okatan, Matthew A Wilson, and Emery N Brown. "Analyzing functional connectivity using a network likelihood model of ensemble neural spiking activity". In: *Neural computation* 17.9 (2005), pp. 1927–1961.

[60] Victor Solo. "Likelihood functions for multivariate point processes with coincidences." In: *Decision and Control, 2007 46th IEEE Conference on*. IEEE. 2007, pp. 4245–4250.

[61] Demba Ba, Simona Temereanca, and Emery N Brown. "Algorithms for the analysis of ensemble neural spiking activity using simultaneous-event multivariate point-process models". In: *Frontiers in computational neuroscience* 8 (2014), p. 6.

[62] Daryl J Daley and David Vere-Jones. *An introduction to the theory of point processes*. Vol. 2. Springer, 1988.

[63] Andrew J. Whalen, Sean N. Brennan, Timothy D. Sauer, and Steven J. Schiff. "Observability and Controllability of Nonlinear Networks: The Role of Symmetry". In: *Phys. Rev. X* 5 (1 Jan. 2015), p. 011005. DOI: 10.1103/PhysRevX.5.011005.

[64] Emery N Brown, Riccardo Barbieri, Valérie Ventura, Robert E Kass, and Loren M Frank. "The time-rescaling theorem and its application to neural spike train data analysis". In: *Neural computation* 14.2 (2002), pp. 325–346.

[65] Takashi Kanamaru, Takehiko Horita, and Yoichi Okabe. "Theoretical analysis of array-enhanced stochastic resonance in the diffusively coupled FitzHugh-Nagumo equation". In: *Physical Review E* 64.3 (2001), p. 031908.

[66] Eugene M Izhikevich and Richard FitzHugh. "Fitzhugh-nagumo model". In: *Scholarpedia* 1.9 (2006), p. 1349.

[67] Frank Gray. *Pulse code communication*. US Patent 2,632,058. Mar. 1953.

[68] Debajit Saha and Baranidharan Raman. "Relating early olfactory processing with behavior: a perspective". In: *Current Opinion in Insect Science* 12 (2015), pp. 54–63.

[69] Debajit Saha, Chao Li, Steven Peterson, William Padovano, Nalin Katta, and Baranidharan Raman. "Behavioural correlates of combinatorial versus temporal features of odour codes". In: *Nature communications* 6 (2015), p. 6953.

[70] Rafal Bogacz, Eric Brown, Jeff Moehlis, Philip Holmes, and Jonathan D Cohen. "The physics of optimal decision making: a formal analysis of models of performance in two-alternative forced-choice tasks." In: *Psychological review* 113.4 (2006), p. 700.

[71] Philip L Smith. "Stochastic dynamic models of response time and accuracy: A foundational primer". In: *Journal of mathematical psychology* 44.3 (2000), pp. 408–463.

[72] Roger Ratcliff. "A theory of memory retrieval." In: *Psychological review* 85.2 (1978), p. 59.

[73] Ray Hyman. "Stimulus information as a determinant of reaction time." In: *Journal of experimental psychology* 45.3 (1953), p. 188.

[74] Martin P Paulus, Nikki Hozack, Lawrence Frank, and Gregory G Brown. "Error rate and outcome predictability affect neural activation in prefrontal cortex and anterior cingulate during decision-making". In: *Neuroimage* 15.4 (2002), pp. 836–846.

[75] Michael N Shadlen and William T Newsome. "Neural basis of a perceptual decision in the parietal cortex (area LIP) of the rhesus monkey". In: *Journal of neurophysiology* 86.4 (2001), pp. 1916–1936.

[76] Xiao-Jing Wang. "Probabilistic decision making by slow reverberation in cortical circuits". In: *Neuron* 36.5 (2002), pp. 955–968.

[77] Wulfram Gerstner, Werner M Kistler, Richard Naud, and Liam Paninski. *Neuronal dynamics: From single neurons to networks and models of cognition*. Cambridge University Press, 2014.

[78] D Vickers. "Evidence for an accumulator model of psychophysical discrimination". In: *Ergonomics* 13.1 (1970), pp. 37–58.

[79] Jerome R Busemeyer and James T Townsend. "Decision field theory: A dynamic-cognitive approach to decision making in an uncertain environment." In: *Psychological review* 100.3 (1993), p. 432.

[80] Marius Usher and James L McClelland. "The time course of perceptual choice: the leaky, competing accumulator model." In: *Psychological review* 108.3 (2001), p. 550.

[81] RHS Carpenter and MLL Williams. "Neural computation of log likelihood in control of saccadic eye movements". In: *Nature* 377.6544 (1995), p. 59.

[82] Ward Edwards. "Optimal strategies for seeking information: Models for statistics, choice reaction times, and human information processing". In: *Journal of Mathematical Psychology* 2.2 (1965), pp. 312–329.

[83] Brian DO Anderson and John B Moore. *Optimal control: linear quadratic methods*. Courier Corporation, 2007.

[84] Arthur Earl Bryson. *Applied optimal control: optimization, estimation and control*. CRC Press, 1975.

[85] Lev Semenovich Pontryagin. *Mathematical theory of optimal processes*. CRC Press, 1987.

[86] Bernard Bonnard and Monique Chyba. *Singular trajectories and their role in control theory*. Vol. 40. Springer Science & Business Media, 2003.

[87] Alberto Bressan and Benedetto Piccoli. *Introduction to the mathematical theory of control*. Vol. 2. American institute of mathematical sciences Springfield, 2007.

[88] Frank H Clarke. *Method of Dynamic and Nonsmooth Optimization*. SIAM, 1989.

[89] Richard Vinter. *Optimal control*. Springer Science & Business Media, 2010.

[90] Ugo Boscain and Benedetto Piccoli. *Optimal syntheses for control systems on 2-D manifolds*. Vol. 43. Springer Science & Business Media, 2003.

[91] Gilbert A Bliss. "Lectures on the Calculus of Variations". In: (1946).

[92] Liam Paninski. "Maximum likelihood estimation of cascade point-process neural encoding models". In: *Network: Computation in Neural Systems* 15.4 (2004), pp. 243–262.

[93] Martin Boerlin, Christian K Machens, and Sophie Denève. "Predictive coding of dynamical variables in balanced spiking networks". In: *PLoS Comput Biol* 9.11 (2013), e1003258.